Decision Time to Return in Seabirds:
application of fine-scale movement data to decision-making analyses

（高精度移動データに基づく海鳥の意思決定分析）

塩見 こずえ

Decision Time to Return in Seabirds:
application of fine-scale movement data to decision-making analyses

（高精度移動データに基づく海鳥の意思決定分析）

塩見こずえ
Kozue Shiomi

東京大学大学院 農学生命科学研究科
水圏生物科学専攻
Department of Aquatic Bioscience
Graduate School of Agricultural and Life Sciences
The University of Tokyo

2011

INDEX

Chapter 1. Introduction

Animals move to search for resources (e.g., prey, mates, refuge) and escape stress sources (e.g., predator, interspecies competition, severe climate) (Jander 1975). Movements from place to place are closely related to all types of animal behavior such as foraging, breeding, and reducing the risk of predation and can be considered to be the underlying basis of their lives in general. Because the environmental and/or animals' internal conditions can change heterogeneously over time (Kronfeld-Schor & Dayan 2003, Henderson 2006, Crystal 2009), the timing of the movements is essential for efficient use of resources and secure avoidance of unfavorable situations. For example, oystercatchers foraging in intertidal zones have been observed to time departures from their resting site such that arrivals at the foraging ground coincide with the time when the ground is exposed to ebb tides in order to increase foraging duration (Daan & Koene 1981). On the other hand, limpets that forage exclusively during high waters have been shown to head home from their foraging areas before they were exposed to the falling tide (Hartnoll & Wright 1977).

Including these examples, the onset of many types of movements is roughly fixed to a certain phase of the year, day, or tidal cycle. Many migratory birds move to their breeding sites and overwintering areas in the spring and autumn, respectively, every year (Gwinner 1996a); zooplanktons move vertically in the water column to shallow and deep water in the night and morning, respectively (e.g., Gabriel & Thomas 1988). These movement patterns probably result from adaptation to the regularity and predictability of environmental changes associated with circadian, circannual, and tidal rhythms. Among these temporally fixed movements, the timing of the migrations has been studied intensively with regard to the associated environmental conditions (e.g., day length, food availability) and changes in the internal states responsible for the onset of movements (e.g., circannual clock, fat accumulation) (e.g., Gwinner 1996b, Prop et al. 2003, Lehikoinen et al. 2004, Studds & Marra 2011). On the other hand, there has been little investigation on the timing of movements between variable sites that are not related to environmental periodicity, either changed or adjusted flexibly according to situations, and/or repeated with shorter temporal cycles than environmental ones. This is partly because, if the departure and arrival sites and times of movements are not fixed and can range beyond our observable area, examination of the timing is almost impossible.

Recent advances in electronics have produced rapid developments in bio-logging science, which is described as the study of using miniaturized animal-attached data loggers to

record and/or relay data about animal movements, behavior, physiology, and/or environment (Naito 2004, Rutz and Hays 2009). Nowadays, a variety of parameters can be recorded by data loggers, such as the ambient temperature, pressure (depth in water), speed, acceleration, global position, heart rate, and body temperature. In addition, data storage capacity is greatly increasing. These tools have dramatically advanced our knowledge of the physiology, biomechanics, and behavioral ecology of free-ranging animals in the wild even in the air and underwater. Since the history of bio-logging techniques started with depth recorders deployed on diving seals (DeVries & Wohlschlag 1964, Kooyman 1966, Kooyman 1968), the spatial positions of animals have always been regarded as important. Horizontal, vertical, and three-dimensional moving paths can be reconstructed in various temporal and spatial scales from seconds to days and from meters to global, respectively (e.g., Davis et al. 1999, Weimerskirch et al. 2002, Block et al. 2011). These movement data can make it possible to investigate flexible movements of wide-ranging animals and the timing of these movements in detail.

Seabirds are one animal group with high mobility for seasonal migration and daily foraging. They spend most of their lifetime at sea and are thus difficult to observe directly and continuously. Highly miniaturized and lightweight animal-borne data loggers have improved this situation and provided a great deal of knowledge on their spatial distribution and movements at sea (Burger & Shaffer 2008, Wakefield et al. 2009). During breeding season, they perform "central place foraging", which is defined as a set of movements: departure from a place ("central place", e.g., nest and roost), foraging at distant sites, and a return to the same place again (Orians & Pearson 1979; Fig. 1-1a). Various species obtain prey in different ways at sea: some feed sitting on the surface, others perform plunge dives, and others dive several tens to hundreds of meters (Ashmole 1971). For such divers, descending to depths and returning to the surface can also be considered as central place foraging (Houston & McNamara 1985; Fig. 1-1b). Because the distribution of their prey at sea is often dynamic, seabirds' movements to search for prey and the consequent foraging sites are also variable. The need to return may constrain their behavioral range and trip duration (Houston & Carbone 1992, Lewis et al. 2004), but the central place provides benefits exceeding the cost; for example, increased breeding success and safe resting sites. Considering the tradeoff between the requirements of foraging and returning, when to start returning to the central place appears to be a fundamental decision in the coordination of their trips. However, the timing of their return has not received much attention so far. On the contrary, diurnal rhythms of departure from and arrival to the central

place, how seabirds search for and where they obtain prey in a vast ocean, and how they can find their way to the nesting colonies in a featureless environment have been well investigated with the help of bio-logging techniques. This thesis used fine-scale movement paths of seabirds recorded by animal-borne loggers to investigate when they start returning to the central place for two different types of central place foraging—diving under the water and flying over the sea. Diving emperor penguins *Aptenodytes forsteri* and flying streaked shearwaters *Calonectris leucomelas* were selected as the model species. Both species were considered to be suitable for this research because they present variable movement patterns and experimental fields and methods have already been established.

Emperor penguins are the largest species in the family Spheniscidae. They breed in the austral winter on the fast ice around the Antarctic continent and make foraging trips to the sea (Jouventin 1995). During the trips, they repeatedly dive to forage and travel horizontally. Their main prey are fish, squid, krill, amphipods, and isopods (Piatkowski & Putz 1994, Robertson et al. 1994, Cherel & Kooyman 1998). Emperor penguins have the greatest diving ability among birds; their deepest recorded diving depth is 564 m (Wienecke et al. 2007), and the longest dive duration is 27.6 min (Sato et al. 2011). For deep and/or long divers like this species, when to start returning to the water surface may be essential because there is an inevitably long time lag between the onset of return and the arrival at the surface. Their inability to take oxygen underwater is likely to act as strong selective pressure to not mistime the decision to return. Chapter 2 examines the onset of return to the surface during dives of emperor penguins in relation to their physiological capacity. Three-dimensional dive paths were reconstructed on a time scale of seconds to investigate their decision time to return; this is the first data of this sort for avian species. This chapter consists of the results published in the *Journal of Experimental Biology* (Shiomi et al. 2012a).

Streaked shearwaters are pelagic birds in the family Procellariidae. They breed in East and Southeast Asia, mainly on the islands in Japan (Oka 2004), and nest underground. They are typical central place foragers; during the chick-rearing period from late August to November, they repeatedly commute to the sea for foraging, traveling up to several hundred kilometers, and return to their island to feed their chicks (Matsumoto 2008). They prey mainly on pelagic fish such as anchovy and saury probably using shallow dives or pecking at the water surface (Matsumoto 2008). Their departure from the colony is usually within a few hours before sunrise, and their return is within several hours after sunset (Yoshida 1962). Chapter 3 examines their decision of when to start returning from wide-ranging trips in relation to the apparent

constraint on arrival times at their breeding colonies by analyzing fine-scale movement paths at sea. The contents of this chapter were published in *Animal Behaviour* (Shiomi et al. 2012b).

Chapter 4 integrates the results from the penguin and shearwater studies. First, methods used to reconstruct animal movements are discussed in terms of the differences between the cases for diving and flying animals. Then, the common characteristics of the movements of the two species are described, and their decision rules for the timing to start returning are compared and summarized. Factors shaping their timing behaviors are also discussed. Finally, future perspectives in this line of research and the potential significance of the present studies are presented.

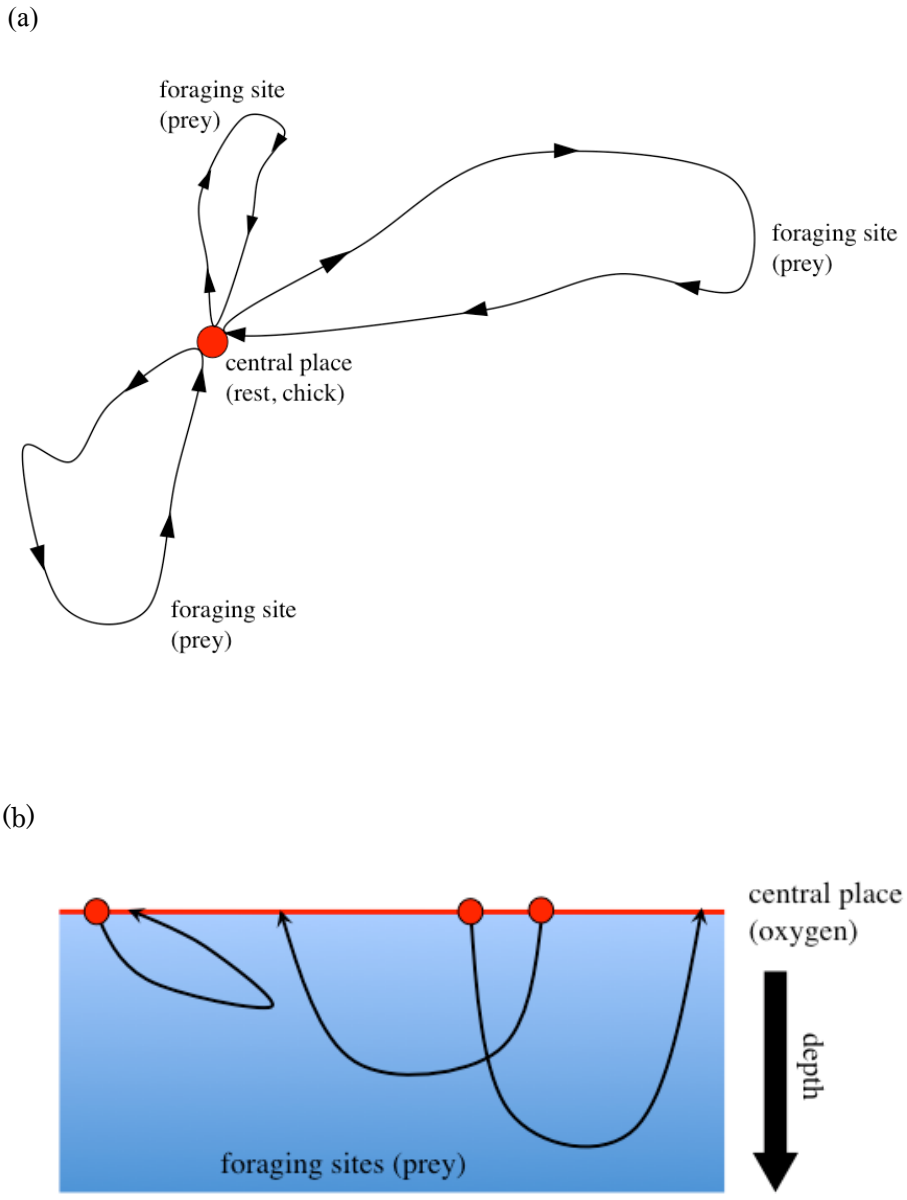

Fig. 1-1. Diagrams of two types of central place foraging performed by seabirds: (a) foraging trips and (b) foraging dives. As presented by red color, the central place is a nesting colony or roost in (a) and the water surface in (b).

Chapter 2. Timing of the decision to return the surface in diving emperor penguins

2-1. Background

Breath-holding divers are always in a dilemma during submergence: while they benefit by exploring and traveling underwater, they must return to the water surface to replenish oxygen stores and to remove accumulated carbon dioxide. Longer dives could allow foragers to exploit more prey or increase distance traveled, but more oxygen consumption might require longer recovery times at the surface as well (Kooyman et al., 1980, Kooyman & Kooyman, 1995). Therefore, deciding when to end a dive may not be straightforward. For a variety of animals, factors affecting the decision have been investigated both theoretically and empirically in terms of foraging ecology and behavioral physiology (Houston & Carbone, 1992, Thompson & Fedak, 2001, Mori et al., 2002). In these studies, dive duration was almost always used as a temporal parameter, which is important to estimate optimal time budgets and to examine physiological capacities. However, given that divers must decide to return the surface well before the end of a dive, the start time to return may also be worth investigating in this context.

In deep dives, the time lag between the decision to return the surface and the end of a dive is inevitably long, and therefore, examination of dive duration alone may not be sufficient to understand their timing strategies. In this chapter about emperor penguins, the decision time defined as the time into a dive at which the animal began to return to the surface was investigated. As the major constraints on diving behaviors are likely to be physiological ones (Butler & Jones, 1997, Kooyman & Ponganis, 1998) and locomotor cost is the main cause of oxygen consumption (Williams et al. 2004), it was hypothesized that cumulative muscle work, and not elapsed time *per se*, determined the time limit of the decision to return to the surface. Based on previous reports that the number of swim strokes during dives related strongly to oxygen consumption and muscle stroke effort (Williams et al., 2004, Williams et al., 2011), the number of strokes at the decision time was investigated as a reasonable index of muscle workload.

2-2. Materials and methods

2-2-1. field experiments

The data sets of dives were obtained under two different conditions; during foraging trips at sea and at the artificial isolated dive hole (hereafter, experiment A and B, respectively).

Experiment A was conducted at a breeding colony of emperor penguins near Cape Washington, Antarctica (74°39' S, 165°24' E; Fig. 2-1a), during the period from 28 October to 17 November 2005. Ten breeding birds were captured at the edge of the colony when they were leaving for foraging trips at sea. Then, either of two types of data logger was attached to the lower central back feathers using waterproof tape (Tesa tape, Beiersdorf AG, Hamburg, Germany; Wilson et al. 1997), instant glue (Loctite epoxy, Henkel, Westlake, OH, USA), and stainless steel cable ties (Metal tie, HellermannTyton Co. Ltd.) (Fig. 2-1b). One type recorded swim speed (1 Hz), depth (1 Hz), and two-axis acceleration (16 Hz)(W1000-PD2GT or W1000L- PD2GT; 122 or 128 mm in length, 22 or 27 mm in diameter, 73 or 127 g in air, Little Leonardo Ltd., Tokyo, Japan). The other type recorded swim speed (1 Hz), depth (1 Hz), three-axis acceleration (8 Hz), and three-axis magnetism (1 Hz)(W1000L-3MPD3GT; 174 mm in length, 26 mm in diameter, 140 g in air, Little Leonardo Ltd., Tokyo, Japan). Using a data set recorded by W1000L-3MPD3GT, three dimensional (3-D) dive paths can be reconstructed (see the section 2-2-3). VHF transmitters (Model MM130, ATS, Isanti, MIN, USA) were also deployed on all the birds to locate them when they returned to the dense colony. The birds were recaptured at the colony 7.9-19.7 days after the deployment, and the instruments were retrieved (Table 2-1).

Experiment B was conducted from 15 November to 4 December 2004 at 'Penguin Ranch' artificially set up on the fast sea ice in McMurdo Sound, Antarctica (77°43'S, 166°07'E; Fig. 2-1a, c) (Kooyman et al., 1992, Sato et al. 2005). Sixteen non-breeding emperor penguins were caught when they were wandering on the ice between a breeding colony and the sea. Then, they were enclosed within an isolated corral on the sea ice (about 25 m and 20 m in long and short spans, respectively). Artificial dive holes were drilled through the 2.3 to 2.5 m thick ice inside the corral, through which the birds were allowed to dive freely. The ice hole was 1.2 m diameter wide and 8 m apart. They foraged daily beneath the sea ice through the isolated dive holes (Ponganis et al. 2000). Loggers, W1000L-3MPD3GT (see above), were attached to three penguins. Three-axis accelerations were recorded at 16 or 32 Hz, and other parameters at 1 Hz. One to three deployments were done for each penguin, and the loggers were retrieved 1.6 to 2.5 days after attachment (Table 2-1).

2-2-2. acceleration and speed data

The acceleration sensor of the data logger measured both specific accelerations by propulsive activity and gravity-based accelerations by gravity (Tanaka et al. 2001, Sato et al. 2003). The

former was used for stroke analyses, and the latter for calculations of animals' postures. Following an assumption that fluctuations in acceleration data caused by changes in animals' posture occurs at the lower frequencies than those by propulsive activities, gravity-based acceleration data were extracted from the acceleration data with a low-pass filter (IFDL Version 4.0; WaveMetrics, Lake Oswego, OR, USA) (Tanaka et al. 2001). To determine a cut-off value of the low-pass filter, the power spectral density (PSD; Fig. 2-2a) of the entire acceleration data set was calculated for each individual by fast Fourier transformation using the function in IGOR Pro version 6.04 (WaveMetrics, Lake Oswego, OR, USA). Considering the frequency with the peak of the PSD as the dominant stroke frequency of each individual, the low-pass finite impulse response (FIR) filters were set to remove the high-frequency components caused by strokes (Sato et al. 2007; Fig. 2-2b). The cut-off values for the filters used for each individual ranged from 1.06 to 1.63 Hz. The specific acceleration data were obtained by subtracting the low-frequency components from the acceleration data.

The speed sensor of the logger consisted of an external propeller and a propeller rotation counter. It has been verified experimentally that the rotations of the propeller per second (rps) are proportional to swimming speeds relative to water with a high coefficient of determination (>0.9) (Tanaka et al. 2001, Sato et al. 2007). To estimate the constant of proportion, *b,* for converting the number of propeller rotations to the swimming speed, the data of the number of propeller rotations per second, longitudinal accelerations, and depths were used. First, the estimated vertical moving rate, R_t, at a given time, t, is described using equation (2-1):

$$R_t = bN_t \sin(p_t) \qquad (2\text{-}1)$$

where N_t is the number of propeller rotations per second, and p_t is the angle of the penguins' longitudinal axis relative to the horizontal plane (pitch angle). Since usually the loggers cannot be deployed to be parallel to the longitudinal axis of animals, the attachment angle of the logger, a, i.e. angle between the longitudinal axis of the logger and of the animal should be considered in calculation of pitch angles (Sato et al. 2003):

$$p = -\arcsin(A_{long}/9.8) - a \qquad (2\text{-}2)$$

where A_{long} is the longitudinal gravity-based acceleration data. The estimated depth profile was then calculated by adding R_t sequentially from the starting time to the ending time of a dive. Because a is usually a positive value in penguin studies, when it is set as zero, the calculated depth at the end of the dive largely deviate from zero (at the surface) (Sato et al. 2003). The appropriate attachment angle of the logger, a, was obtained by repeating the calculation of depth profiles with different values of a, so that the estimated depth at the end of a dive become zero (Sato et al. 2003). Then, the optimal value of the conversion coefficient, b, was determined by repeating the calculation of the estimated dive profile with different values of b. With the optimal value, the estimated depth profile fitted the depth profile measured with the depth sensor well (Fig. 2-3). Those procedures to calculate the attachment angle, a, and the constant, b, were conducted for all dives of each deployment using a customized macro. Selecting dives for which the estimated dive profile was consistent with the measured one, the average values were obtained. They were used for calculating actual swimming speeds (= bN_t). The stall speed of the logger was determined experimentally to be 0.3 m s^{-1} when the sampling frequency is set as 1 Hz (Tanaka et al. 2001). Speeds below this value were considered indistinguishable from zero.

Mean swim speed was calculated from the swim speeds in a dive, and an averaged value was obtained for each bird. To test the difference of swim speeds between the two experiments, two types of linear mixed models (LMM) were fitted to the pooled data of mean swim speed during a dive for all birds. The LMM takes the effect of dependence among data points on estimation of parameters into account by including those factors as random effects. In the present study, 'bird identity' was considered as a random effect. One model included 'experiment' (during foraging trips or at the isolated ice hole) as a fixed effect, and the other did not. To judge whether inclusion of 'experiment' improve the model, Akaike Information Criteria (AIC) were compared between the two fitted models. AIC is calculated with log likelihood and the number of parameters: the model with the smallest value of AIC can be considered as the most parsimonious one. For the model fitting, R 2.10 (R Development Core Team, 2009) was used with *lmer* function in R package *lme4* (Bates & Maechler, 2009).

2-2-3. reconstruction of 3-D dive paths

Using data recorded by the logger W1000L-3MPD3GT, 3-D dive paths of one bird (CW13) in experiment A and of three birds in experiment B were calculated using a customized macro (Narazaki & Shiomi, 2010) compliant with IGOR Pro. The heading on the horizontal plane, h_t, at each time point was determined from the rotation angles of the longitudinal and lateral axes

(pitch, roll) and the data of three-axis geomagnetism (Johnson & Tyack 2003). The extracted low-frequency components of acceleration were used as gravity-based ones to calculate pitch (p; see equation (2-2)) and roll (r) with equations introduced by Johnson & Tyack (2003):

$$r = \begin{cases} \arctan(A_{lat}/A_{dv}) & (A_{dv} < 0) \\ \arctan(A_{lat}/A_{dv}) + \pi & (A_{lat} \le 0 \text{ and } A_{dv} > 0) \\ \arctan(A_{lat}/A_{dv}) - \pi & (A_{lat} > 0 \text{ and } A_{dv} > 0) \\ \pi/2 & (A_{lat} < 0 \text{ and } A_{dv} = 0) \\ -\pi/2 & (A_{lat} > 0 \text{ and } A_{dv} = 0) \end{cases} \quad (2\text{-}3)$$

where A_{lat} is lateral gravity-based acceleration, and A_{dv} is dorso-ventral gravity-based acceleration. Then, the locomotion vector in a given period from *t-1* to *t* with reference to the fixed frame (x_t, y_t, z_t) was calculated with the data on heading, h_{t-1}, pitch, p_{t-1}, depth change, ($D_t - D_{t-1}$), and swimming speed, U_t, using equation (2-4). The x-axis is northward, the y-axis is westward, and the z-axis is upward (depth presented as negative):

$$\begin{cases} x_t = U_t \cos(p_{t-1}) \cos(h_{t-1} + d) \\ y_t = -U_t \cos(p_{t-1}) \sin(h_{t-1} + d) \\ z_t = D_t - D_{t-1} \end{cases} \quad (2\text{-}4)$$

where d is the declination of earth's magnetism in the experimental fields, 133.2° for bird CW13 and 144.8° for birds in experiment B, respectively (Maus et al. 2005). Finally, the dive path was reconstructed by adding the locomotion vectors during a dive in chronological order (dead-reckoning principle; Wilson & Wilson 1988, Mitani et al. 2003)(Fig. 2-4).

2-2-4. decision-to-return time

A dive was defined as any submersion deeper than 2 m and longer than 3 seconds. As the interest in this study was in the time at which the bird decided to return to the water surface, the elapsed time after the start of a dive until a continuous final ascent started was analyzed (Fig. 2-5a). The ascent start time (AST) was obtained from time-series depth data as the elapsed time until the last positive change of depth occurred. To avoid detecting instantaneous changes of depth during final ascent, the AST was defined to occur at a depth deeper than half of the maximum depth of a dive.

In dive path analyses, only dives in which mean swim speed was greater than 1 m s^{-1} were considered as reliable data. This is because cruising swim speed of emperor penguins is relatively constant with the mean speed of around 2 m s^{-1} (Sato et al., 2010). In dives with swim speeds less than 1 m s^{-1}, it is highly possible that rotation of the propellers, which is used for measuring swim speeds, probably stopped or slowed as a result of ice accumulation around the propeller. To describe property of horizontal movements, the farthest horizontal distance (FHD) from the starting point of a dive and the elapsed time (farthest horizontal time; FHT) until the bird reached the farthest horizontal point were calculated for each dive path (Fig. 2-5b).

2-2-5. number of strokes

Emperor penguins perform stroke and glide swimming, in which they stroke intermittently with a glide phase between consecutive strokes (van Dam et al., 2002). As an index of muscle workload until the decision to return, the number of strokes during the period from the start of a dive to the decision-to-return time was calculated using the longitudinal specific acceleration data, which reflect stroking activities as regular peaks (van Dam et al., 2002; Fig. 2-2b). A set of up- and down- beats was recognized as one stroke. Stroke rate (the number of strokes per second) of each bird was estimated as a slope of a linear regression line, in which a number of strokes was a response variable, and the decision-to-return time an explanatory variable. To determine a difference of stroke rates between the two experiments (during foraging trips or at the artificial dive hole), two types of generalized linear mixed models (GLMM) were fitted to the pooled data with Poisson error distribution and logarithm link function, in which a number of strokes was a response variable with logarithm of the decision time as an offset term, and 'bird identity within an experiment' as a random effect. One model included 'experiment' (during foraging trips or at the isolated ice hole) as a fixed effect, and the other did not. Akaike Information Criteria (AIC) were compared between the two fitted models. For the model fitting, R 2.10 (R Development Core Team, 2009) was used with *glmer* function in R package *lme4* (Bates & Maechler, 2009).

2-3. Results

2-3-1. dives during foraging trips (experiment A)

In total, 15,978 dives were recorded from ten free-ranging birds breeding near Cape Washington. Dive depths (maximum depth in a dive) ranged from less than 10 m to more than 500 m (Fig.

2-6a). A histogram of mean swim speed in a dive for each bird was bell-shaped (Fig. 2-7), and the average value for a bird ranged from 2.0 to 2.3 m s^{-1} (Table 2-1). Note that as mean swim speeds were largely variable for shallow dives, which could result from short dive durations, only dives deeper than 50 m were used to describe characteristics of their swim speeds (N = 4,251 dives).

On visual examination of the plot of the ascent start time (AST) against dive depth, the upper boundary of the AST conditional on dive depth seemed asymptotic (Fig. 2-6a). Therefore, nonlinear quantile regression (Koenker & Park, 1996) was applied to estimate the asymptotes. A similar approach was adopted in a previous study to estimate the asymptotes of dive duration in leatherback turtles (Bradshaw et al., 2007). Quantile regression gives a functional relationship between variables for a certain portion of a probability distribution of responses (Cade & Noon, 2003, Koenker & Bassett, 1978). It is useful for investigating limiting factors by providing an estimate of the upper boundary of the conditional distribution of responses (Cade & Noon 2003). Because this method is robust to the presence of outliers (Cade et al., 1999), it seemed suitable to the present data, which had some exceptional data points (large AST) in relatively shallow dives (Fig. 2-6a). An exponential-rise model

$$Y = a\ \{1\text{-}exp\ (\text{-}bX)\} \qquad (2\text{-}5)$$

was fitted on the 95th percentile of the AST (Y, in min) against dive depth (X, in m) (Fig. 2-6a). For the model fitting, R 2.10 (R Development Core Team, 2009) was used with *nlrq* function in R package *quantreg* (Koenker, 2009). The regression coefficient (a) for each bird, which corresponded to an estimated asymptote value of the AST, was 5.7 ± 0.56 min (mean ± s.d., range 4.9-6.7 min; Table 2-2). Of dives in which the AST exceeded the asymptote of each bird, 42.2 ± 25.4% (mean ± s.d., range 14.3-100%) were shallower than 100 m (Fig. 2-6a).

For one bird CW13 deployed with W1000L-3MPD3GT, three-dimensional (3-D) dive paths of 2411 dives were reconstructed. Dives appeared to be divided roughly into two groups; in group I, the farthest horizontal times (FHT) nearly equaled the end times of the dive (i.e. dive duration), and those of group II were less than the dive duration. A histogram of the ratio of the FHT to the dive duration had a prominent peak just below 1.0 and a low peak between 0.4 and 0.75, corresponding with group I and II respectively (Fig. 2-8a). That is, the dive paths of group II indicated that the bird began to return toward the starting point around at the middle of the dive (see Fig. 2-5b). For these U-turn dives, the FHT should be more indicative of the timing of

the decision to return than the AST. If U-turn dives are defined as dives in which the ratio of the FHT to dive duration was between 0.4 and 0.75 and in which the farthest horizontal distance (FHD) was greater than the dive depth, the FHT of these U-turn dives positively correlated with the FHD (Pearson's correlation coefficient r_c = 0.96, P < 0.0001, N = 217 dives; green circles in Fig. 2-8b). The maximum FHT and FHD were 9.5 min and 865.2 m, respectively. The outliers of shallow dives in the plot of the AST against dive depth disappeared when replacing the AST and dive depth with the FHT and the FHD for the U-turn dives, respectively (compare Figs. 2-6a and 2-8b).

2-3-2. dives at the isolated ice hole (experiment B)

In experiment B, 3-D paths of 495 dives were reconstructed for three birds. All the dives were U-turn dives because there was neither another ice hole nor an ice crack through which to exit within several kilometers around the artificial hole. For comparison with dive paths of the bird CW13 in experiment A, the ratio of the FHT to dive duration in dives in which birds clearly performed U-turns (FHD > 100 m) was calculated. The histogram had a peak around 0.5, similar to the U-turn dives of bird CW13 (Fig. 2-8a). Mean swim speed in a dive ranged from 1.6 to 1.9 m s^{-1} on average for each bird (Table 2-1 and Fig. 2-7). Note that for the same reason as that in experiment A, only dives reaching farther than 50 m from the starting point of a dive were used for calculations (N = 321 dives). The mean swim speeds were significantly smaller than those in experiment A: AIC of the LMM with and without 'experiment' as a fixed effect was 1021 and 1009, respectively, and swim speeds estimated by the LMM were 2.2 m s^{-1} for birds in experiment A and 1.8 m s^{-1} for birds in experiment B. The difference of swim speeds between during foraging trips at sea and in dives at the isolated ice hole has been reported in a previous study (Sato et al. 2010), although the reason remains unknown. While dive depth did not exceed 100 m, the maximum value of the FHD in each bird was 1047.8 ± 108.6 m (mean ± s.d.) in experiment B. The FHT correlated with the FHD for all birds (Pearson's correlation coefficient r_c = 0.96 to 0.98, P < 0.0001, Fig. 2-6b). In 23.7 ± 7.7% (mean ± s.d., range 18.4 – 32.5%) of the dives in each bird, the FHT exceeded the average upper limit of the AST (5.7 min) in birds in experiment A (Fig. 2-6b).

2-3-3. number of strokes

The following results of stroke analyses do not include data from bird CW13, because acceleration was recorded at the lower sampling frequency (8 Hz), and the algorithm to detect

strokes did not appear to work well when using the same threshold as for the other data sampled at 16 or 32 Hz. In all the other twelve birds from both experiment A and B, the number of strokes significantly increased with the decision time, i.e. the AST and the FHT (linear regression: r^2 = 0.89 to 0.97 for each bird, $P < 0.0001$). AIC of the model with 'experiment' as a fixed effect, which was fitted on the number of strokes with the decision time as a fixed effect, was smaller than the one not considering 'experiment' (AIC: 35,556 and 35,575 respectively). This means that the number of strokes for dives of similar duration was different between experiments. The estimated slope (i.e. stroke rate until the decision time) was smaller for birds in experiment B than in experiment A (0.45 and 0.79 beats s^{-1} respectively), which is consistent with a previous report that stroke rates were higher in dives during foraging trips than in dives through the artificial ice hole (Sato et al., 2011). Stroke rate of individual birds estimated as a slope of the linear regression line ranged from 0.34 to 0.83 beats s^{-1} (Table 2-2 and 2-3) and was inversely related with the upper limit of the decision time (hereafter, decision time limit) obtained by the 95th percentile regression on the AST against dive depth in experiment A and by the maximum FHT multiplied by 0.95 in experiment B, respectively (linear regression using reciprocals of stroke rate: r^2 = 0.995, $P < 0.0001$, N = 12 birds, *decision time limit* = 3.97×(1/*stroke rate*); Fig. 2-9a).

In experiment A, the number of strokes at the AST appeared asymptotic conditional on dive depth (Fig. 2-9b) as the AST did. Fitting an exponential model (equation (2-5)) to estimate the 95th percentile conditional on dive depth, the estimated upper limit of the number of strokes at the AST was 255 ± 31 beats (range: 196–295 beats) in each bird (Table 2-2). The number of strokes at the FHT in experiment B was 237 ± 27 beats at maximum (Table 2-3), which distributed within a similar range to that of birds in experiment A (Fig. 2-9b).

2-4. Discussion

2-4-1. decision rule to return the surface

The AST in experiment A was largely variable for a given dive depth (Fig. 2-6a). This may have resulted from differences in prey patch conditions, social interaction, and/or the degree of satiety, although it cannot be discussed with the present data set. Despite of the variation, there appeared to be both lower and upper boundaries in the plot of the AST. While the linear increase in the lower limit with dive depth reflected V-shaped dives with no apparent foraging times, the asymptotic distribution of the upper limit suggested that there was a decision time

limit independent of dive depth. There were some shallow dives (dive depth <100 m) in which the AST largely exceeded the decision time limit estimated by percentile regression (Fig. 2-6a), but fine-scale 3-D dive paths of bird CW13 yielded the possible explanation. In most of those shallow dives, the bird traveled horizontally a far distance and then returned toward the starting point of the dive (see Fig. 2-5b). This shape of the dive paths was similar to those of birds diving at the isolated dive hole in experiment B, where they dived shallower than 100 m, probably for foraging fish beneath the surface of the sea ice (Ponganis et al., 2000), and always returned to the ice hole because the fast sea ice prevented them from surfacing at other places. Also in shallow and long dives during foraging trips at sea, birds might dive under the sea ice and explore not vertically but horizontally, as has been suggested in previous studies (Kooyman & Kooyman, 1995, Watanuki et al., 1997, Wienecke et al., 2007). Under such circumstances, they might decide to return toward the starting point of a dive unless another exit is found. Considering that replacing the AST with the FHT for the U-turn dives of bird CW13 eliminated the outliers among shallow dives in the plot of AST against dive depth (Fig. 2-8b), there appeared to be a decision rule irrespective of whether dives were vertical or horizontal. Those inferences from the results in the bird CW13 are likely applicable to shallow and long dives of the other nine birds in experiment A as well, although their dive paths were unknown.

However, it was found that the FHT of birds in experiment B often exceeded the decision time limit, avg. 5.7 min, obtained in experiment A (Fig. 2-6b). This did not fit the inference above that there is a common decision time limit to return. Stroke analyses helped to address this inconsistency. In experiment B, the combination of the lower stroke rate and the higher value of the maximum FHT than in experiment A resulted in the maximum number of strokes on the FHT for each bird, ranging from 218 to 267 beats, which were within the range of the upper limit of the number of strokes at the AST in experiment A obtained by the 95th percentile regression, 196-295 beats (Fig. 2-9b). These results suggest that the accumulated number of strokes, but not the elapsed time, was related to their decision time limit to return. This concept was also supported by the decision time limits of individual birds, which were longer for birds with the lower stroke rate (Fig. 2-9a). The limit of the number of strokes expected from the regression line, *decision time limit* = 3.97 (1/*stroke rate*), is 238 beats (= 3.97×60), which is consistent with the empirical values for each bird presented in Tables 2-2 and 2-3.

2-4-2. difference of stroke rates

One remaining question is why the stroke rates were so different between birds in experiment A and B. I try to explain it from biomechanical aspects.

Swimming pattern in stroke-glide mode of emperor penguins is constant as a set of gliding phase following one stroke (Fig. 2-10), while some other aquatic animals such as seals swim with several consecutive strokes followed by prolonged gliding (e.g. Watanabe et al. 2006; Fig. 2-10). Whichever a stroke pattern is, their average swim speeds keep relatively constant during cruising (Sato et al. 2007), while instantaneous swim speeds increase and decrease accompanied by strokes and glides, respectively (Watanabe et al. 2006). Aquatic animals also have relatively constant stroke frequencies (reciprocal of stroke cycle duration) expected from their body size (Sato et al. 2007), with which the acceleration (output force) by one stroke is probably within a narrow range. It is implied that, in order to keep the average swim speed constant, they have to stroke when the instantaneous speed decreases by the same amount as the increase with the previous stroke(s); this can be seen in the empirical data (Fig. 2-10).

Stroke rate is nearly equal to a reciprocal of glide duration. And from the prediction above, the glide duration is the time taken for deceleration to a given swim speed after the preceding stroke. The deceleration rate, dU/dt, is affected by drag and buoyancy parallel to swimming direction (Fig. 2-11) and presented as

$$m\frac{dU}{dt} = \{D - (B - mg)\sin\beta\} \qquad (2\text{-}6)$$

where m is body mass, U is swimming speed, t is time, D is drag, B is buoyancy, g is gravity, and β is pitch angle. Integrating both sides of the equation about t during the glide duration G taken for instantaneous speed to decrease by the same amount as the acceleration by one stroke, the equation (2-7) is obtained:

$$m(U_G - U_0) = \int_0^G \{D - (B - mg)\sin\beta\}dt \qquad (2\text{-}7).$$

As drag and buoyancy are dependent of speed and depth (ambient pressure), respectively, these parameters change during a glide in a strict sense. But for simplification, I assume here that drag

and buoyancy is constant during one period of gliding, which leads to the relationship (2-8) from the equation (2-7):

$$m(U_G - U_0) \cong \{D - (B - mg)\sin\beta\}G \qquad (2\text{-}8).$$

And duration of gliding, *G,* is expressed as

$$G \cong \frac{m(U_G - U_0)}{\{D - (B - mg)\sin\beta\}} \qquad (2\text{-}9).$$

Drag and buoyancy are obtained with the below equations:

$$D = \frac{1}{2} S C_d \rho_w U_{avg}{}^2 \qquad (2\text{-}10)$$

$$B - mg = \{(\frac{A_0}{v/10 + 1} + \frac{m}{\rho_t})\rho_w - m\}g \qquad (2\text{-}11)$$

where U_{avg} is calculated as $(U_G+U_0)/2$, S is wetted surface area of the body, C_d is drag coefficient, ρ_w is the density of sea water, ρ_t is the density of the body tissue of a penguin, A_0 is air volume inside of the penguin body, and v is current depth. Among the parameters affecting G, air volume has been suggested to be smaller in shallower dives even when those were extremely long dives (Sato et al. 2011), which implies that air volume A_0 was smaller in experiment B than experiment A. Additionally, swim speeds and pitch angles were also smaller in experiment B: the latter is because of their horizontal swimming, which means that pitch angles kept around zero unlike birds swimming mainly vertically during foraging trips at sea. By setting the parameters required in equation (2-7) as showed in Table 2-4, stroke rates when a penguin achieves 240 beats (according to the empirical upper limit) underwater are calculated with variable air volume, swim speed, and pitch angles (Fig. 2-12). The model estimations suggest that birds in experiment B with smaller air volumes, lower swim speeds, and shallower pitch angles would flap their wings at the lower rate than birds in experiment A. Thus, biomechanical factors are likely to explain, at least qualitatively, the difference of stroke rates in experiment A and B.

2-4-3. conclusion

In the present study, it was found in experiment A that emperor penguins at sea had a decision time limit to return the water surface, which was independent of the distance to the surface (vertical or horizontal). However, in combination with the results from experiment B at the isolated dive hole, it is suggested that the decision was constrained not by elapsed time, but by the number of strokes.

The cost of diving consists of basal metabolic cost and locomotor cost, and the number of strokes is a reasonable index of the latter, i.e. muscle workload (Williams et al., 2004, Williams et al., 2011). The results of the present study suggest that the cumulative work in muscle triggered the onset of the return to the surface. Comparison between experiments A and B and among individuals indicated that a decrease in stroke rate prolonged the decision time limit, which increased the maximum distance traveled by the time of the decision (up to more than 1 km in experiment B). Intermittent stroking of aquatic animals has been elucidated as a swimming strategy to save locomotor cost (Weihs, 1974, Williams, 2001). In emperor penguins, this locomotion pattern was reported as a potential energy conservation mechanism to achieve long dives (van Dam et al., 2002) in addition to physiological adaptations, such as bradycardia and peripheral vasoconstriction, reducing the basal metabolic rate of diving (Meir et al., 2008, Ponganis et al., 2003). It was shown here that stroking patterns may affect the decision to end a dive and consequently the dive duration.

These new insights were revealed by focusing on the start time to return to the surface, reconstructing fine-scale dive paths, and analyzing stroking activities with acceleration data. Although previous studies on diving animals postulated that total oxygen stores and oxygen consumption rate constrain dive duration (Hansen & Ricklefs, 2004, Hays et al., 2000), the duration of a dive should be a consequence of the prior decision to return to the surface. Therefore, it may be important to investigate the timing of the initiation of the return as well to fully understand diving strategies.

Table 2-1. Basic information for each experimental bird.

Bird	experiment	Body mass (kg)	Type of loggers	Data length (days)	Mean swim speed during a dive (m s^{-1})		Number of dives for speed analyses
					mean	s.d.	
CW1	A	29.0	W1000-PD2GT	4.0	2.1	0.23	124
CW2	A	23.0	W1000-PD2GT	4.1	2.2	0.30	359
CW3	A	21.5	W1000-PD2GT	4.1	2.2	0.28	314
CW4	A	23.5	W1000-PD2GT	3.9	2.3	0.30	294
CW7	A	24.0	W1000-PD2GT	4.0	2.2	0.30	300
CW8	A	27.5	W1000-PD2GT	3.9	2.0	0.22	232
CW9	A	24.0	W1000-PD2GT	4.0	2.1	0.25	345
CW10	A	25.5	W1000L-PD2GT	14.3	2.2	0.29	513
CW11	A	22.0	W1000L-PD2GT	14.5	2.2	0.25	1196
CW13	A	26.0	W1000L-3MPD3GT	11.5	2.2	0.24	574
PR1	B	27.4	W1000L-3MPD3GT	4.1	1.9	0.29	116
PR2	B	24.7	W1000L-3MPD3GT	6.3	1.9	0.28	147
PR3	B	24.4	W1000L-3MPD3GT	2.3	1.6	0.27	58

* Body mass was measured before deploying the logger.

* Data length for birds PR1 and PR2 was presented as the sum of two and three deployments, respectively.

Table 2-2. Results of the 95th percentile regression analyses on the ascent start time (AST) and the cumulative number of strokes at the AST against dive depth for birds in experiment A.

		Ascent start time (min)		Number of strokes at the AST			
Bird	Number of dives	coefficient *a*	coefficient *b*	coefficient *a*	coefficient *b*	Stroke rate (beats s^{-1})	s.e.
CW1	676	5.7	0.05	196	0.05	0.60	0.007
CW2	994	5.9	0.02	257	0.03	0.70	0.005
CW3	876	4.9	0.04	236	0.04	0.78	0.007
CW4	875	6.3	0.03	271	0.03	0.69	0.005
CW7	997	5.6	0.03	294	0.03	0.83	0.005
CW8	852	5.9	0.03	295	0.02	0.63	0.008
CW9	818	5.4	0.04	239	0.05	0.72	0.005
CW10	3061	5.1	0.04	256	0.03	0.82	0.004
CW11	4156	5.1	0.04	255	0.04	0.80	0.003
CW13	2673	6.7	0.03	-	-	-	-
mean		5.7	0.03	255	0.03	0.73	
s.d.		0.6	0.01	31	0.01	0.08	

The regression equation was $Y = a[1\text{-}\exp(-bX)]$, where Y is the AST or the number of strokes at the AST and X the dive depth.

Stroke rates were obtained as a slope of the linear regression line to predict the number of strokes from the AST (decision-to-return time).

Table 2-3. Upper limit of the FHT (decision-to-return time) and results of stroke analyses for birds in experiment B.

Bird	Number of dives	Maximum FHT (min)	Maximum number of strokes at the FHT	Stroke rate (beats s^{-1})	s.e.
PR1	158	10.8	218	0.39	0.009
PR2	254	9.8	267	0.46	0.006
PR3	83	11.7	225	0.34	0.008
mean		10.8	237	0.40	
s.d.		1.0	27	0.06	

Table 2-4. List of parameters for stroke and glide swimming model (see Section 2-4-2).

symbol	parameter	value (unit)		citation
m	body mass	25	(kg)	
U_G-U_0	increase of speed by one stroke	0.4	(m s^{-1})	
S	wetted surface area	0.68	(m^2)	Clark & Bemis (1979)
g	gravitational acceleration	9.8	(m s^{-2})	
C_d	drag coefficient	0.003		Clark & Bemis (1979)
ρ_w	density of water	1027	(kg m^{-3})	
ρ_t	density of body tissue	1020	(kg m^{-3})	Wilson et al. (1992)

(a)

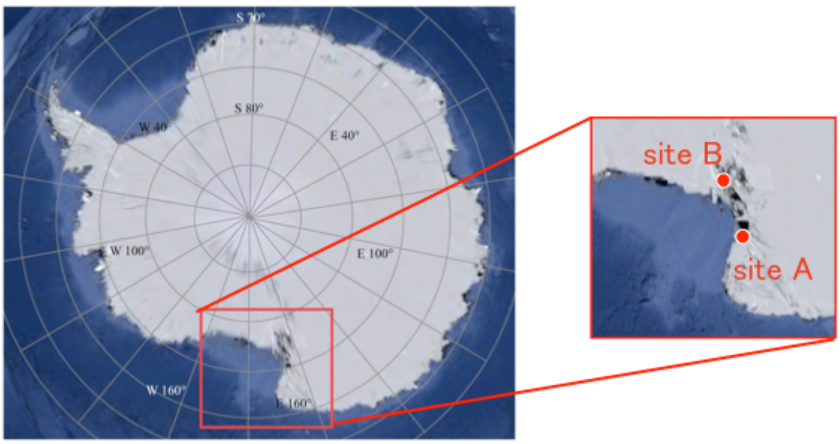

(b)

(c)

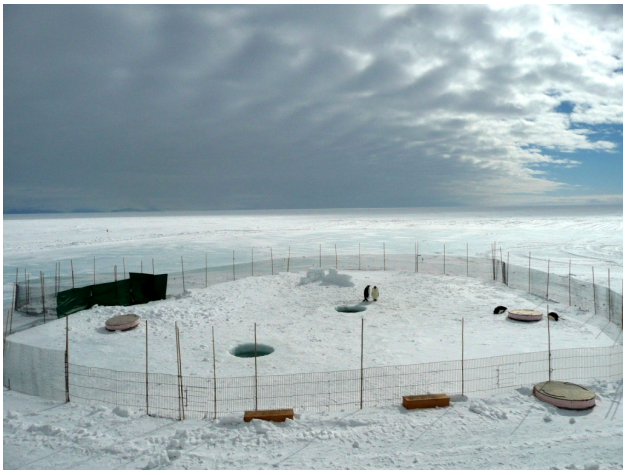

Fig. 2-1. (a) Map of Antarctica and the enlarged part near the sites for experiments A (site A: near Cape Washington, 74°39'S, 165°24'E) and B (site B: McMurdo Sound, 77°43'S, 166°07'E). The map was made by modifying the image obtained from Google earth (http://www.earth.google.com). Pictures of (b) a penguin with a data logger, W1000L-3MPD3GT, on the lower central back and (c) the experimental site B ('Penguin Ranch'), where penguins stand near isolated dive holes inside the artificial corral on the fast sea ice (Photos by Kozue Shiomi).

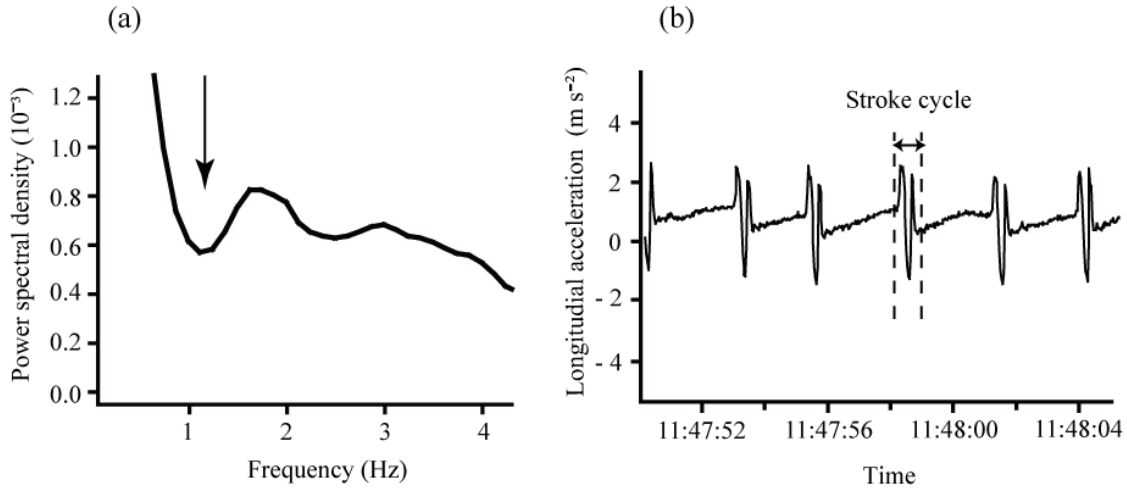

Fig. 2-2. (a) Power spectral densities of longitudinal acceleration data calculated by fast Fourier transformation. An arrow indicates the trough providing a threshold of the low-pass filter to extract gravity-based acceleration components (see the section 2-2-2). (b) Time-series data of longitudinal acceleration. Double-headed arrows show a stroke cycle (a set of up- and down strokes) detected as regular peaks. Stroke frequency is a reciprocal of stroke cycle duration.

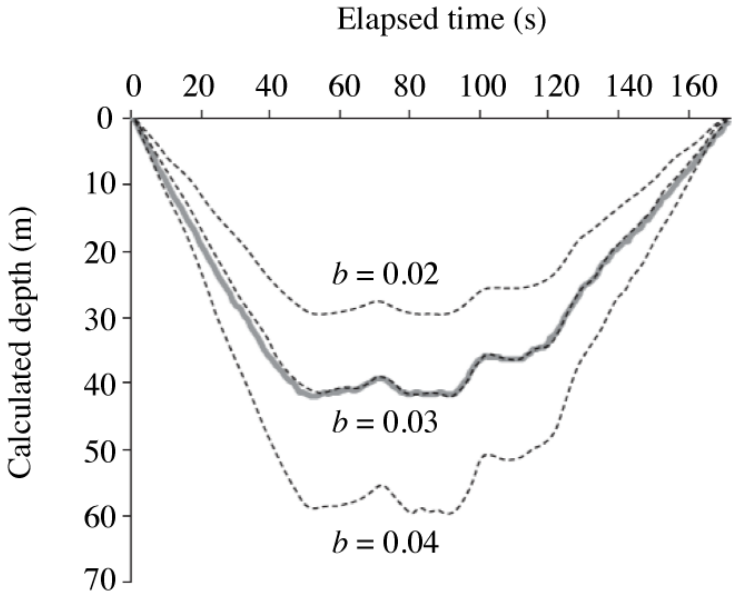

Fig. 2-3. Comparison of depth profiles to deteremine the constant *b* for converting the number of propeller rotations per second to the swimming speed. Gray line presents that recorded by a data logger, and dashed lines those calculated with recorded pitch angles, the number of propeller rotations, and several assumed values of *b*. For this dive, 0.03 is appropriate.

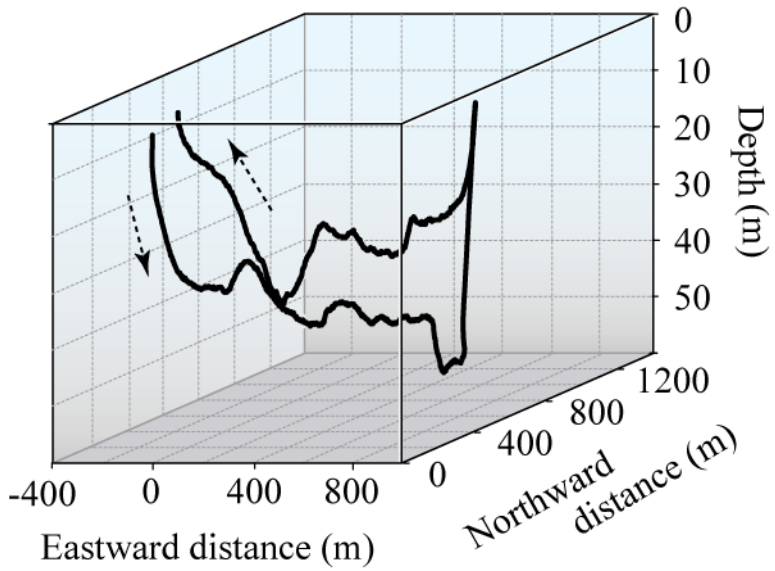

Fig. 2-4. Example of reconstructed three-dimensional dive path of an emperor penguin. Dashed arrows indicate the direction of travel.

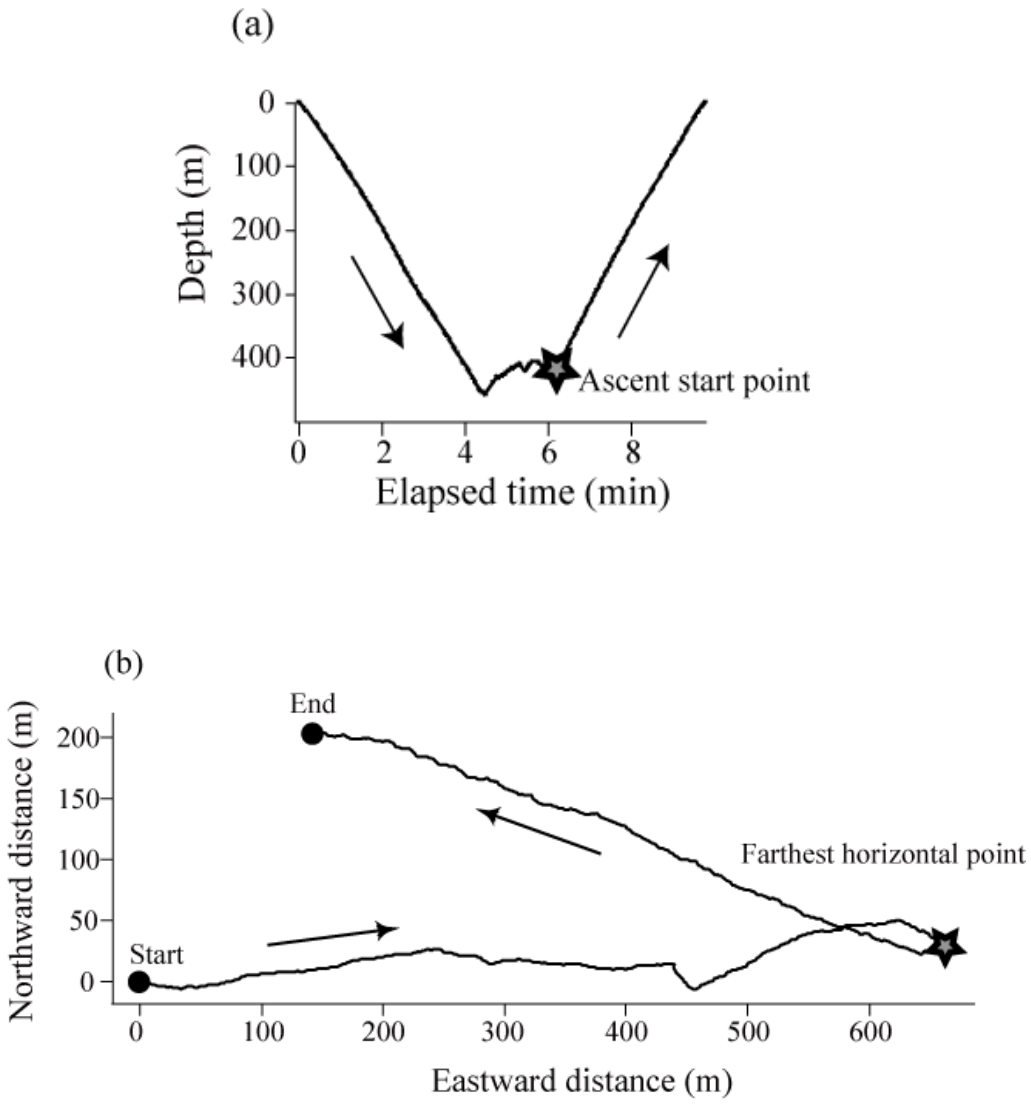

Fig. 2-5. Illustration of the point of decision to return the surface in non-U-turn dives (a; time-series depth data) and in U-turn dives (b; an aerial view of a dive path). The onset of ascent and U-turn were considered as the decision point in (a) and (b), respectively.

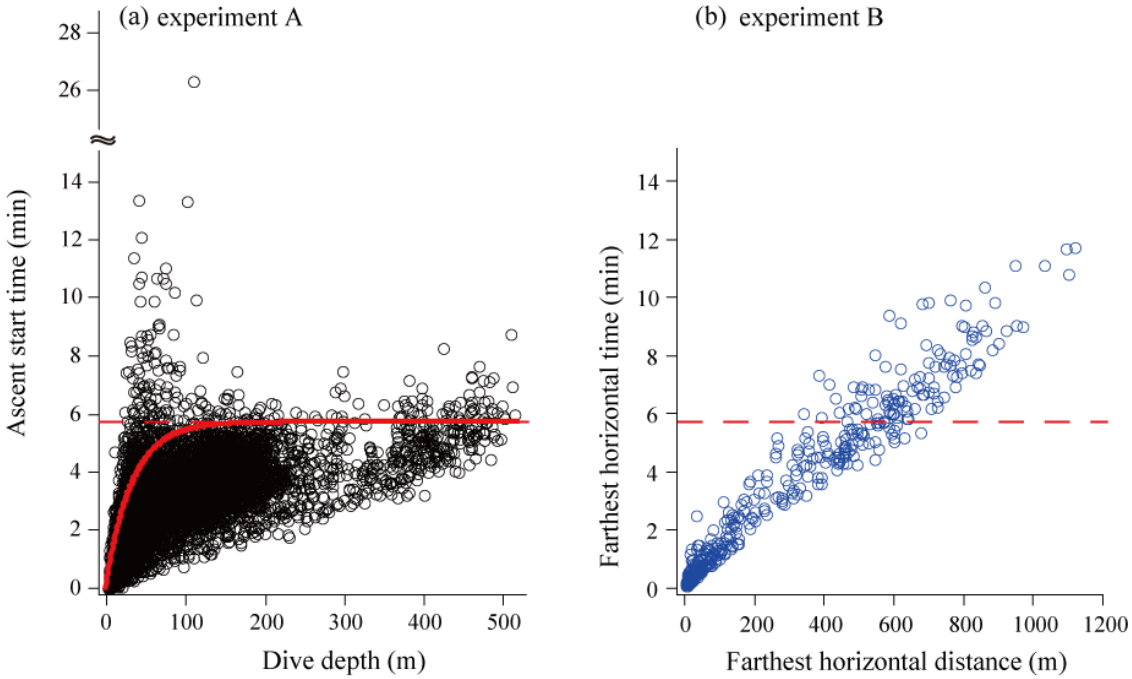

Fig. 2-6. Relationships between the decision-to-return time and vertical or horizontal distance from the starting point of the dive. (a) Plots of ascent start time (AST) against dive depth obtained from birds diving during foraging trips (experiment A; *N*=15,978 dives from 10 birds) and (b) those of farthest horizontal time (FHT) against the farthest horizontal distance (FHD) obtained from birds diving at the isolated dive hole (experiment B; *N*=495 dives from three birds). A red line represents the 95th percentile regression line, AST=a{1–exp[–b(dive depth)]}, using average regression coefficients from 10 birds in experiment A; dashed lines represent an average asymptote (5.7 min) estimated as coefficient *a* in experiment A (see Table 1).

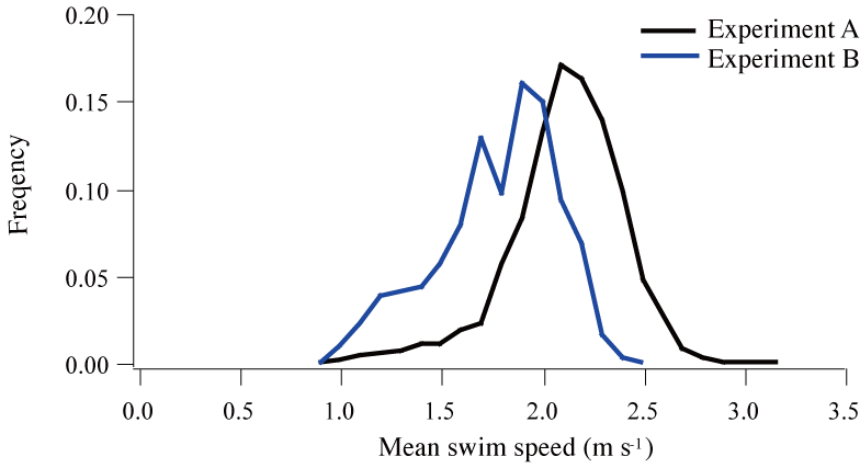

Fig. 2-7. Histograms of mean swim speed in a dive of birds diving during foraging trips (expetiment A; black line) and of birds diving at the artificial dive hole (experiment B; blue line).

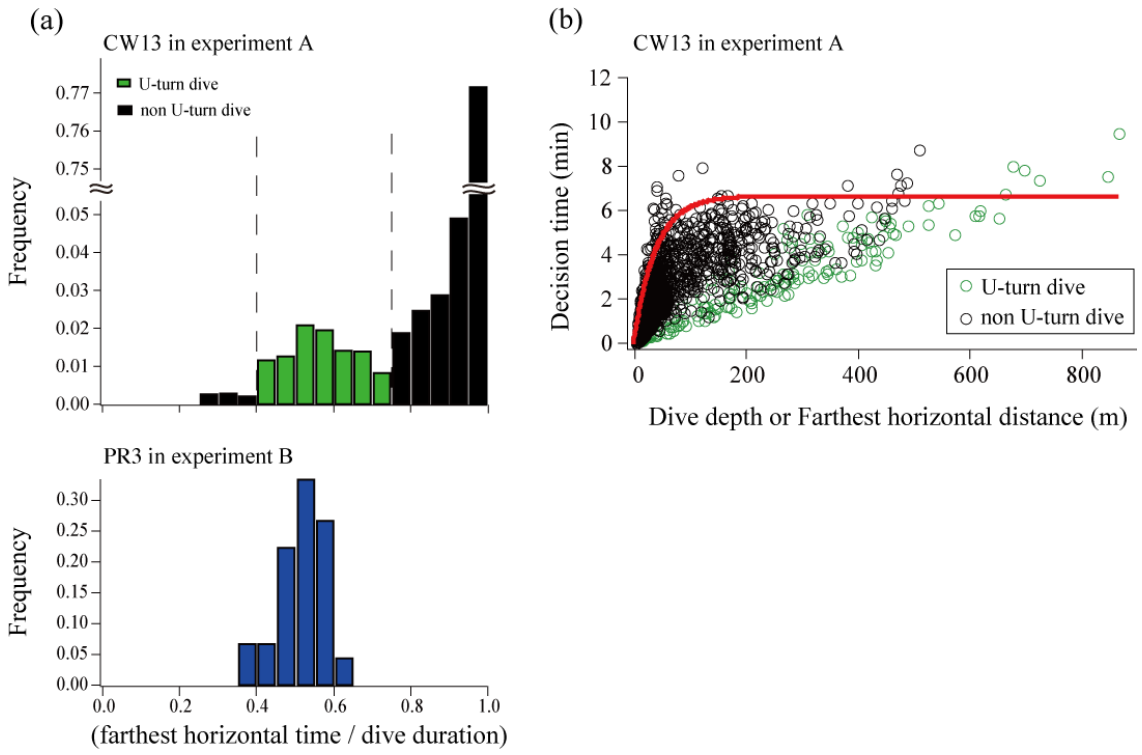

Fig. 2-8. Classification of U-turn dives using dive paths of bird CW13 in experiment A. (a) Histogram of the ratio of the farthest horizontal time (FHT) to dive duration (top). For reference, a histogram obtained from bird PR3 in experiment B, where birds always returned to the starting point of a dive, is presented (bottom). (b) Relationship between decision-to-return time (i.e. AST for non-U-turn dives, FHT for U-turn dives) and dive depth for non-U-turn dives (black) and farthest horizontal distance (FHD) for U-turn dives (green). The red line presents the 95th percentile regression line, AST=a{1–exp[–b(dive depth)]}, obtained from bird CW13.

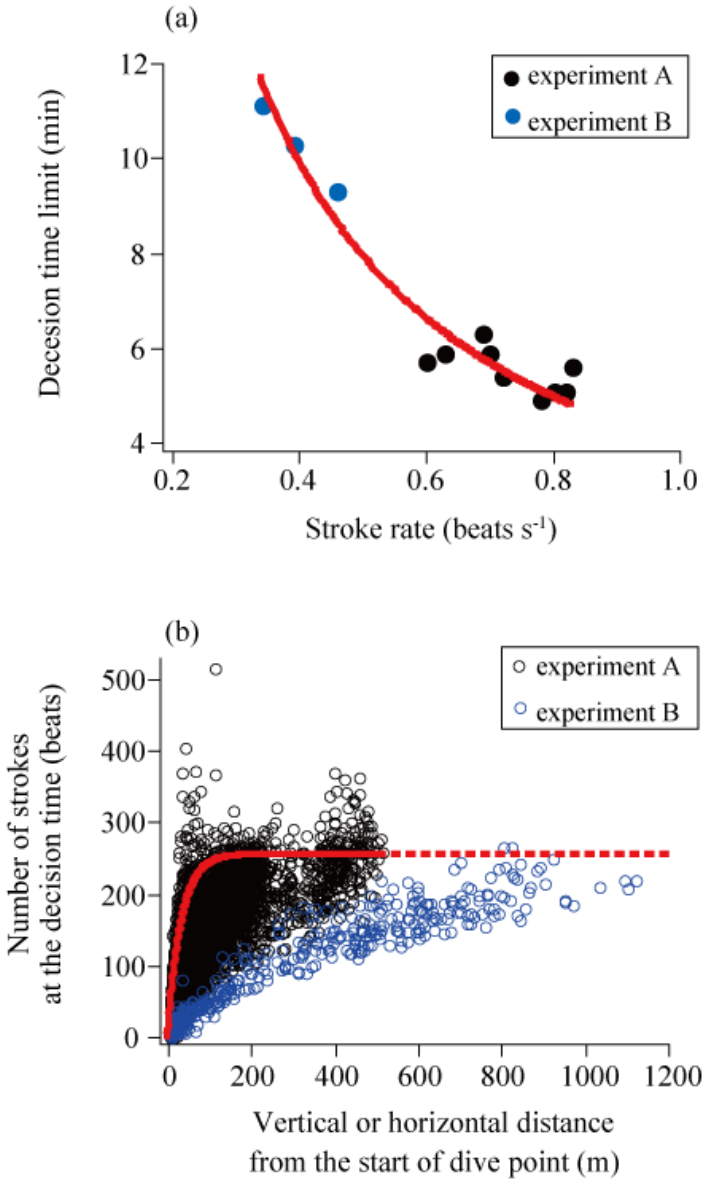

Fig. 2-9. Results of stroke analyses. (a) Relationship between the upper limit of the decision-to-return time (decision time limit) and stroke rate in each bird in experiment A (black) and B (blue). The decision time limit was estimated by the 95th percentile regression on AST in experiment A, and as the maximum FHT multiplied by 0.95 in experiment B. The red line indicates the regression line: decision time limit=3.97/stroke rate. (b) Relationship between the number of strokes at the decision to return and the dive depth and farthest horizontal distance (FHD)(black, dives in experiment A; blue, dives in experiment B). The red line presents the 95th percentile regression line averaged for birds in experiment A (see Table 2-2).

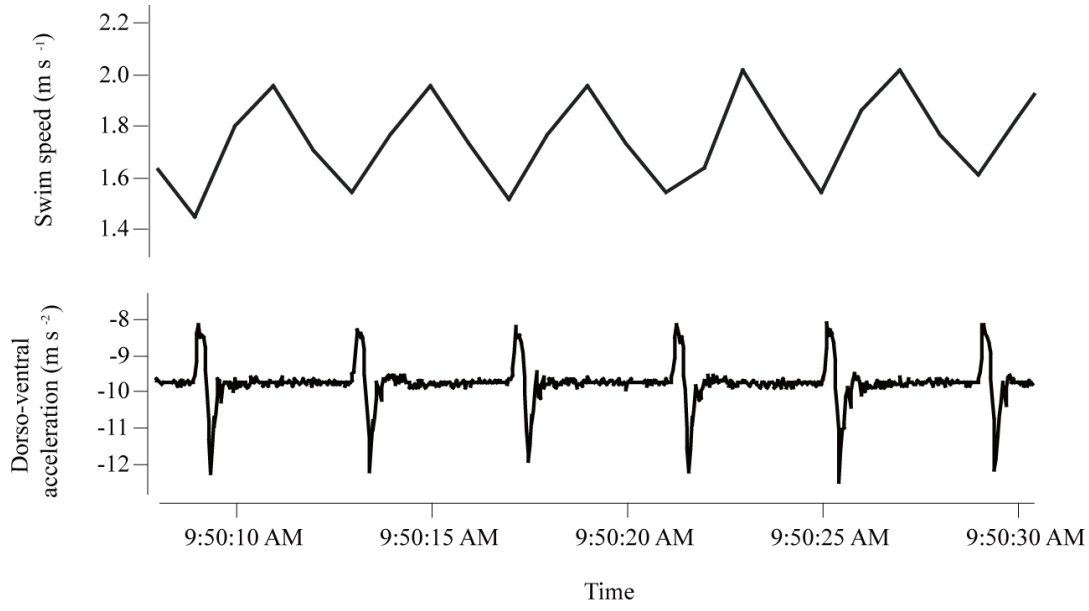

Fig. 2-10. Time-series data of swim speed and dorso-ventral acceleration. Regular peaks in the acceleration reflect up- and down strokes of flippers. Instantaneous increase and decrease in the speed reflect stroke and glide, respectively.

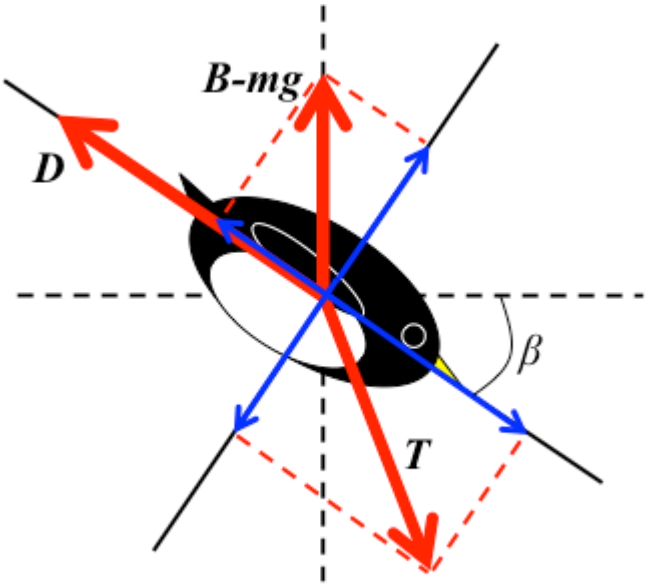

Fig. 2-11. Diagram of hydrodynamic and mechanical forces on a swimming penguin. *D* is drag, *B* is buoyancy, *m* is body mass, *g* is gravity acceleration, *T* is thrust, and *β* is pitch angle relative to horizontal plane. During gliding phase, thrust component parallel to swim direction is expected to be smaller than drag and buoyancy component, and therefore, a bird would gradually decelerate.

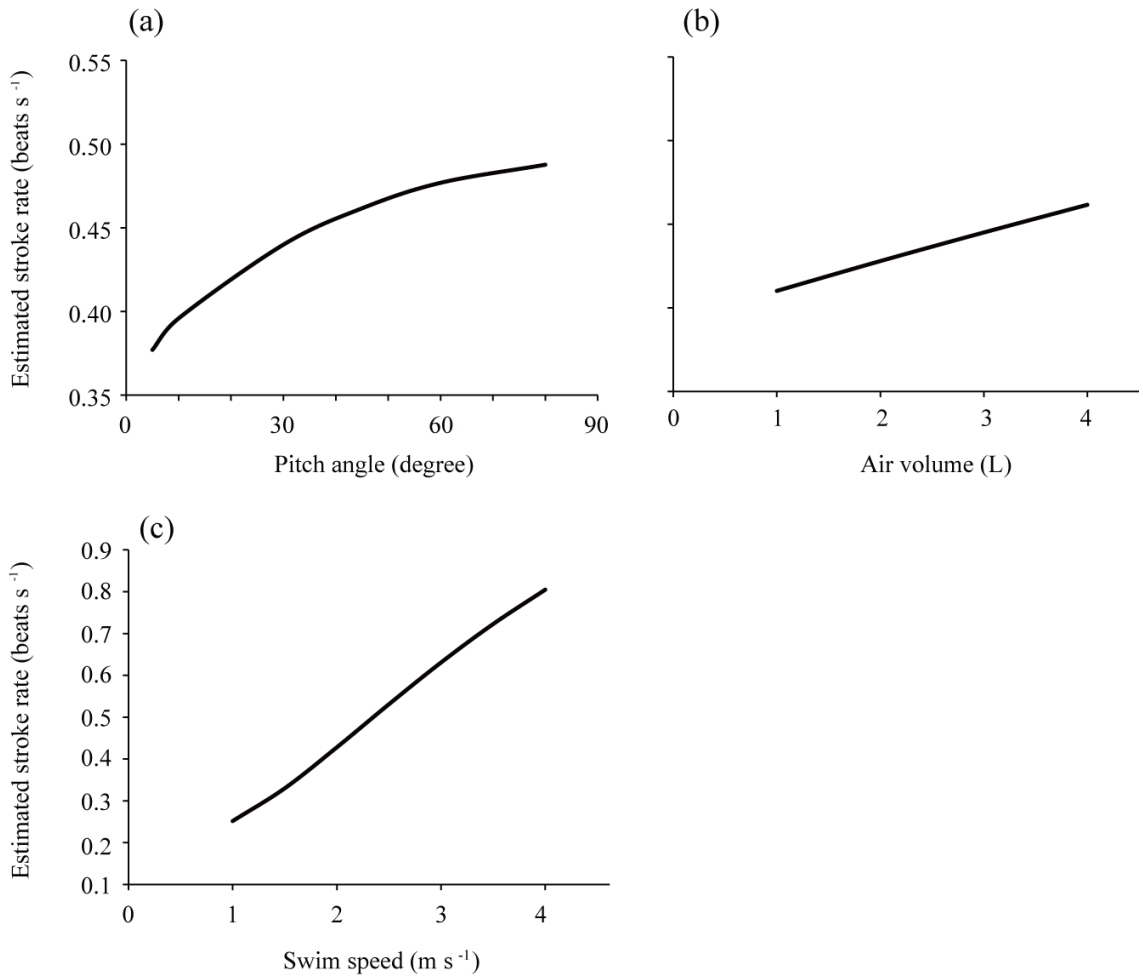

Fig. 2-12. Model calculation of stroke rates of emperor penguins, based on estimation of glide duration with (a) different pitch angles, (b) air volumes, and (c) swim speed. In (a), air volume is set as 4 L, in (b), pitch angle is set as 45 degree, and in (c), air volume is set as 2 L and pitch angle as 45 degree.

Chapter 3. Timing of the decision to start homing in streaked shearwaters

3-1. Background

Previous studies have reported that a variety of traveling animals from invertebrates to mammals arrive at their goal sites including nests and foraging areas within a narrow time window of the day, such as in the twilight hours (e.g. Davis et al. 1962, Hobson 1972, Rodway & Cooke 2001, Bijlsma & van den Brink 2005, Narendra et al. 2010). These temporal patterns require the ability to time movements between distant places accurately so as to reach destinations at the appropriate time, neither too late nor too early.

Some seabird species of the families Procellariidae and Alcidae have also been observed to return to their breeding colonies within a specific time window at the end of their foraging trips (e.g. Matthews 1953, Warham 1958, Miyazaki 1996). This has been interpreted as an adaptation for avoidance of predators or kleptoparasitism (Miyazaki 1996, Riou & Hamer 2008). On the other hand, their foraging areas often distributed over more than several hundred kilometers (e.g. Kato et al. 2003; Guilford et al. 2008; Thalmann et al. 2009), which means that homeward distances to the colony can vary to a large extent for each trip. The timing of arrivals over widely variable distances is conceivably a major challenge in breeding ecology, but so far no study has investigated it. This may be partly because behaviors after departure and before arrival are difficult to observe in highly mobile animals.

Miniaturized and lightweight GPS data loggers provide us with fine-scale movement paths of free-ranging animals, including flying seabirds (von Hünerbein et al. 2000, Steiner et al. 2000). GPS is a satellite-based navigation system. Twenty-five stationary US satellites are placed in four orbits around the Earth and send a particular signal. The position of a receiver is calculated based on measurements of the signal delay, i.e., the distance between the receiver and the satellites. Since the satellite positions are known, the receiver can calculate its position by solving a set of simultaneous equations. Three-dimensional positioning requires the solution of four equations with four unknowns: three spatial coordinates plus the clock bias (Sisak 1998). Since May 1, 2000, when selective availability—degradation of the GPS signal to prevent foreign military use— was turned off, the accuracy of the positions has increased (Steiner et al. 2000).

In the present study, GPS data loggers were deployed on streaked shearwaters (*Calonectris leucomelas*) breeding on islands in northern Japan to record their at-sea homing paths associated with arrival times. Although they perform foraging dives at sea, those are

shallow in depth and short in duration (Matsumoto 2008). Therefore, the lack of positional data while submergence seems negligible. Fine-scale movement data allowed to investigate the relationships between the timing of homing flights, homeward distance, travel speed, and arrival time at the colony.

3-2. Materials and methods

3-2-1. field experiments

Experiments were carried out during chick-rearing period of streaked shearwaters at breeding colonies on two islands (ca. 11 km apart; Fig. 3-1), Sanganjima Island (39°18'N, 141°59'E; September 2008; N = 11 birds; Table 3-1) and Funakoshi-Ohshima Island (39°24'N, 141°59'E; September 2009; N = 10 birds; Table 3-1), Japan. The study birds were caught by hand when present in their nest burrow. GPS loggers (TechnoSmArt, Guidonia Monteceilo, Italy) packed with heat-shrinking tube for waterproof (deployment mass ca. 25 g) were attached on birs' back feathers using waterproof tape (Tesa, Hamburg, Germany) and instant glue (Loctite, Henkel, Dusseldorf, USA) in the same manner as for penguins in Chapter 2. The mass of the loggers was 4.5% of the birds' body mass on average (range 3.8-5.3%; Table 3-1). Loggers were set to take one positional fix every 20 s or 1 min. About one week after the deployments, recapture of the birds for retrieving the loggers was started. There appeared to be no damage to their feathers from the attachments of the loggers. Experimental periods lasted 16 days and 3 weeks, respectively and no birds abandoned their chicks during the experiments. The procedures of the field study were approved by the Animal Experimental Committee of the University of Tokyo, and this work was conducted with permission from the Ministry of the Environment and Agency for Cultural Affairs, Japan.

3-2-2. definition of homing start

For analyses of the data obtained with GPS data loggers, MATLAB (Mathworks) software was used. All positional fixes were mapped using the Universal Transverse Mercator coordinate system. Horizontal ground speed was calculated from consecutive positional fixes. The frequency distribution of speeds was bimodal (Fig. 3-2), as has previously been found in other seabird species (Guilford et al. 2008, Weimerskirch et al. 2002, Zavalaga et al. 2010). The lower values were considered to relate to drifting on the sea surface, while higher values were interpreted as flight (Guilford et al. 2008, Weimerskirch et al. 2002, Zavalaga et al. 2010).

Because intermediate values are difficult to separate flight from drifting, a conservative value, 15 km h^{-1}, was used as the threshold of flight to reduce pseudo flights, based on the histogram (Fig. 3-2).

For each positional fix, distance to the island was calculated, and the rate of change in distance over the following one-hour period (i.e. average approach speed for the hour) was used to estimate the speed with which shearwaters approached their nesting colonies. The values were negative during outward journeys and positive during homeward ones. Considering the last phase, during which average approach speeds remained positive, the start of homing for each trip was defined as the first point when average approach speed was >15 km h^{-1} (for the criterion of horizontal ground speed relating to flight, see Fig. 3-2). Following this procedure, the homing start time (in hours relative to sunset) and the distance (km) from the island at that point were obtained (Fig. 3-3).

3-2-3. model fitting

Linear mixed models were used to estimate the associations between homing start distance, *D* and (i) homing start time, *T*, (ii) trip-end (arrival) time, (iii) mean flight speed during homing and (iv) percentage of flight time during homing. Although 'colony identity (and/or year)' was included as a random effect in the model, there was no significant improvement compared to the model without it. Therefore, only 'bird identity' was considered as a random effect in the present analysis. For model fitting, R 2.10 (R Development Core Team 2009) was used with the *lmer* function in R package *lme4* (Bates & Maechler 2009), and 95% confidence intervals and *P* values of each parameter were obtained from 100,000 Markov Chain Monte Carlo runs using the *pvals.fnc* function in R package *languageR* (Baayen 2009).

3-3. Results

According to movement paths obtained using GPS data loggers, streaked shearwaters (*N* = 21 birds) breeding on the two islands commuted between their nesting colonies and foraging areas at sea (Fig. 3-1), similar to most seabird species during their breeding seasons (Gaston 2004). During deployment of the loggers, they performed a total of 68 foraging trips lasting 0.6 to 7.8 days. The maximum distance from the colony during a trip (hereafter, 'trip range') varied between 17.6 and 526.9 km. None of the tagged birds spent time on the islands during daylight hours, and birds arrived at their nesting colonies mostly during several hours after sunset as

reported previously (Yoshida 1962) (Fig. 3-4a). Using this data set, I discussed their homing behaviors at sea to arrive within an appropriate daily time window despite substantial variation in their trip ranges.

Analysis of consecutive GPS locations during a trip indicated that birds initiated their homeward journeys at a well-defined point in time, from when the distance of positional fixes to the island started decreasing markedly (Fig. 3-3, see the section 3-2-2). In some short-range trips (<100 km), however, the changes in the distances to the birds' colony were continuously gentle or irregular, and the homing initiation was not well defined. The decision to start homing may be more flexible when returning over shorter distances because the time constraint is expected to be weaker than when returning from much more distant places. Although it cannot be elucidated at present, considering the purpose of the present study, that is, to investigate homing behaviors from distant places, the focus was placed on long-range trips (> 100 km, N = 26 trips by 17 birds), which all exhibited a distinctive homing phase. In these trips, the distance from the island (D) at the onset of homing varied from 96.6 to 457.2 km; note that the 'homing start distance' was not identical to, and less than, the trip range which was used when subsampling for homing analyses. 'Homing start time' (T) varied from 19.9 to 1.9 h before sunset and was strongly negatively correlated with D (Fig. 3-5a, Table 3-2). Thus, birds initiated homing earlier in the day when they were farther away from their nesting colonies: a linear mixed model estimated $T = -0.036D + 0.84$. In 69.2% of the >100 km trips, birds arrived at the colonies within 3 h after sunset (Fig. 3-4a) and arrival times did not correlate with the homing start distance D (Fig. 3-5c, Table 3-2).

The mean value ± s.d. of the flight speeds during homing was 34.7 ± 5.3 km h^{-1}. On the basis of the definition of flight, birds did not fly continuously to the islands from the homing start but sometimes landed on the water. The average percentage ± s.d. of flight time after the start of homing to trip end was 80.9% ± 11.5%. Neither the mean flight speed nor the percentage of time spent flying during homing correlated with the homing start distance D (Table 3-2).

3-4. Discussion

In the present study, streaked shearwaters were present at the colony exclusively at night. Comparison between histograms of trip end times and times of arrival within a 3 km radius of the islands indicated that diurnal colony attendance was strictly avoided. On some trips,

shearwaters arrived near the island before sunset (Fig. 3-4b), but they never entered the colony during daylight hours (Fig. 3-4a). This may reflect diurnal predator (such as raptor) avoidance on the island (Yoshida 1981).

For long-range trips, the wide-ranging homeward distance *D* seems to make it difficult to arrive at the island within a specific time window. Although one possible solution would be to change movement speeds according to travel distance, faster from the farther place, neither the flight speeds nor the percentage of flight time of the shearwaters correlated with the homeward distance (Table 3-2). Another solution can be to time the onset of the homeward journey by leaving earlier from farther locations, as observed in the present study. For birds flying at 34.7 km h^{-1} with a percentage of flight time of 80.9% (see the section 3-3), homeward travel time would increase by 0.036 h per km of travel distance. This expected value is identical to the absolute value of the slope of the empirical model for *T* against *D*, -0.036 (95% CI: -0.046 to -0.024). In the present data set, seven of 17 individuals performed more than one (two or three) long-range trips (>100 km) during deployment of the loggers. The data points from each bird, showed that individuals distinctly changed the homing start times depending on the distances (Fig. 3-5b). Thus, streaked shearwaters adjusted the onset of homing to the difference in the travel time, as expected from their flight performance. This temporal tuning strategy could maximize foraging time for each location and ensure an appropriate arrival time. Although why they preferred to arrive within several hours after sunset remained to elucidate, it may associate with their navigational mechanisms in addition to avoidance of diurnal predators. A previous study on Manx shearwaters suggested that shearwaters have to finish homeward journeys until around sunset because their navigation depends on diurnal cues such as sun (Matthews 1953). This may be the case also for streaked shearwaters and result in the concentration of arrival times at the beginning of night.

Anticipatory movements associated with arrival times have been well known mainly in seasonal migrants and intertidal foragers (e.g. Daan & Koene 1981, Hartnoll & Wright 1977). However, no study has investigated the quantitative relationship between travel distances, movement speeds, and timing of the movements associated with arrival times. Additionally, in most of those studies, animals did not need to adjust the onset of the movement on each trip because the distances between departure and arrival sites were mostly fixed. This study of streaked shearwaters is, to my knowledge, the first to show the temporal tuning of movements to travel time to achieve arrivals within a specific time window. It was clearly demonstrated that the requirement for constant arrival times at home sites affected the at-sea decision about when

to leave. Although what mechanism(s) underlie(s) the observed tuning behavior is still an open question, departure was timed as if they knew the travel time from the foraging areas to the island and the time of day. They may have learned what time they should start homing trips from each foraging area in previous trips or indeed recognized the required time to the islands from travel time during the outward journey and/or distance from the island obtained by path integration or an internal map sense, which are also possible mechanisms for navigation (Wiltschko & Wiltschko 2003). The strong correlation between *T* and *D* and the striking agreement of expected and empirical relationships imply that tuning the onset of homing is an ecologically important biological phenomenon. This kind of timing ability may be found in other animal species from phylogenetically diverse taxa achieving punctual homing.

Table 3-1. Basic information of experimental birds.

ID	Field	Sex	Body mass (g)	Proportion of logger mass to body mass (%)
S1	Sanganjima	female	473	5.29
S2	Sanganjima	female	485	5.15
S3	Sanganjima	male	650	3.85
S4	Sanganjima	male	639	3.91
S5	Sanganjima	female	581	4.30
S6	Sanganjima	male	592	4.22
S7	Sanganjima	male	538	4.65
S8	Sanganjima	male	558	4.48
S9	Sanganjima	female	533	4.69
S10	Sanganjima	female	520	4.81
S11	Sanganjima	male	550	4.55
T1	Funakoshi-Oshima	female	580	4.31
T2	Funakoshi-Oshima	female	510	4.90
T3	Funakoshi-Oshima	male	640	3.91
T4	Funakoshi-Oshima	female	635	3.94
T5	Funakoshi-Oshima	male	625	4.00
T6	Funakoshi-Oshima	female	635	3.94
T7	Funakoshi-Oshima	unknown	555	4.50
T8	Funakoshi-Oshima	female	565	4.42
T9	Funakoshi-Oshima	male	665	3.76
T10	Funakoshi-Oshima	male	585	4.27
			mean	4.37
			s.d.	0.44

* Sex was determined with voice: calls of males are high pitched, whereas those of females are low pitched (Arima & Sugawa 2004).

Table 3-2. Results of fitting of linear mixed models for shearwaters' homing behavior. AIC of the models with, and without, a fixed effect of homing start distance are compared to detect the effect of homing start distance on each dependent variable. For all the dependent variables, except for homing start time, the 95% CI of the estimated slope included zero.

	Fixed effect					
	None		'Homing start distance'			
				95% CI for a slope		
Dependent variables	AIC		AIC	Lower	Upper	*P* value
Homing start time	156.1	>	138.8	-0.0461	-0.0242	<0.0001
Average flight speed during homing	163.7	<	169.4	-0.0006	0.0396	0.062
Proportion of flight time during homing	-27.7	<	-11.1	-0.0004	0.0006	0.64
Arrival time	106.4	<	118	-0.007	0.0067	0.96

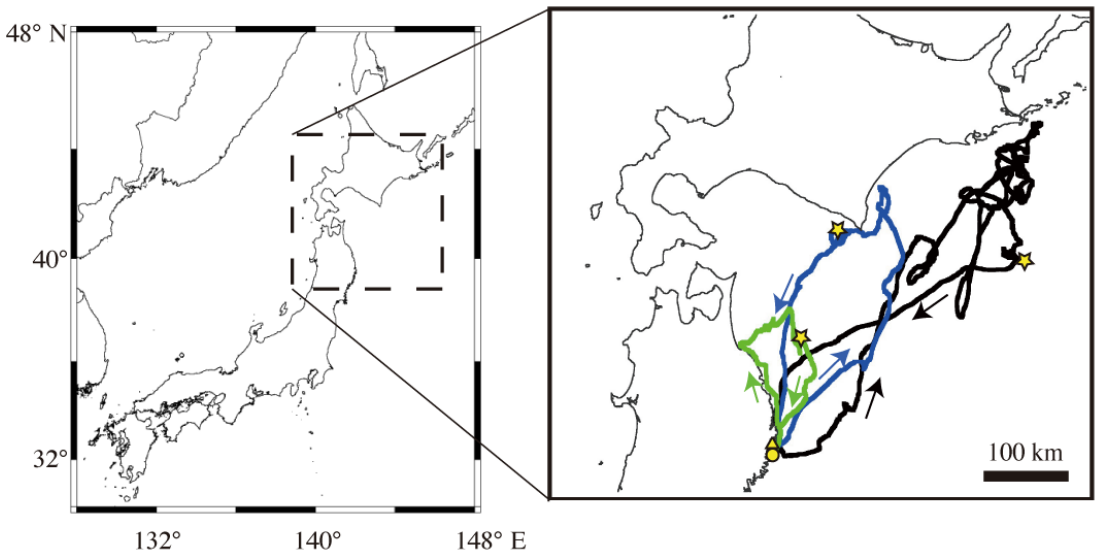

Fig. 3-1. Three examples of tracks of shearwaters recorded by GPS loggers. The maximum distance from the colony during the respective foraging trips was 179.7 km (green), 360.7 km (blue) and 526.9 km (black; these are the same trips as shown in Fig. 3-3). Arrows indicate travel directions, and a yellow circle and triangle show the positions of the breeding colonies on Sanganjima and Funakoshi-Ohshima Islands, respectively. Yellow stars show the homing start point for each trip.

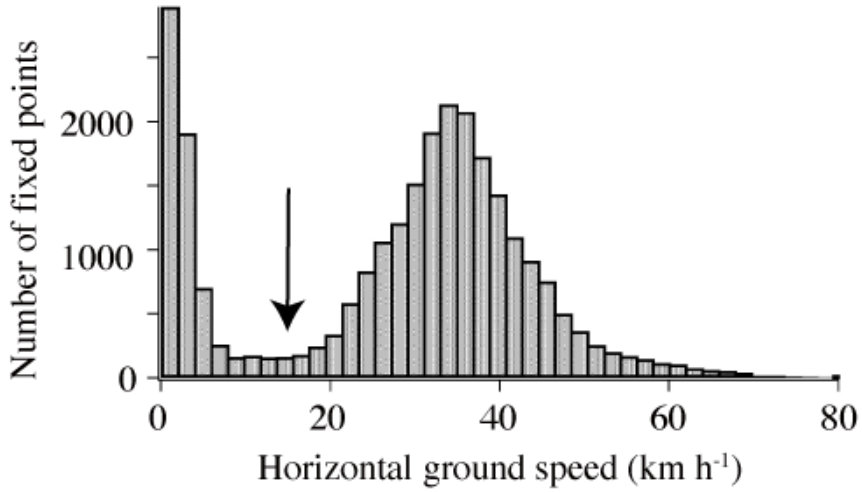

Fig. 3-2. Histogram of horizontal ground speeds during homing of shearwaters. Data are pooled for the homing phases of all analysed foraging trips (*N* = 26 trips by 17 birds). The black arrow indicates the cut-off value of 15 km h^{-1}, which was used for the threshold of 'flight'.

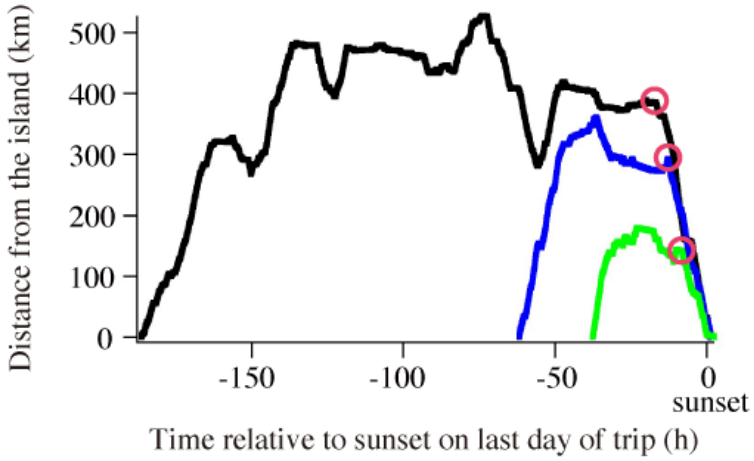

Fig. 3-3. Time-series data of the distance from the island during three sample foraging trips (cf. Fig. 3-1). Red circles indicate homing start points determined with approaching speed to the island.

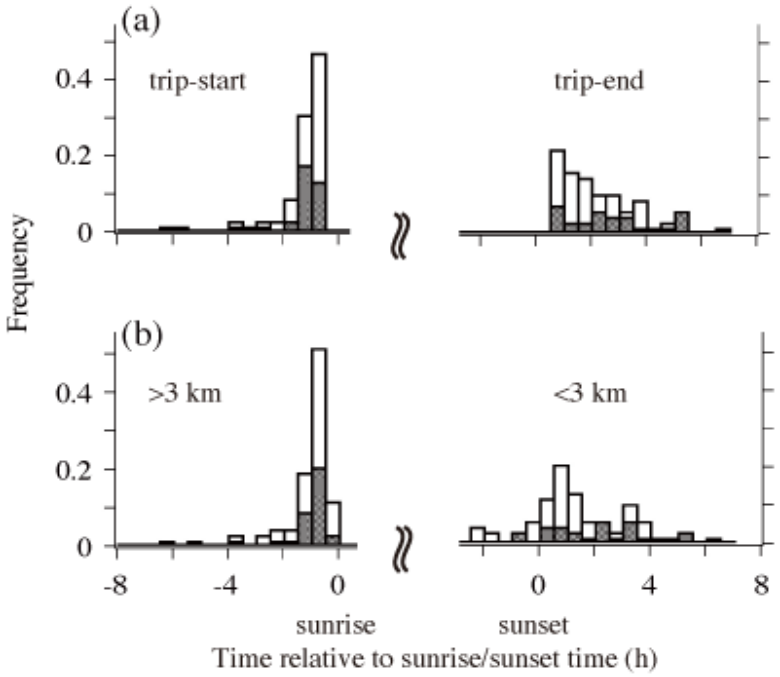

Fig. 3-4. Histograms of times of departure from and arrival at the shearwaters' nesting islands (*N* = 68 trips by 21 birds). (a) Trip start and end times and (b) times when exiting and entering a 3 km radius from the islands. Times are presented relative to sunrise and sunset, respectively. White bars indicate short-range (<100 km) trips, grey ones long-range (>100 km) trips.

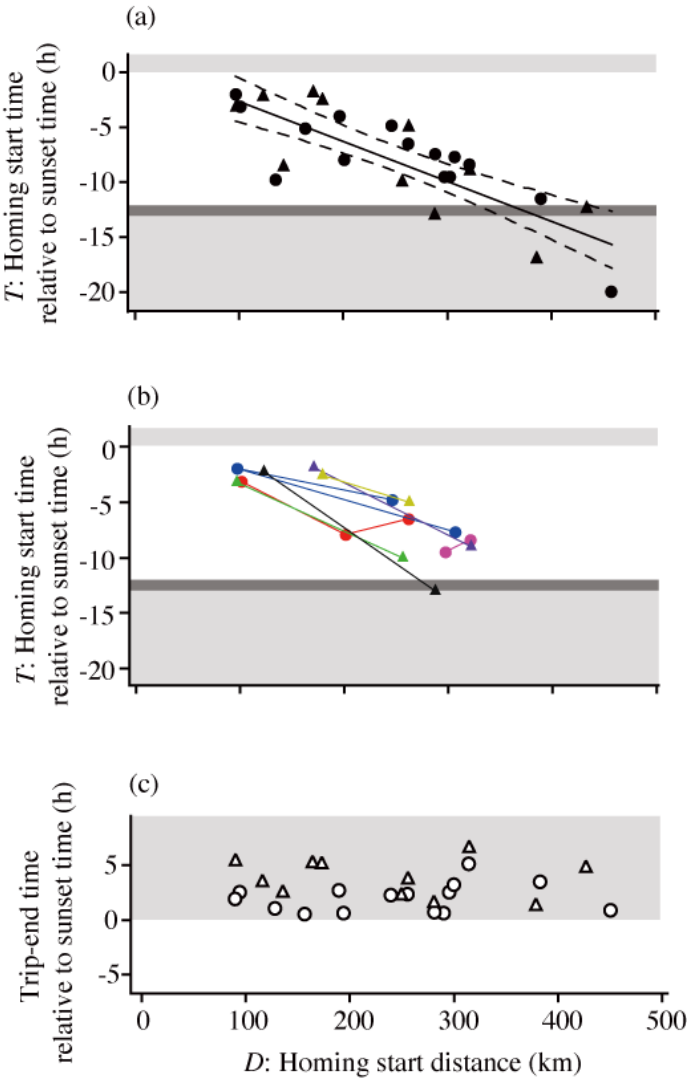

Fig. 3-5. Results of the analysis of homing start and arrival time in relation with distance at the start of homing (N = 26 trips by 17 birds). (a, b) Relationships between homing start time, T, and homing start distance, D, and (c) between trip end time and D (circle: Sanganjima birds; triangle: Funakoshi-Ohshima birds). The solid line in (a) is a best fit estimated by a linear mixed model, with the dashed lines giving 95% confidence intervals. For (b) I used the data points of individuals performing more than one trip during deployment of the loggers (N = 16 trips by seven birds). The data from each bird are shown in the same colour and are connected with lines. Light-grey zones indicate night, and the dark-grey zones represent the range of sunrise time (dependent on date).

Chapter 4. General discussion

Central place foraging is performed by many species from diverse taxa, ranging from invertebrates to primates, and is thus considered primitive behavior in the animal kingdom. This thesis investigated the timing to start returning for two model species of central place foragers—diving emperor penguins and flying streaked shearwaters—by analyzing fine-scale movement data collected during their trips. The decision could be a fundamental part of central place foraging because it affects their physiological condition, arrival times at the central place, and foraging efficiency. In this final chapter, the methods to obtain fine-scale movement data of diving and flying animals are compared, and the properties of the paths obtained with each method are presented. Next, the moving speeds in fluid are examined because this is one of the main parameters characterizing animal movements. Insights into the decision time to return by seabirds are summarized based on a comparison of the results for the penguin and shearwater studies. Future perspectives on this line of research are also presented.

4-1. Methodology

Irrespective of whether the subject species is aquatic or terrestrial, it is impossible for us to follow free-ranging animals for a long period and record their movements accurately and continuously. This limited the investigation of the behavior of wide-ranging central place foragers after departure and before arrival; thus far, the timing of their movements has only been described for their departure and arrival as observed at the central place. The novel bio-logging technique allows us to "observe" the undisturbed movements of those animals remotely (Naito 2004, Rutz & Hays 2009). In the present study, the fine-scale movement data of penguins and shearwaters were analyzed to find rules for the timing of their decision to return to the central places, which has never been examined before. Although the present results indicate the usefulness of the data obtained with animal-borne loggers, there are still some constraints to recording the movements of free-ranging animals. The dive paths of emperor penguins were reconstructed by the dead-reckoning method, where locomotion vectors relative to the water were added in chorological order (Fig. 4-1a), and flight paths of streaked shearwaters were constructed by connecting consecutive positional fixes recorded by GPS loggers (Fig. 4-1b). Here, the opposite characteristics of the two methods to reconstruct the movement paths from locomotion vectors and positional fixes are discussed.

4-1-1. dive paths

For diving animals, records of vertical movements, i.e. dive depth, have been available using pressure sensors since the beginning of bio-logging science (DeVries & Wohlschlag 1964, Kooyman 1966, Kooyman 1968). Nowadays, we can obtain the depth profile at spatial and temporal scales of centimeters and seconds, respectively. In contrast, the reconstruction of horizontal movements and consequently the 3-D dive paths underwater had been difficult until recently, especially for wide-ranging animals. As diving animals move and forage in 3-D environments, investigations of their movements in 3-D should be helpful to better understand their behavioral ecology and the physiology of diving.

Currently, there are two methods for reconstructing the 3-D movements of aquatic animals (Wilson et al. 2007): acoustic telemetry (Lagardère et al. 1990, Hindell et al. 2002) and dead-reckoning (Wilson & Wilson 1988). Acoustic telemetry necessitates that receivers are within a few hundred meters of the animal to be tracked; hence, data on fast and wide-ranging species are difficult to obtain with this method (Wilson et al. 2007). The dead-reckoning technique used in the penguin study overcomes this problem; it requires data on speed, heading, and change in depth (or pitch angle), with which the locomotion vectors per measurement interval are calculated. By integrating those vectors, 3-D movements of the animals can be reconstructed. With data sets sampled at the second scale, temporally finely resolved, dive paths can be obtained without the constraint of the measuring range.

In the penguin study in Chapter 2, three-dimensional (3-D) movements of emperor penguins were reconstructed by dead-reckoning to deepen the understanding of their decision rule to return to the surface. The study was the first to report fine-scale dive paths for avian divers. Their foraging trips range up to several hundred kilometers from their breeding colonies (Ancel et al. 1992), although one dive is performed within several hundred meters from the starting point of the dive. Therefore, dead-reckoning is helpful to investigate their underwater movements and the decision to return to the surface.

However, in dead-reckoning, errors accumulate in positional fixes over time due to the lack of reference when estimating the absolute positions relative to the ground (Mitani et al. 2003, Wilson et al. 2007; Fig. 4-1a). Error accumulation due to ocean current drift and data processing artifacts occurred in the estimated dive paths of emperor penguins (see Appendix 1). This situation when acquiring the movement paths of aquatic animals is different from that for terrestrial animals, for which the positions at each time instant can be recorded by GPS loggers with high accuracy. Nevertheless, when investigating decisions made during animal movements,

movement paths excluding passive transports by fluids (water and air) may be more helpful because they can purely present the body's locomotion. In the penguin study, the decision time of emperor penguins was defined as the moment when the birds changed their heading to go toward the surface, which is likely to be clearly shown in the path obtained by dead-reckoning. Additionally, when considering the cost of traveling, moving speeds relative to water are more important than those relative to the ground for calculation of the energy required for swimming.

4-1-2. flight paths

Horizontal movement paths of animals including volant birds can be reconstructed from positional data obtained by geolocation, satellite telemetry, and global positioning system (GPS). There are trade-offs of the spatiotemporal scales and accuracy of positional data, costs of the devices and running costs, and volume and weight of the devices. GPS data loggers, which provide most accurate positional data (error < ±2.5 m for the GPS logger made by TechnoSmArt, Italy), have made it possible to know in detail how animals get to a specific place after departure from another place.

Animal-borne GPS loggers do not have a long history: after global full-time coverage for GPS was achieved in 1993 (Sisak 1998), GPS units were developed and deployed on some terrestrial and aquatic species (e.g. Sisak 1998, Schofield 2007). In the early period, the use of GPS loggers had been limited to only relatively large animals because of its volume and mass (e.g. several kilogram for marine mammals). Especially for flying birds, the effect of additional mass could be serious (e.g. Passos et al. 2010) because they have evolved as light as possible within physical and physiological constraints to adapt to flight behaviors. However, since von Hünerbein et al. (2000) and Steiner et al. (2000) developed a miniaturized one (total mass of around 30 g) for pigeon, the size and weight were rapidly becoming smaller and lighter. Now, the lightest GPS is less than 10 g, which can be deployed small mammals and flying birds (Wikelski et al. 2007). Because there are no obstacles to interrupt satellite signals in pelagic zones, the flight paths of seabirds during foraging trips can be recorded with excellent quality.

Considering that animals move interactively with their environments (e.g., topographical features, physical conditions) and probably update their courses according to the information (Nathan et al. 2008), data on where they passed through are very useful to investigate the mechanisms of animal movements. However, when we are interested in what direction they intend to move in and the energy cost of traveling, movement paths obtained from GPS loggers should be interpreted carefully. Movements of air or water can change the

moving directions and speeds of animals in the fluid, and we get the positional data from GPS loggers as the sum of the animal and fluid movements (Fig. 4-1b). This is also the case for other positional systems that estimate absolute positions, such as satellite telemetry. One of the major purposes of obtaining time-series positional fixes of animals is to investigate their orientation and navigation mechanisms. In those studies, the directions that individuals head toward are especially important; therefore, we need to take both movements of animals and fluids into account when analyzing tracks. For example, Girard et al. (2006) considered ocean currents as a factor that causes drift in the movements of sea turtles tracked by satellite telemetry. After examining the turtles' orientation ability, they concluded that the turtles could not compensate for the deflecting actions of ocean currents.

In our study on shearwaters, birds appeared to experience wind drift during homing (see Appendix 2). The differences between moving vectors relative to the ground obtained from GPS loggers and those relative to the air after considering wind drift are unlikely to affect the analysis results for the timing to start homing because relative changes in the approaching speeds to the nesting islands were used as indices to determine the onset of homeward flights. However, the differences may be a limitation when discussing flight speeds in terms of energy efficiency of movements (see below) and orientation strategies.

4-1-3. future perspective about record of movement paths

Dead-reckoning can reconstruct movements faithful to animals' body orientations, and positional data obtained from GPS loggers can be used to investigate the interactions between animal movements and environmental conditions. Applying both methods to the same individuals, which can reveal movements relative to both the fluid and the ground, may be a significant step toward a comprehensive understanding of their decisions in terms of moving directions and speeds when traveling. Because the spatial and temporal scales of ocean current and wind data provided by satellite systems are sparse compared to the movement data from the animal-borne data loggers, it is difficult to estimate the effect of drift on movements using those data sets. Then, deployment of two types of devices, which allow reconstructing movement paths by both dead-reckoning and connecting absolute positions, may be plausible. Although absolute positional data cannot be obtained underwater, the positional information at the surface as obtained from a GPS logger can be used to compensate for errors that accumulate during positional estimation by dead-reckoning (Wilson et al. 2007, Matsumura et al. 2011). The combination of dead-reckoning and GPS can help reveal more about the animals' orientation

strategies and the energy aspect of their movements in fluids.

4-2. Moving speeds

The histograms of the swimming and flight speeds showed peaks for both the penguins and shearwaters, and the moving speeds seemed to be constrained to a specific range for each species. This common feature of movements underwater and in the air is discussed here from a physical aspect using biomechanical models.

4-2-1. swimming speeds

Recently, Sato et al. (2010) suggested a biomechanical model to estimate the swim speed that minimizes the cost of transport. The model incorporates work against mechanical forces (drag and buoyancy), the pitch angle, and the metabolic rate of diving penguins. The cost of transport during diving consists of the mechanical cost and basal metabolic cost. The former can be estimated by integrating the sum of the drag and buoyancy parallel to the swimming direction; the latter is the product of the basal metabolic rate and time. While drag increases with the square of speed, the time to travel a given distance inversely decreases; therefore, there is a tradeoff in swimming speed between the mechanical and basal metabolic costs.

Sato et al. (2010) calculated the most energy-efficient speed assuming that a penguin aims to reach a given depth; however, as shown in Chapter 2, emperor penguins swim not only vertically but also horizontally. Therefore, their model was slightly modified for this study to deal with the case where a penguin travels a given 3-D distance irrespective of whether it is vertically or horizontally. However, the main results of the model estimation were not affected by these changes.

Assuming that the swim speed and pitch angle of a penguin remain constant, the relationship of the thrust T, drag D, and buoyancy B is

$$T\cos(\alpha - \beta) = D - (B - mg)\sin\beta \qquad (4\text{-}1)$$

where α is the angle of thrust, β is the pitch angle of the swimming direction relative to the horizontal plane, m is the body mass (kg), and g is the gravitational acceleration (= 9.8 m s^{-2}) (Fig. 4-2). The cost to travel a unit distance C_t (J m^{-1}) is described as:

$$C_t = T\cos(\alpha - \beta) \qquad (4\text{-}2)$$

From equations (4-1) and (4-2), the following equation is obtained:

$$C_t = D - (B - mg)\sin\beta \qquad (4\text{-}3)$$

The required energy E_t (J) to travel a distance I (m) is calculated by integrating the cost per unit distance C_t:

$$E_t = \int_0^I \{D - (B - mg)\sin\beta\} di \qquad (4\text{-}4)$$

where i is the current traveled distance (m). Thus, E_t is determined by the drag (D), buoyancy (B-mg), and pitch angle (β). The drag and buoyancy are

$$D = \frac{1}{2}\rho_w \lambda C_d S U^2 \qquad (4\text{-}5)$$

$$B - mg = \{(\frac{m}{\rho_t} + \frac{A_0}{i\sin|\beta|/10 + 1})\rho_w - m\}g \qquad (4\text{-}6)$$

where ρ_w is the density of seawater (1027 kg m^{-3}), λ is the ratio of the drag of an active swimmer to that of a passive object (Hind & Gurney 1997), C_d is the drag coefficient, S is the wetted surface area (m^2), U is the swimming speed (m s^{-1}), ρ_t is the density of the penguin body tissue (1020 kg m^{-3}; Wilson et al. 1992), and A_0 is the air volume in the body at sea surface. From equations (4-4), (4-5), and (4-6),

$$E_t = 10A_0\rho_w g(\ln|\frac{I\sin|\beta|}{10} + 1|) + \{\frac{\rho_w \lambda C_d S U^2}{2} - (\frac{\rho_w}{\rho_t} - 1)mg\sin\beta\}I \qquad (4\text{-}7)$$

The basal metabolic cost M_t (J) is the product of the basal metabolic rate M_b (J s^{-1}) and time (s) taken to travel a given distance:

$$M_t = M_b \frac{I}{U} \qquad (4\text{-}8)$$

M_b was obtained from an allometric relationship for avian groups (McKechnie et al. 2006):

$$M_b = 3.65 m^{0.744} \qquad (4\text{-}9)$$

The energy invested for muscle contractions is partly lost through translation into thrust. Therefore, the actual mechanical energy required to generate thrust is considered to be $E_t/(\varepsilon_p \varepsilon_A)$, where ε_A presents the efficiency with which chemical energy is translated into muscle work and ε_p is the propeller efficiency with which muscular movements are translated into thrust. The total energetic cost E to travel a distance I is

$$\frac{E_t}{\varepsilon_p \varepsilon_A} + M_t = \frac{10 A_0 \rho_w g}{\varepsilon_p \varepsilon_A} (\ln | \frac{I \sin | \beta |}{10} + 1 |) + \{ \frac{\rho_w \lambda C_d S U^2}{2} - (\frac{\rho_w}{\rho_t} - 1) mg \sin \beta \} \frac{I}{\varepsilon_p \varepsilon_A} + \frac{M_b I}{U} \qquad (4\text{-}10)$$

By substituting assumed values into each parameter of equation (4-10) as shown in Table 4-1, the relationship between the swim speed U and the total cost of transport E is obtained (Fig. 4-3a). At the swim speed U_{opt} that minimizes the cost of transport, $\frac{dE}{dU} = 0$. From the equation (4-10),

$$\frac{d(E_t / \varepsilon_A \varepsilon_p + M_t)}{dU} = \frac{\rho_w \lambda C_d S I}{\varepsilon_A \varepsilon_p} U - M_b I U = 0 \qquad (4\text{-}11)$$

Then, U_{opt} is presented as

$$U_{opt} = (M_b \varepsilon_p \varepsilon_A / \rho_w \lambda C_d S)^{1/3} \qquad (4\text{-}12)$$

As estimated by the previous model (Sato et al. 2010), U_{opt} is 1.8 m s^{-1} for emperor penguins.

According to equation (4-11), the optimal swim speed is independent of the traveled distance *I*. Although some theoretical models have indicated that swim speeds should be changed depending on the situation such as the prey patch condition and dive depth (e.g., Thompson et al. 1993), the cost of transport is also considered to be a basic constraint in those models. The empirical values for the swim speed of emperor penguins (1.0-3.2 m s^{-1}) appear to be consistent with the range of estimated speeds to achieve a low cost of transport (Fig. 4-3a). Although the biomechanical model above only considers swim speeds during descent for a given distance, penguins seem to avoid changing swim speeds, largely due to energy efficiency.

4-2-2. flight speeds

Theoretical models to estimate energy-efficient air speeds have also been suggested for avian flight. The aerodynamic power P_{aero} required for forward flight has been modeled in several ways (e.g., Norberg 1990, Pennycuick 2008). The general prediction common to all the models is that P_{aero} should vary with flight air speed according to a U-shaped curve (Tobalske 2007). As performed in a previous study on flight speeds of cormorants (Watanabe et al. 2011), the cost of flight was estimated for streaked shearwaters, based on the Pennycuick (2008) and Norberg (1990) models. These models estimate the cost of traveling for a unit of time; they were modified to calculate the speed to minimize the cost of traveling a given distance. The estimated flight speeds with the minimum cost of transport were compared with the empirical data.

The power P_{aero} is the sum of induced power P_{ind} to produce lift, parasite power P_{par} to overcome drag on the body, and profile power P_{pro} to overcome drag on the wings:

$$P_{aero} = P_{ind} + P_{pro} + P_{par} \quad (4\text{-}13)$$

Each component—i.e. P_{ind}, $P_{pro,}$ and P_{par}—is described as below. The only difference between the Pennycuick and Norberg models is the equation to estimate the profile power P_{pro}; the latter assumes that it depends on speeds, while the former does not.

$$P_{ind} = 2km^2g^2 / U\pi L_w^2\rho_a \quad (4\text{-}14)$$

$$P_{par} = \frac{1}{2}\rho_a S_b C_d U^3 \quad (4\text{-}15)$$

$$\begin{cases} P_{pro} = (4km^2g^2/3\pi L_w^2\rho_a^2 S_b C_d)^{1/4} C_{pro} S_w / L_w^2 & \text{for Pennycuick model} \quad (4\text{-}16) \\ P_{pro} = \frac{1}{2}\rho_a S_w C'_{pro} U^3 & \text{for Norberg model} \quad (4\text{-}17) \end{cases}$$

where k is the induced power factor, m is the body mass, g is gravitational acceleration, U is the flight air speed, L_w is the wingspan, ρ_a is the air density, S_b is the frontal area of the body, C_d is the body drag coefficient, C_{pro} is the profile power coefficient for Pennycuick model, S_w is the wing area, and C'_{pro} is the profile power coefficient for the Norberg model. Then, the total metabolic cost of flight M at a given flight speed is obtained as

$$M = R(P_{aero}/\varepsilon + M_b) \quad (4\text{-}18)$$

where R is the respiration factor, M_b is the basal metabolic rate, and ε is the efficiency of converting metabolic power into mechanical power. While P_{ind} decreases with flight speed, P_{par} in both models and P_{par} in the Norberg model increase. The tradeoff results in the U-shape curve of power required for flight over a range of air speeds (Fig. 4-3b). This relationship has been supported by the measurement of the mass-specific power of pectoralis muscles in doves, cockatiels, and magpies and the oxygen consumption in cockatiels (index of metabolic power output) over a range of flight speeds; all of these were also U-shaped (Tobalske 2003, Bundle et al. 2007). Based on the models, the energy cost E to travel a given distance I with flight speed U can be calculated as

$$E = \frac{MI}{U} \quad (4\text{-}19)$$

By setting the parameters for streaked shearwaters to be those given in Table 4-2, the speed minimizing E, which is called the maximum range flight speed U_{mr}, is estimated to be 22.0 and 10.3 m s^{-1} by the Pennycuick and Norberg models, respectively (Fig. 4-3b).

Guilford et al. (2008) reported that in Manx shearwaters, a related species of streaked shearwater, the ground speeds during flight are distributed close to the U_{mr} obtained from the Pennycuick model. In the present study, the empirical average ground speed in each

homeward flight of streaked shearwaters was 9.6 ± 1.5 m s^{-1} (mean ± s.d., N = 26 trips by 17 birds; Fig. 4-3b), which is close to the U_{mr} estimated by the Norberg model while being much less than the value estimated by the Pennycuick model. At present, the model, which is more plausible, is unknown, but the U-shaped models implies that the flight speeds of the shearwaters may be constrained to a narrow range for cost-efficient traveling.

It should be noted that the ground speeds are affected by wind drift and differ from air speed, which is the parameter considered in the biomechanical models presented above. When using air speeds calculated for the shearwaters with wind data obtained from satellites (see Appendix 2), the peak of the histogram shifts to a slightly larger value (Fig. 4-3c), although the spatiotemporal resolution of the wind data was insufficient to discuss the obtained air speeds in detail. Watanabe et al. (2011) were the first to report the air speeds of flying birds directly measured by an external propeller and discussed their moving speeds in terms of energy cost for flight. In future studies, the air speeds of shearwaters should also be measured. In addition, streaked shearwaters, which have wings with a high aspect ratio, not only flap their wings while flying but also continuously soar in the air, as do other species in Procellariiformes (Sato et al. 2009). Optimal flight speeds for the flap-gliding mode have not yet been modeled (Videler 2005). Despite the present imperfect data, it can be assumed that shearwaters have probably not evolved to adjust moving speeds for various ranges of traveling distances because one component—air speed—is highly likely to be constrained by mechanical and physiological factors, and the other—wind speed—cannot be controlled.

4-3. Decision time of seabirds to return

4-3-1. results from the two model species

To achieve energy-efficient movements in relation to the mechanical cost and basal metabolic cost, the species appeared to keep their moving speeds in fluids at a moderate level. Therefore, it seems unrealistic for them to drastically change swimming and flying speeds according to the situation. Given this prediction, the importance of the timing to start moving becomes increasingly evident to be at the right place at the right time.

In both emperor penguins and streaked shearwaters, a variation was found in the onset time of returning to their central places—in emperor penguins, the decision times strongly varied for a given dive depth (Fig. 2-6a); in the shearwater study, a difference of several hours was found in the timing to start homeward flights from similar distances (Fig.

4-4a). If we assume that animals always make the appropriate decision for each situation, the empirical variations in the decision time indicate variable conditions—physical, physiological, and ecological—that they experienced in the wild. For example, weather, foraging success, and interactions with conspecific individuals may alter the optimal time to move and/or the performance of their timing ability. Thus, simultaneous and sometimes conflicting requirements may affect their decision-making.

Even in the apparently complicated situations, however, some tendencies in the timing to start returning to the central place were found for each species. These are likely to reflect internal and/or external factors that dominate others. Streaked shearwaters adjusted the onset time of homeward flights to the distance to their breeding islands by leaving earlier from the further place (Fig. 4-4a). This pattern of movements appeared to anticipate the inward travel time to arrive at the island within the appropriate time of day. This flexible timing ability probably resulted from a combination of the adaptations to dynamic prey distributions at sea, which forces them to travel variable distances in each trip, and the narrow time window available for arrival at the colony, which may be due to the presence of diurnal predators and their poor navigational ability at night. Thus, for the shearwaters, ecological and cognitive factors appear to dominate their timing of the decision to return. The combination of wide-ranging foraging areas and narrow time window for arrivals is not unique to streaked shearwaters, but has also been observed for some other seabirds. And species from diverse taxa arrive punctually at their central places. Therefore, the timing ability found in streaked shearwaters may be shared among a variety of species.

In the penguin study, the upper limit of the time to start returning to the surface did not correlate to the distance from the surface and was inversely proportional to the stroke rate (Fig. 4-4b). In other words, muscle workload appeared to be responsible for their decision time limit to return. Unlike shearwaters, in dives at the upper boundaries, the penguins' decision to return seemed reactive rather than anticipatory. In breath-holding divers, there must be strong selective pressure to not mistime the return to the surface by leaving the depth too late because failure directly leads to death by asphyxia. It appears reasonable for emperor penguins to have a decision rule associated with their physiological capacity. However, most studies on penguins diving in open water have reported that the dive duration is generally proportional to the dive depth (e.g., Sato et al. 2004), and a relatively asymptotic distribution like that of emperor penguins has only been found in Adélie penguins diving under the sea ice (Watanuki et al. 1997). This fact suggests the possibility that not only the need to breath at the surface but

also the sea ice, which can prevent them from surfacing, can affect the asymptotic upper limit of the decision time to return in relation to the distance.

Emperor penguins and streaked shearwaters range widely underwater and over the sea, respectively, and movements between their foraging areas and central place (i.e., water surface and breeding colony) for each dive and trip are highly variable. The flexible behaviors greatly contributed to the present findings on the decision rule for the onset of returning to the central place; while moving speeds were kept relatively constant, timing was adjusted according to internal and/or external conditions. If the birds used specific areas, i.e., movement patterns were relatively constant, it would be difficult to detect the dominant factors in the wild and the abilities of animals that could meet several different requirements at the same time. In addition, by using the two species in largely different situations—i.e., diving and flight— that return to a central place to breathe and to feed their chicks, this study revealed that different types of factors can affect the timing of movements. As a general condition of central place foraging, there is a tradeoff between continuing to forage and returning to the central place. Additionally, ecological and cognitive factors appear to affect the timing of homeward trips in shearwaters, while the physiological capacity and physical environment affect the onset of returning to the water surface in dives of emperor penguins. Their anticipatory or reactive timing mechanisms likely evolved under a combination of these constraints.

4-3-2. future studies

In both studies on diving and flying seabirds, internal mechanisms associated with their decision to return and why they present such timing behaviors still need to be clarified, although some hypotheses have been suggested. For the penguins, physiological measurements such as oxygen depletion in the muscle and blood with recording of the animal movements may help uncover the proximate mechanisms responsible for the timing behaviors found in this study. For the shearwaters, experiments during seasons when the sun set at different times from those in the present study and experimental approaches involving translocation experiments and circadian clock resetting will be required to clarify the mechanisms involved with the timing of homeward journeys. For both penguins and shearwaters, comparative analyses with species presenting similar and/or different behavioral characteristics should also be helpful to determine the ultimate mechanisms of timing behaviors.

In this thesis, the focus was mainly on the timing of the onset of seabirds' returning journeys as a temporal aspect, and only a one-dimensional spatial parameter (i.e.,

distance) was used. Fine-scale movement data can provide more spatial information on the birds' movements, and sophisticated spatial analyses of movement paths have been performed in studies on foraging and homing behaviors as separate subjects (e.g., Bonadonna et al. 2005, Weimerskirch et al. 2007, Bailleul et al. 2010). Considering that when and how to arrive at the goal sites can be determined by the timing of the onset of movements, moving speeds, and navigational capacities and that the timing of movements can be affected by preceding behaviors such as the outward journeys and foraging, more comprehensive analyses of both temporal and spatial data may help in understanding the birds' decision rules related to their movements.

4-4. Concluding remarks

Since the dawn of ethology, many insights into the decision rules of wild or captive animals have been obtained by carefully observing their behaviors and investigating which conditions trigger changes in behavior and what constraints exist (McFarland 1977). "Observing" the fine-scale movement data recorded by animal-attached loggers makes it possible to access animals' decision-making in the wild, which we cannot see directly. Investigating the movements in space and time as a consequence of the animals' decision process can be a powerful approach to revealing the manner in which animals interact with their internal and external environments and the parameters that are significant for their life. To the best of my knowledge, the studies presented in this thesis are the first reports on the flexible timing of the decision by central place foragers to return to their central. Novel analyses of fine-scale movement data indicated that seabirds timed their inward movements to solve variable constraints in addition to the tradeoff between foraging and returning. The decision rules on when to return were presented by free-ranging seabirds, even though the internal and external conditions can vary for each trip under natural conditions. The timing ability for the onset of return is thus expected to be the key to central place foraging. Mistiming may lead to fatal effects, and the timing behavior has a great significance to the birds' survival. I believe that the present studies can be the beginning of growth in research on the timing of decision-making by free-ranging wild animals.

Table 4-1. List of parameters used in the model to estimate swim speed minimizing cost of traveling.

symbol	parameter	value (unit)	citation
A_0	air volume in the body at the water surface	0.004 (m^3)	
ρ_w	density of water	1027 (kg m^{-3})	
g	gravitational acceleration	9.8 (m s^{-2})	
I	traveled distance	500 (m)	
β	pitch angle	45 (degree)	
ρ_t	density of body tissue	1020 (kg m^{-3})	Wilson et al. (1992)
m	body mass	30 (kg)	Clark & Bemis (1979)
λ	ratio of the drag of an active object to that of a passive one	0.58	Hind & Gurney (1997)
C_d	drag coefficient	0.003	Clark & Bemis (1979)
S	wetted surface area	0.68 (m^2)	Clark & Bemis (1979)
ε_p	propeller efficiency	0.85	Hind & Gurney (1997)
ε_A	chamical efficiency	0.17	Hind & Gurney (1997)
M_b	basal metabolic rate	45.8 (J s^{-1})	McKechnie et al. (2006)

Table 4-2. List of parameters used in the model to estimate flight speed minimizing cost of traveling. Parameters presented as "measured" values were obtained from breeding birds caught at Funakoshi Ohshima Island in 2011 (N = 11 birds for m, L_w, and S_w and 4 birds for S_b).

symbol	parameter	value	(unit)	citation
k		1.2		Pennycuick (2008)
m	body mass	0.58	(kg)	measured
g	gravitational acceleration	9.8	(m s^{-2})	
L_w	wing span	1.09	(m)	measured
ρ_a	density of air	1.26	(kg m^{-3})	
S_b	frontal area	0.0077	(m^2)	measured
C_d	drag coefficient	0.1		Pennycuick (1996)
C_{pro}	profile coefficient for Pennycuick model	8.4		Pennycuick (2008)
C'_{pro}	profile coefficient for Norberg model	0.02		Rayner (1979)
S_w	wing area	0.11	(m^2)	measured
R	respiration factor	1.1		Pennycuick (2008)
ε	efficiency of energy convertion	0.23		Pennycuick (2008)
M_b	basal metabolic rate	3.67	(J s^{-1})	Ellis & Gabrielsen (2002)
I	traveled distance	200,000	(m)	

(a)

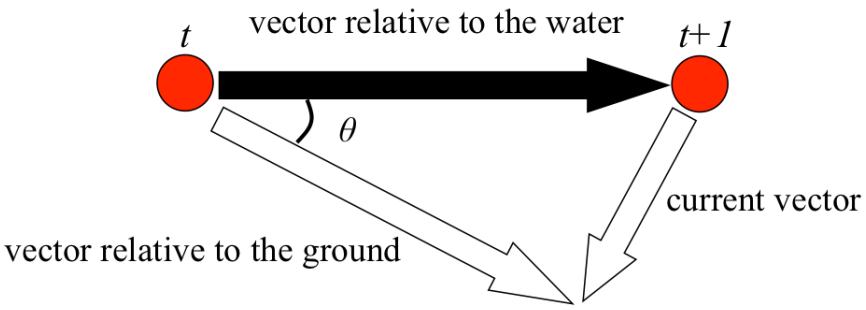

(b)

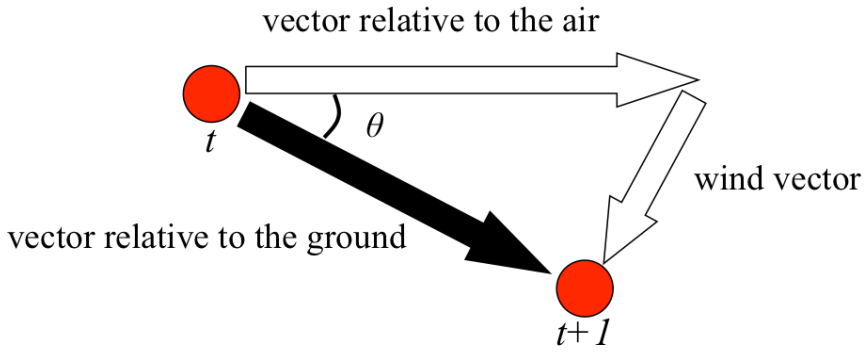

Fig. 4-1. Diagrams of the difference between two methods to obtain moving paths: (a) dead-reckoning and (b) GPS logger. Red circles represent positional data obtained by each method. Measured vectors are represented by black arrows, and unknown vectors by white arrows. While dead-reckoning reconstructs movements relative to the fluid (water and air), connecting positional fixes recorded by the GPS loggers results in movements relative to the ground.

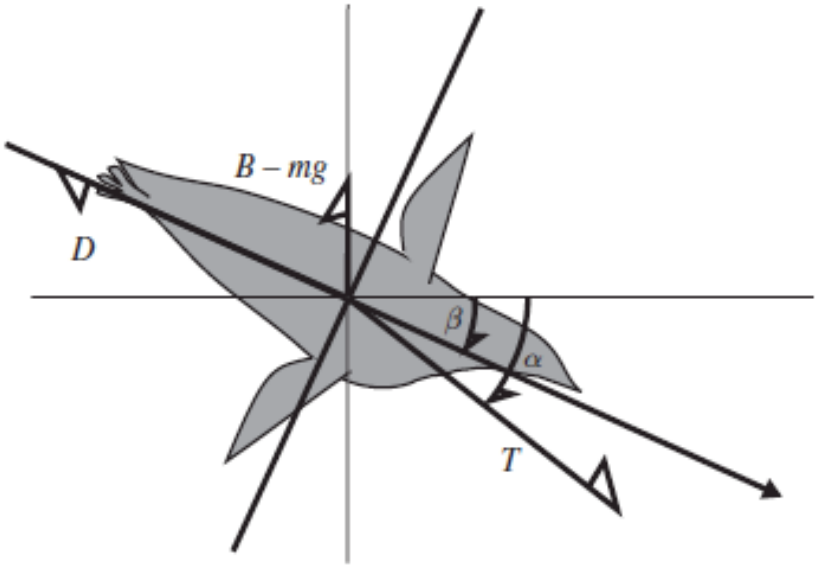

Fig. 4-2. Diagram of hydrodynamic and mechanical forces on a descending penguin (cited from Sato et al. 2010). *D* is drag, *B* is buoyancy, *m* is body mass, *g* is gravitational acceleration, *T* is thrust force produced by flapping, β is pitch angle, and α is the angle of thrust force relative to the horizontal plane.

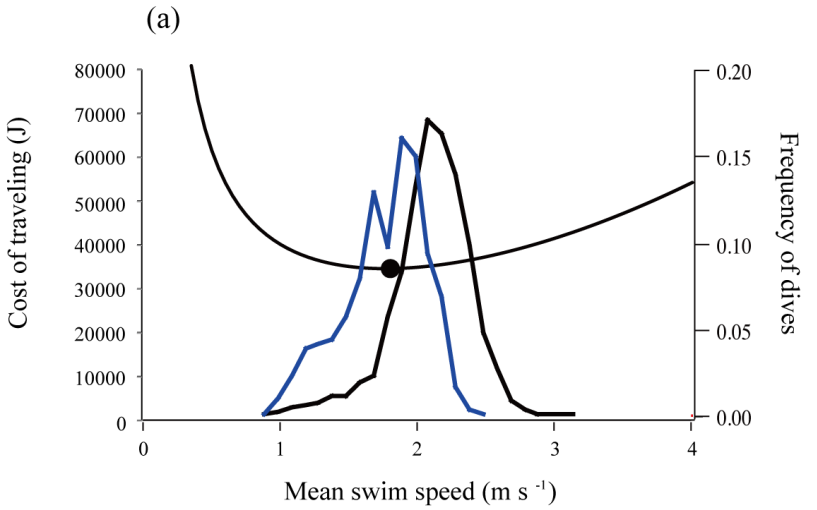
(a)
Cost of traveling (J)
Frequency of dives
Mean swim speed (m s -1)

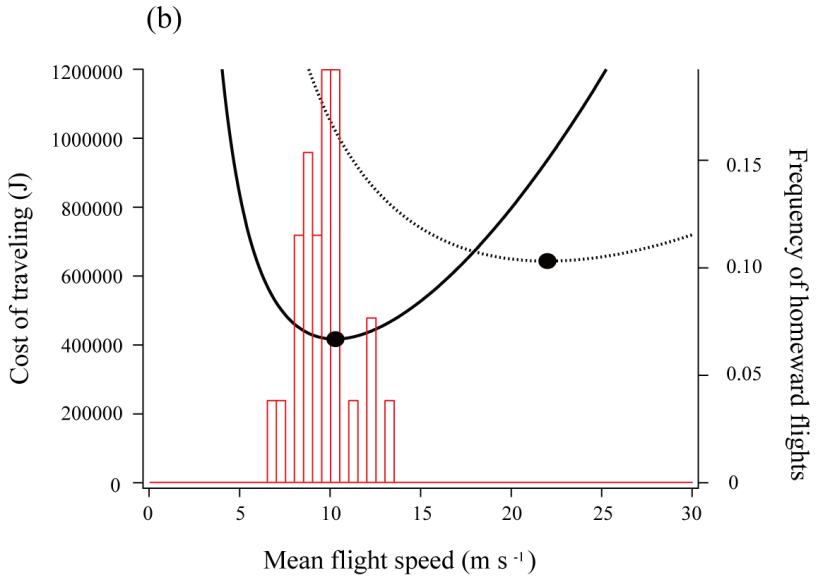
(b)
Cost of traveling (J)
Frequency of homeward flights
Mean flight speed (m s -1)

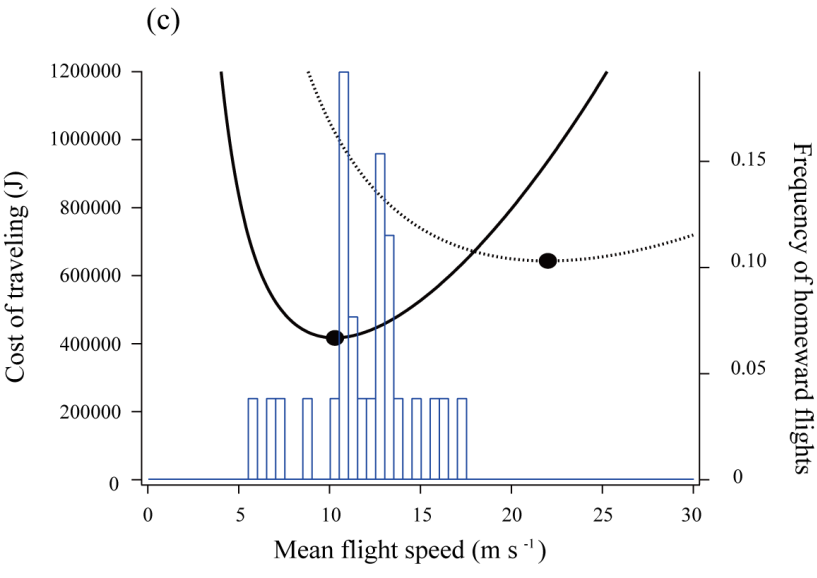
(c)
Cost of traveling (J)
Frequency of homeward flights
Mean flight speed (m s -1)

Fig. 4-3. Comparisons of moving speeds to minimize the cost of traveling as estimated by the biomechanical models (curve lines) with empirical values (histograms) of (a) swimming emperor penguins and (b, c) flying streaked shearwaters. To estimate optimal swim speeds that minimize the cost (black circles), the model suggested by Sato et al. (2010) was used with minor modifications. For flight speeds, models by Pennycuick (2008) (dashed line) and Norberg (1990) (solid line) were applied. Each histogram was made (a) with mean swim speeds during the return to the surface in a dive, (b) with mean ground speeds during a homeward flight, and (c) with mean air speeds during a homeward flight (c). See Table 4-1 and 4-2 for parameter values used in the estimations.

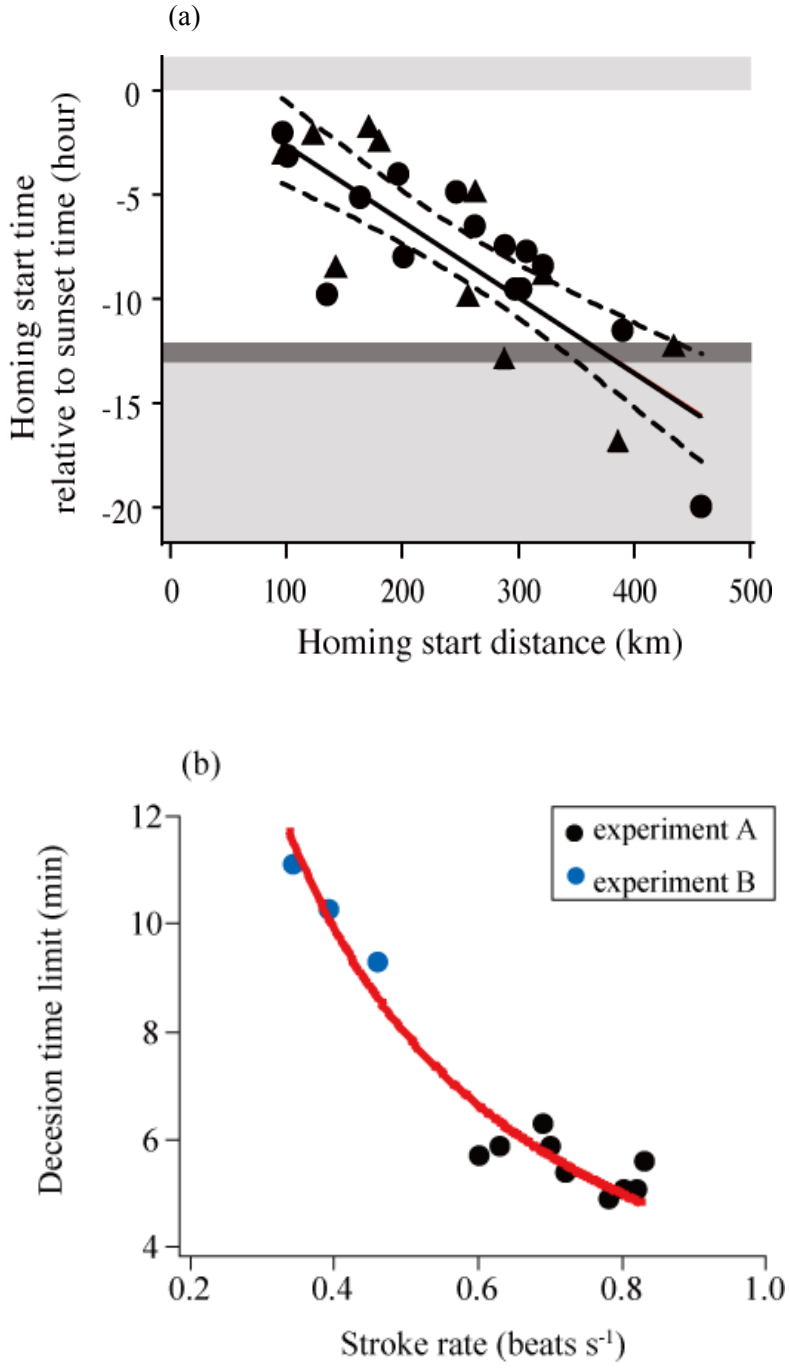

Fig. 4-4. Relationships between the decision time to return (vertical axes) and the factor affecting the decision (abscissa axes) for (a) streaked shearwaters and (b) emperor penguins.

Appendices

Appendix 1: Evaluation of dive paths obtained by dead-reckoning

Positional data obtained by dead-reckoning necessarily include an accumulative error, due to the lack of reference points underwater (Mitani et al. 2003, Wilson et al. 2007). It is important to understand the limitation of the method in interpreting diving behaviors appropriately with the dive paths. Here, the dominant cause of the error is first tested, and next, another cause which can affect estimation of dive paths at a fine-scale. The contents of Appendix 1 were published in *Aquatic Biology* (Shiomi et al. 2008, Shiomi et al. 2010).

A1-1. Dominant cause of errors: ocean current

A1-1-1. hypotheses

The dead-reckoning method is based on the assumption that animals are always moving in a direction parallel to their longitudinal body axis. This assumption is not always true, especially for animals in moving fluids. Any movements not meeting this assumption, such as passive transport by water currents, are not included in the calculation and can cause errors in estimated positions (Fig. A1-1). Based on this fact, Wilson et al. (1991) described that positional fixes estimated by dead-reckoning become more inaccurate with time and that the greatest source of inaccuracy is ocean current.

If ocean current actually affects the dive paths, it is hypothesized that the directions of the estimated points relative to the real positions (error direction) will not be uniformly distributed, but will be opposite to the direction of the prevailing current. The aims of the section A1-1 are: (1) to confirm whether the error directions of the dive paths estimated by dead-reckoning are distributed in a certain direction, and, if so, (2) to examine the relationship between the error directions and the current direction using the data of dive paths obtained in experiment B (at the artificial dive hole) in Chapter 2.

A1-1-2. test of the hypotheses

The hypotheses above were tested in the unique condition, Penguin Ranch, where emperor penguins dive through a fixed artificial dive hole and return to the same hole at the end of dives. Under this condition, where the start and end points of dives were known, the errors in positional estimation by dead-reckoning can be evaluated quantitatively. The net error was

calculated as the difference between the starting and ending points of reconstructed dive paths (Mitani et al. 2003, Wilson et al. 2007, Fig. A1-2). In addition, the direction of the estimated ending point relative to the starting point was calculated as the error direction (Mitani 2002), to test whether the directions were distributed opposite to the ocean current direction. A southward-flowing current was found to predominate near the site for experiment B (77°49' S, 166° 07' E) by Barry & Dayton (1988). The uniformity of the distribution of the error directions during each deployment was examined using a Rayleigh test, and the mean error directions were compared among all deployments using the Watson-Williams test (Zar 1999, Chap. 27). Only dives in which the dive depth was >25 m and the farthest horizontal distance (FHD) was >100 m were used for the error analysis. The other dives were not considered to be suitable for the analysis, because the penguins swam tortuously and irregularly near the dive holes during those dives. Results are presented as means (± s.d.), and the results of tests were assumed to be significant at $P < 0.05$.

A1-1-3. results and discussion

The calculated ending points of the dive paths were always inconsistent with the known starting point as shown in Fig. A1-2. The mean net error of a dive in each deployment ranged from 113.3 ± 79.8 to 215.1 ± 190.2 m, and the net error correlated positively with the dive duration (Pearson's correlation coefficient; $r_c = 0.64$ to 0.82, $P < 0.01$; Fig. A1-3, Table A1-1). The net error divided by the dive duration, i.e. the error-per-second of a dive, varied between 0.18 ± 0.09 and 0.37 ± 0.15 m s^{-1} for six deployments. In all deployments, the directions of the ending points relative to the starting point were biased significantly (Fig. A1-4; Rayleigh test; $P < 0.001$, length of mean vector $R_r = 0.53$ to 0.84). Although the mean angles were different between deployments (Watson-Williams test; $P < 0.001$), most of the estimated ending points were north relative to the starting points (Fig. A1-4).

In a previous study, a positive correlation was found between the dive duration of Weddell seals *Leptonychotes weddellii* and the distance between the starting and ending points of their dive paths as calculated by dead-reckoning (Mitani et al. 2003). In addition, the distributions of the estimated ending points of the dive paths in each deployment were significantly biased relative to the starting point (Mitani 2002). However, it could not be confirmed that the directions of the estimated ending points represented the error directions, because the free-ranging seals did not necessarily use the same ice hole at the start and end of their dives. In view of this problem, Penguin Ranch, where the animals absolutely returned to

the same place, was chosen for the test of hypotheses. The calculated ending points of the emperor penguin dive paths were always inconsistent with the starting point, as shown in Fig. A1-2, and the longer the birds dived, the larger the net errors became (Fig. A1-3, Table A1-1), as Wilson et al. (1991) suspected. Thus, the error was incurred in a time-based cumulative manner. Additionally, in all six deployments, the distribution of the estimated ending points was biased significantly, and the error directions tended to be north relative to the starting point (Fig. A1-4). A southward-flowing current was predominate near Penguin Ranch (Barry & Dayton 1988), and the mean angles of the error directions were close to the major axis of the current identified by principle component analysis (see Fig. 3a in Barry & Dayton 1988). Those results verified the hypothesis that the positions estimated by dead-reckoning deviate towards the opposite of the ocean current direction relative to the real ones. However, it should be noted that the error-per-second values (Table A1-1) were much larger than the mean current speed (0.076 m s^{-1}; Barry & Dayton 1988). In the present study, the difference could be explained only by the possibility that the current speed in the experimental period was faster than that studied by Barry & Dayton (1988). In future studies, the current speed and direction should be measured in the experimental site. Other potential factors that may have caused error include the drift secondary to the centrifugal force when the penguins veered, the inaccuracy of the data used for calculating the dive paths, and the difference between the headings of the attached data logger and the penguins' longitude axis (Wilson et al. 2007). But the direction of the error deriving from those factors is probably variable, depending on the direction of the penguins' movement. Considering that the penguins swam in various directions (Shiomi et al. 2009) and that the error direction was biased significantly in all deployments, it seems highly unlikely that those factors were the main cause of accumulative errors.

Finally, it is concluded that the ocean current affected the dive paths calculated by dead-reckoning. In order to correct the estimated positional data, the net error is divided by the time elapsed between the subsequent known positions, and the fraction is applied to each estimated position (Mitani et al. 2003, Wilson et al. 2007). This method assumes a constant linear drift, accumulating the error in amplitude and direction over time. The results in this study showed that the method generally used for error compensation could realistically be viable, assuming the effect of the current does not change significantly depending on depth, the animal's body angle, and heading. In free-ranging animals, GPS loggers would be helpful to check and correct the error (Wilson et al. 2007, Matsumura et al. 2011). If the animal moves across different layers of current, or if the distances between the subsequent known points are

relatively long, obtaining the direction and speed of the dominant current in each area is advantageous in order to correct the positional data as accurately as possible.

A1-2. Another cause of errors: data processing artifacts

A1-2-1. unrealistic movements in estimated dive paths

As described above, in dead-reckoning, locomotion vectors per measurement interval are integrated from the start to the end of a dive to reconstruct paths (Wilson & Wilson 1988). The vectors can be obtained with animal-borne recorders, such as gimbaled compass loggers (e.g. Davis et al. 1999) and tri-axis magnetic and acceleration loggers (e.g. Johnson & Tyack 2003). It is suspected that other sources of error additional to ocean current arise when the direction of locomotion vectors are obtained using magnetic and acceleration data loggers. In this method, the heading at each measurement interval is not recorded directly, but is calculated indirectly from tri-axis magnetic and acceleration data. The process of the calculations with a combination of multiple parameters can include some factors that cause errors in the estimated paths.

When looking at the dive paths of emperor penguins closely, apparently unrealistic movements were found. In the headings, infrequent abrupt changes were observed (Fig. A1-5). The abrupt heading changes occurred by several tens of degrees during stroke cycles (Fig. A1-6). At the abrupt changes, penguins changed their headings drastically twice within a single stroke (Fig. A1-6), which appears to be physically difficult. The loggers used in the present study provide up to 1 Hz of parameters except for accelerations; consequently, headings were calculated at 1 Hz. Based on sampling theory, the calculated headings allow us to discuss only fluctuations derived from body posture changes at less than 0.5 Hz (Nyquist frequency). Changes at frequencies higher than 0.5 Hz caused aliasing in the data sampled at 1 Hz. Considering the mobility of penguins, a sampling frequency of magnetism (1 Hz) might be insufficient to record their movements thoroughly. It is possible that the loggers recorded just one segment of the series of actual movements during the sampling interval of 1 s, and that the incomplete data record due to sampling intervals caused unrealistic changes in the calculated headings. From this perspective, tri-axis accelerations that were sampled at a higher frequency of 16 or 32 Hz were checked visually. If penguins changed their swimming direction so rapidly, then the sharp turns must be detected as acceleration signals, such as prominent peaks on some or all of the 3-axis. However, no specific signals were detected in the vicinity of the abrupt

changes of the calculated heading. Therefore, the abrupt heading changes in the penguins' paths seemed to be artifacts.

When penguins stroke, their pitch changes slightly in the vertical plane with up- and down-beat motions, respectively (Clark & Bemis 1979). That is, the frequency of changes in gravity-based acceleration and magnetism data during stroke cycles is the same as that of strokes. A problem possibly occurred on combining the magnetism with the low-pass filtered acceleration data. The acceleration sensors in the data loggers record both specific accelerations and gravity-based accelerations, although only the latter, which reflect body posture, are required for heading calculations. Currently, frequency-based filters or running mean procedures are used to separate specific and gravity-based acceleration (e.g. Tanaka et al. 2001, Wilson et al. 2006). The low-frequency components of acceleration and smoothed acceleration obtained using each method are thought to be derived from changes in body posture relative to gravitational acceleration (Tanaka et al. 2001, Wilson et al. 2006). With both methods, however, accurately extracting true gravity-based acceleration is impossible in principle because, as mentioned above, some movements such as strokes can cause concurrent changes in both specific and gravity-based accelerations (Shepard et al. 2008, Shiomi et al. 2008). Dominant stroke frequencies of emperor penguins were larger than 0.5 Hz (Fig. 2-2a), and therefore, pitch angles could also change at a frequency higher than the Nyquist frequency. While low-pass filters naturally had eliminated high-frequency components of the gravity-based acceleration from such movements, the sampling rate of magnetism (1 Hz) did not allow the application of the same filter. As a result, aliasing was found in the magnetism data (Fig. A1-6), which seemed to lead to unrealistic changes in the calculated headings.

A1-2-2. simulation tests

Simulations with artificial data sets of tri-axis magnetism and gravity-based acceleration at 32 Hz examined the inferences about the source of the artifacts. The simulation data assumed that a penguin swim horizontally toward north, east, south, or west, at constant speeds of 2.0 m s^{-1}, which is similar with empirical values (see Chapter 2). Pitches and rolls of the animals were set to 0 degree except during stroke cycles, when pitches change down (–20 degree) and up (20 degree) corresponding with up- and down-beat motions, respectively. Based on the real values recorded for birds swimming horizontally, stroke cycle durations and stroke rate were set as 0.5 s and 0.4 Hz. Then, headings were estimated with the simulated magnetism and gravity-based acceleration data after any one of the three patterns of data processing below.

Simulation A: original magnetism and gravity-based acceleration. Magnetism and gravity-based acceleration of 32 Hz were down-sampled to 1 Hz by picking up data points at 1 s intervals. The data were then used for the heading calculation without any filtering.

Simulation B: filtered magnetism and filtered gravity- based acceleration. Magnetism and gravity-based acceleration data were processed by the same lowpass filter. Headings were then estimated with filtered magnetism and filtered acceleration after being downsampled to 1 Hz.

Simulation C: original magnetism and filtered gravity-based acceleration. Magnetism data were downsampled to 1 Hz without any filtering. Gravity-based acceleration data were processed by low-pass filters and down-sampled to 1 Hz. Headings were estimated with the magnetism and filtered acceleration. That is, this simulation followed the same data process used for the field experimental data.

As a result, headings calculated in Simulations A and B were always consistent with the 'true' headings (0, 90, 180, or 270 degree), providing the smooth straight paths (Figs. A1-7a and b). Although the baselines of the calculated headings in Simulation C showed the 'true' values, abrupt changes occurred in calculated headings during stroke cycles. As a consequence, the estimated path was similar to the paths obtained from the real penguin data (compare Figs. A1-5 and A1-7c). Results of these simulations supported the speculation that unrealistic movements in the estimated paths are attributed mainly to the changes in body postures concurrent with strokes and the combination of filtered acceleration with non-filtered magnetism in the heading calculation. Because it is practically impossible to obtain true gravity-based acceleration data like in Simulation A, magnetism data should be processed, if possible, by the same filter as applied to the acceleration data, like in Simulation B. It should be noted, however, that both filtered magnetism and filtered acceleration data do not reflect changes in body posture at frequencies higher than the cut-off value of low-pass filters.

A1-3. Conclusion

The reconstruction of 3-D dive paths undoubtedly provides useful information for examining the behavioral, ecological, and physiological significance of underwater activities such as

foraging (e.g. Davis et al. 1999, Mitani et al. 2004) and orientation (e.g. Davis et al. 2001, Narazaki et al. 2009). User-friendly programs for IGOR Pro and MATLAB (MathWorks) provided at http://bre.soc.i.kyoto-u.ac.jp/bls/index.php?3D_path (Narazaki & Shiomi 2010) enable one to easily apply the method used in the present study to various diving animals. Unfortunately, however, the 3-D dive paths estimated by dead-reckoning with multiple parameters were elucidated to be susceptible to errors derived from passive transport by ocean current (section A1-1) and data processing for the calculation (section A1-2). In order to avoid misinterpretation of estimated dive paths, it is necessary to understand the assumptions and inherent problems of the method being used as well as the behavioral characteristics of study animals. In the analyses in Chapter 2, the FHD may be affected by accumulated errors in positional estimation. However, the conclusion can be robust that the upper limit of the decision to return is related with the number of strokes because the FHT is determined based on the relative shape of dive paths and is unlikely to change even if taking linear drift into account.

Table A1-1. Results of error analyses for estimated dive paths of emperor penguins.

	Net error (m)		Error-per-second (m s^{-1})		Correlation	
Deployment	mean	s.d.	mean	s.d.	coefficient	Significance
PR1-1	117.5	102.5	0.24	0.14	0.64	**
PR1-2	113.3	79.8	0.18	0.09	0.73	**
PR2-1	179.4	96.4	0.31	0.13	0.62	**
PR2-2	197.7	122.6	0.32	0.1	0.81	**
PR2-3	180.0	135.9	0.37	0.15	0.82	**
PR3	215.1	190.2	0.28	0.15	0.81	**

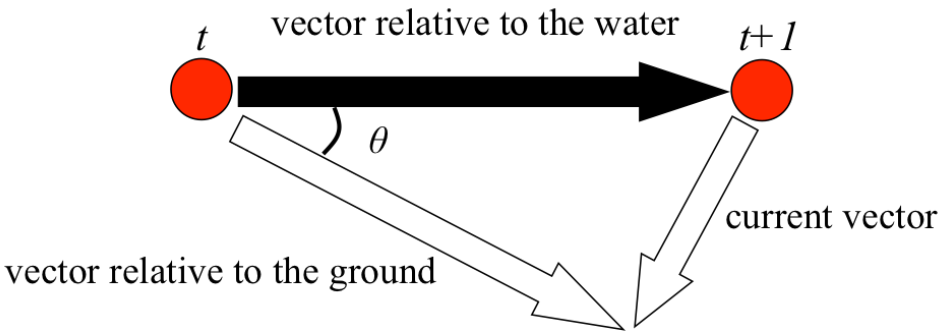

Fig. A1-1. Diagram of ocean current drift. Red circles present positional fixes at the times, *t* and *t+1*, estimated by dead-reckoning. A brack arrow presents the measured vector, and white arrows unknown vectors. θ is the angle between movements relative to the water and to the ground.

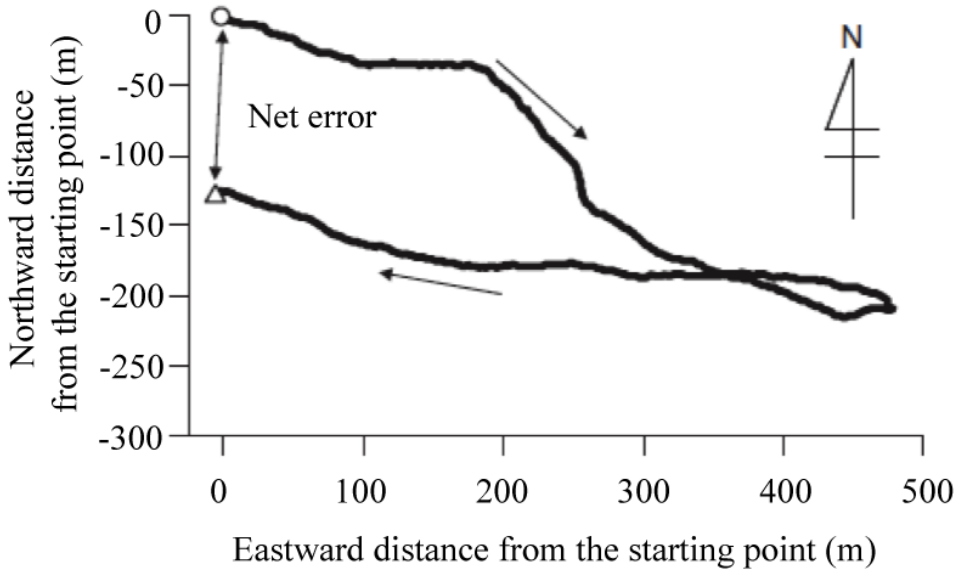

Fig. A1-2. Overhead view of a dive path calculated by dead-reckoning. Open circle: the coordinate (0,0) presents the starting point of the dive; open triangle: the estimated ending point of the dive. Note that the *x*-axis is eastward and the *y*-axis is northward. The amplitude of net error in this dive path is displayed by a two-headed arrow.

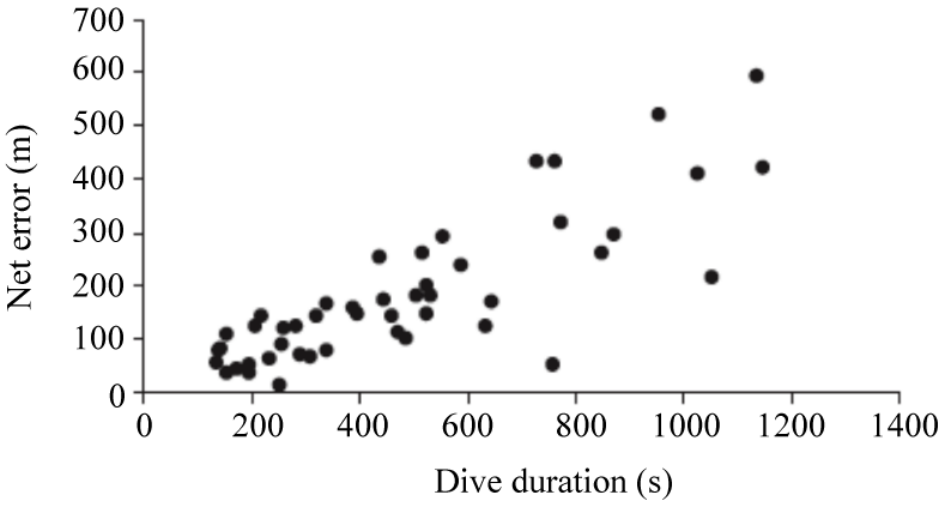

Fig. A1-3. Relationship between dive duration and net error in a deployment (PR3; n = 47 dives). The correlation coefficient, r_c, was 0.82. Note that only the data of dives in which dive depth was >25 m and the FHD was >100 m are displayed.

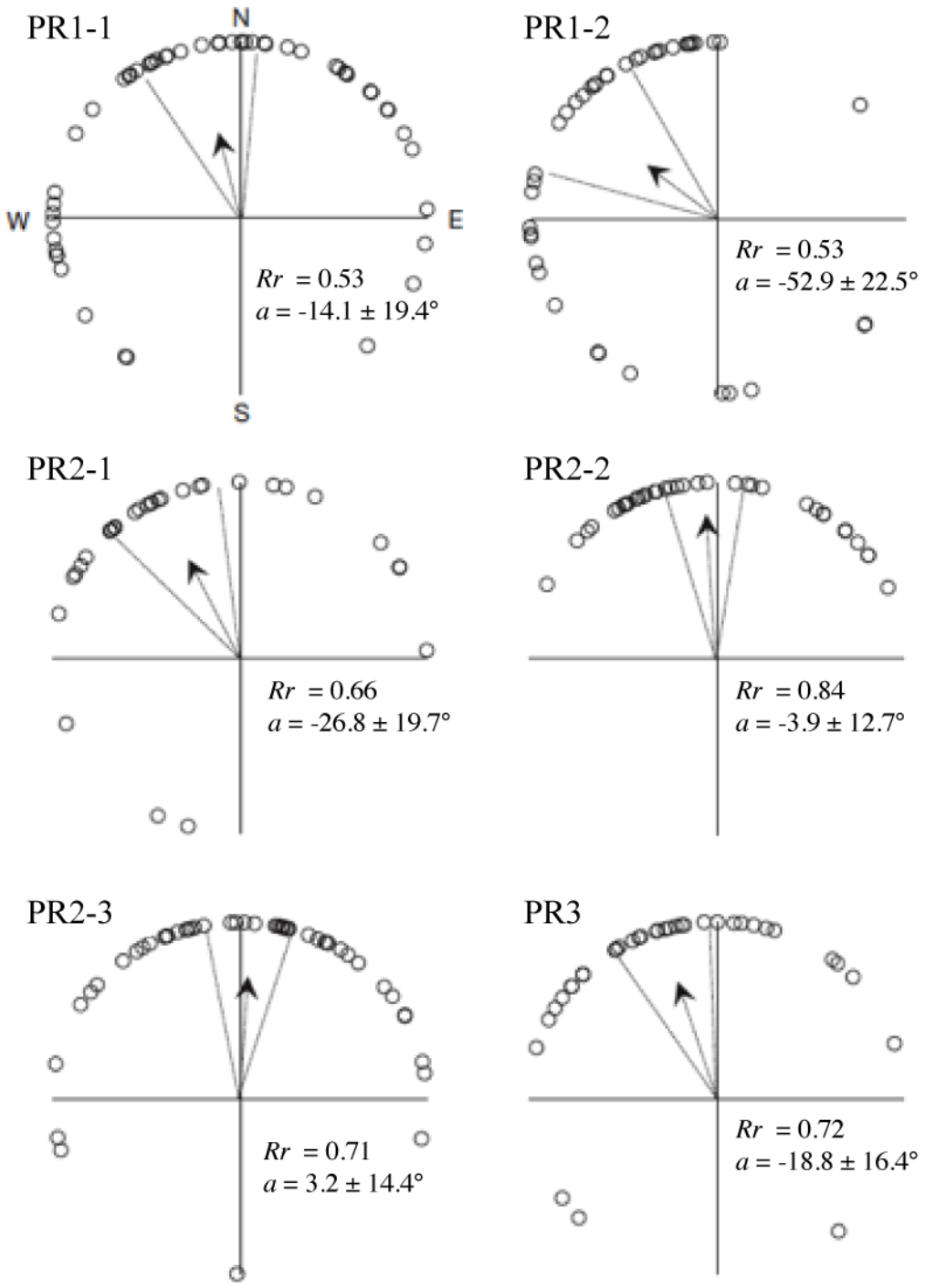

Fig. A1-4. Distribution of estimated ending point directions for each dive, relative to the starting point. The dashed arrows present the mean vectors; R_r is the length of the mean vector and a is the mean angle. The length of the vector is drawn proportional to the radius of the circle = l. The confidence limit for the mean angle was marked by dashed lines.

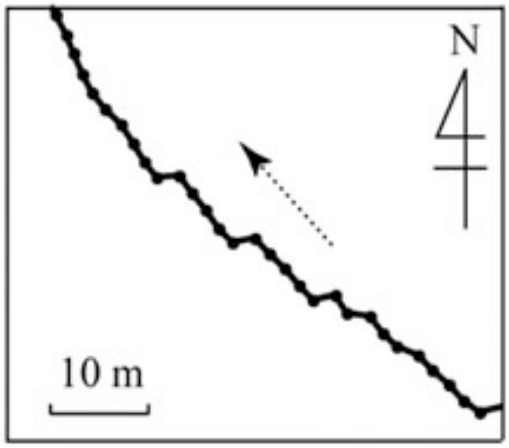

Fig. A1-5. Enlarged part of an overhead view of a dive path of an emperor penguin. Dashed arrows indicate the direction of travel. Note that there are some abrupt heading changes in the path.

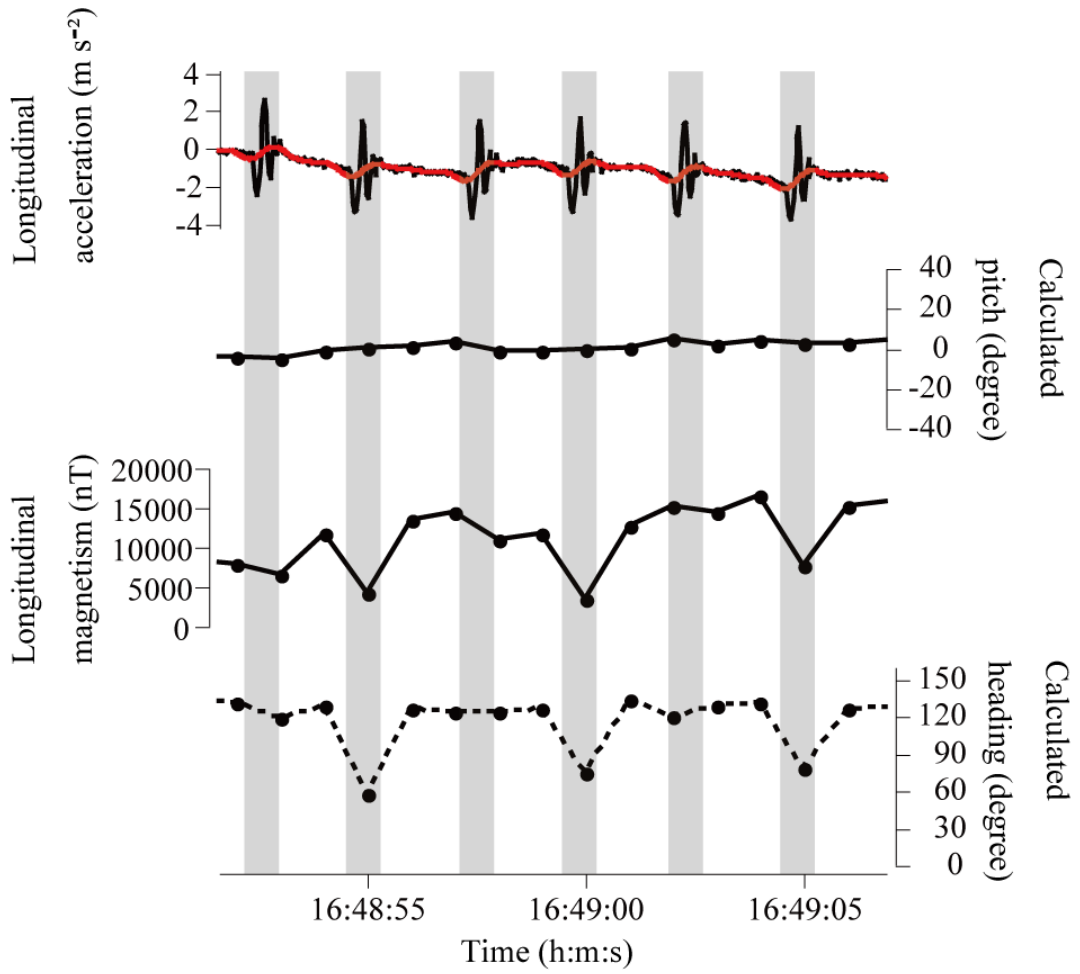

Fig. A1-6. Time-series data of longitudinal acceleration, calculated pitch, longitudinal magnetism, and calculated heading. Red lines indicate low-frequency components of longitudinal acceleration, which were extracted with frequency-based low-pass filter. Emperor penguins stroked intermittently, and gray zones indicate stroke cycles of the penguin.

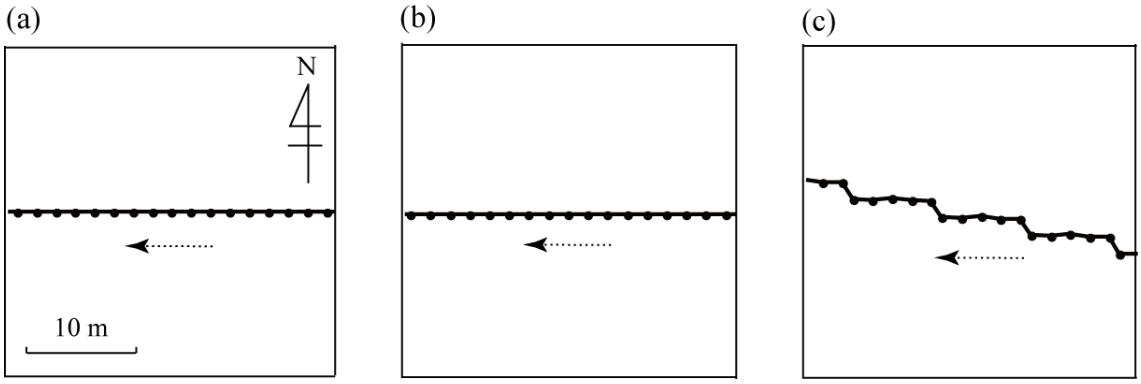

Fig. A1-7. Enlarged sections of the overhead views of an emperor penguin's paths obtained by the simulations. Dashed arrows indicate the direction of travel assumed to be western (270°) in these examples.

Appendix 2: Evaluation of flight paths obtained with GPS

Appendix 1 discusses the problems with positional estimation by dead-reckoning. Unlike for diving penguins, the positions of shearwaters can be accurately recorded by GPS data loggers. GPS technology has facilitated detailed investigations of prey-searching strategies (Weimerskirch et al. 2007), navigational mechanisms (Biro et al. 2004), and collective movements (Nagy et al. 2010) of flying birds. However, for animals moving in fluids such as the air and water, locomotion vectors calculated from consecutive GPS positions are the sum of animal movements relative to the fluid and movements of the fluid itself (Fig. A2-1). Therefore, those directions and speeds may differ from the animals' active movements. At sea, the ocean wind is likely to alter the locomotion vectors of seabirds. Here, the wind experienced by streaked shearwaters is examined, and the degree to which the wind can affect their movement paths is inferred.

A2-1. Wind data

Wind speeds and directions (hereafter, wing vector) along the homing paths of each shearwater were obtained using MATLAB (Mathworks) with the *xtractomatic_bdap* function; the data are released by National Oceanic and Atmospheric Administration (NOAA). For the procedure, the same data set of movement paths as that presented in Chapter 3 was used (N = 26 long-range trips by 17 birds). The sets of wind data were created based on data from the National Aeronautics and Space Administration (NASA) SeaWinds scatterometer aboard the QuikSCAT satellite platform. Wind vector fields arranged over a 0.125°-gridded ocean surface were averaged in 24 h ("TQSux101day" for zonal winds and "TQSuy101day" for meridional winds: http://coastwatch.pfel.noaa.gov/coastwatch/CWBrowserWW360.jsp? get=griddata). These data are intended for science-quality research applications.

A2-2. Data analyses

Moving vectors relative to the ground (hereafter, ground vector; (x_g,y_g)) during flight were calculated from consecutive positions recorded by GPS loggers. The ground vectors and wind vectors (x_{wind},y_{wind}) were then used to estimate moving vectors relative to the air (hereafter, air vector; (x_{air},y_{air})) (Fig. A2-1).

$$\begin{cases} x_{air} = x_g - x_{wind} \\ y_{air} = y_g - y_{wind} \end{cases} \quad \text{(A2-1)}$$

The angle between the two moving vectors θ was calculated based on the cosine law as an index of the difference between the ground vectors and air vectors,:

$$\theta = \arccos[(U_{air}{}^2 + U_g{}^2 - U_{wind}{}^2)/2U_{air}U_g] \quad \text{(A2-2)}$$

where U_{air}, U_g, and U_{wind} are the lengths of the air, ground, and wind vectors, respectively.

A2-3. Results and discussion

For some portions of the trips, the program to obtain wind data returned null values because there were no data of wind vectors in the area near land. According to calculations with the available data, the wind mainly came from south-southeast to west-northeast (Fig. A2-2). The mean deviation angle θ between the ground and air vectors for each trip was from 3.4 to 45.1 degree s^{-1}, with an average of 17.8 degree s^{-1} (Fig. A2-3a). The mean distance between the end points of the two vectors (equal to wind speeds) for each trip was from 1.7 to 7.4 m s^{-1}, with an average of 4.3 m s^{-1} (Fig. A2-3b). The mean ground speeds during flight for each homeward trip was from 6.9 to 13.3 m s^{-1}, with an average of 9.6 m s^{-1}. If shearwaters have no reference to compensate for wind drift, which is highly possible at sea far from coast, accumulative deviation may occur between birds' aimed movements and actual ones due to wind along the way. How they manage wind at sea is worth investigating in future studies.

While the deviation between moving vectors relative to the ground and to the air could be a limitation when discussing flight speeds in terms of energy efficiency and orientation strategies for homing, the results for the timing to start homing presented in Chapter 3 should be robust irrespective of whether moving vectors relative to the ground or to the air were used because the average approaching speed to the birds' nesting islands that was used to extract the homing start time was a relative index during the trip.

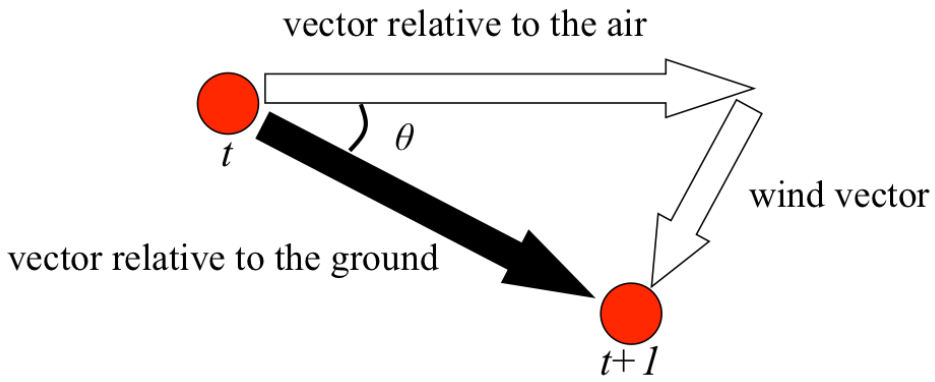

Fig. A2-1. Diagram of wind drift. Red circles represent positional fixes at times *t* and *t+1* recorded by a GPS logger. The brack arrow represents the measured vector, and the white arrows are unknown vectors. θ is the angle between movements relative to the air and to the ground.

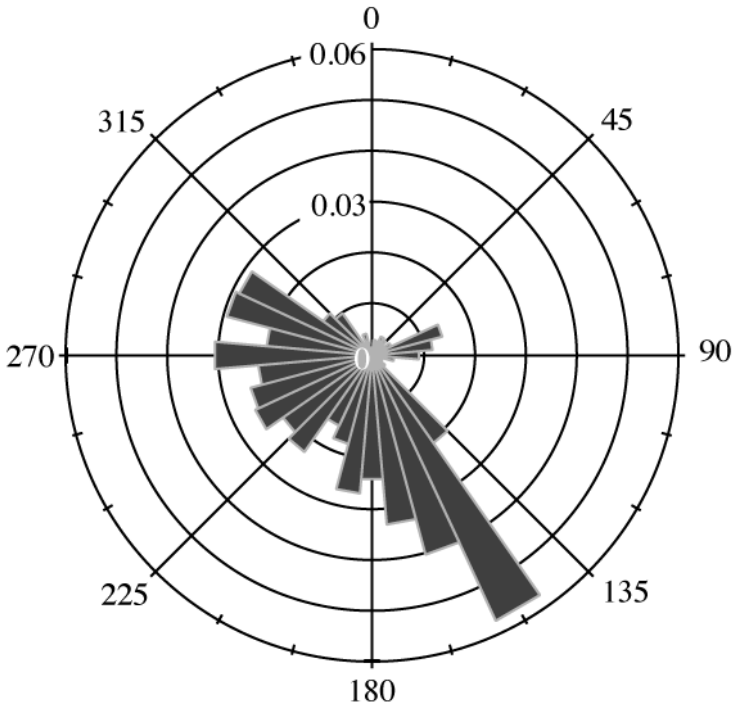

Fig. A2-2. Histogram of wind directions (i.e., direction that winds come from). All data obtained for each positional fix in homeward flights (N = 26 long range trips by 17 birds) were included.

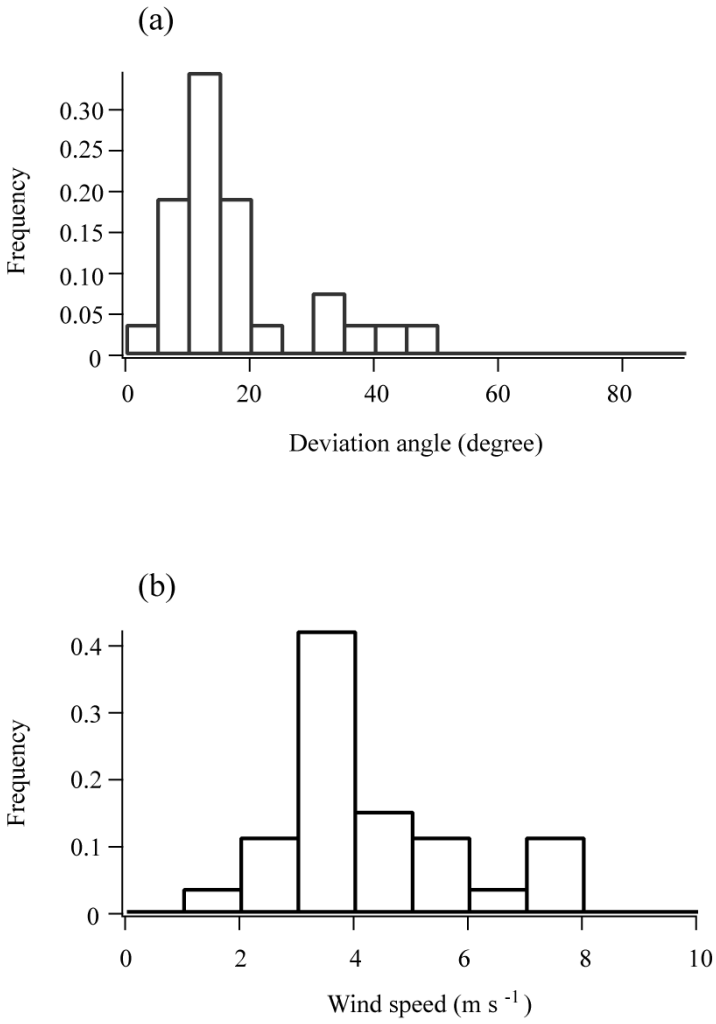

Fig. A2-3. Histograms of (a) deviation angles between moving vectors relative to the ground and to the air (θ in Fig. A2-1) and (b) deviation distances between the end points of the two vectors (= wind speed).

Acknowledgements

Dr. Katsufumi Sato supervised all of my studies and always gave me fruitful comments. Dr. Nobuaki Arai introduced me to the field of bio-logging science and gave opportunities to conduct various studies. Dr. Paul J. Ponganis helped with field experiments on emperor penguins in Antarctica, data analyses, and writing manuscripts. Dr. Ken Yoda gave me a chance to start research on streaked shearwaters and provided advice on field experiments, data analyses, and writing a manuscript. Dr. Cassondra Williams, Dr. Jessica Meir, Dr. Katherine Ponganis, and Mr. Brendan Tribble helped with field experiments in Antarctica. Mr. Nobuhiro Katsumata advised for field experiments of shearwaters and helped with writing a manuscript. Mr. Yukihisa Kogure, Mr. Syoichi Machino, Ms. Risako Tsutsumi, Mr. Itsumi Nakamura, Ms. Karin Onitsuka, Mr. Naoyuki Miyata, Dr. Takashi Yamamoto, Dr. Shinichi Watanabe, Dr. Yutaka Watanuki, Mr. Atsuo Ito, Dr. Kenichiro Sakamoto, Dr. Yoshiaki Habara, Ms. Emiko Oda, Mr. Go Sakamoto, Dr. Yuji Ohgi, Dr. Koichi Kaneda, Ms. Mahoro Suzuki helped me obtain data on shearwaters. Dr. Carlos Zavalaga and Ms. Madoka Yamaguchi explained methods for experiments with GPS data loggers. Mr. Norio Miura, Mr. Tatsuo Abe, Mr. Tsuguo Tashiro, Mr. Takanori Abe, Mr. Kimiko Abe, Mr. Masataka Kurosawa, Mr. Koichi Morita, Mr. Masaaki Hirano, and fishermen and staff of the Kamaishi and Funakoshi-wan fishery cooperatives in Iwate Prefecture supported me in carrying out safe field experiments at the islands. The staff of the International Coastal Research Center supported my research life in Otsuchi. Dr. Christian Rutz and Dr. Serge Daan gave many fruitful comments on the manuscript of the shearwater study. Dr. Yasuhiko Naito always encouraged me. Dr. Tomoko Narazaki cooperated with me and provided advices on writing the manuscript. Dr. Hiromichi Mitamura, Dr. Tohya Yasuda, Dr. Junichi Okuyama, Dr. Kotaro Ichikawa, Dr. Takashi Yokota, and Dr. Yuuki Kawabata taught me the basics of research. Dr. Patrick Miller gave an advice on reconstructing the dive paths of penguins. Dr. C. A. Bost helped establish the field of the shearwater study and provided GPS loggers for the experiments. Dr. Kenichiro Shimatani advised me on data analyses and writing the manuscript. Dr. Nobuyuki Miyazaki helped write the manuscript, and his sponsorship (UTBLS; Bio-Logging Science, University of Tokyo) supported research. Dr. Katsumi Tsukamoto, Dr. Hiroyoshi Higuchi, Dr. Ichiro Aoki, and Dr. Akinori Takahashi reviewed this thesis and gave comments to improve the manuscript. T. Stockard, T. Zenteno-Savin, J. St. Leger, and E. Stockard assisted on field experiments of emperor penguins. The staff of McMurdo Station, especially Fixed Wing Operations, provided logistical support for the penguin studies. My parents, brother, sister, and aunt always supported me to continue my research. I greatly appreciate all the help, cooperation, and advice from the people in relation to my research.

References

Ancel, A., Kooyman, G. L., Ponganis, P. J., Gendner, J. P., Lignon, J., Mestre, X., Huin, N., Thorson, P. H., Robisson, P. & Le Maho, Y. (1992). Foraging behavior of emperor penguins as a resource detector in winter and summer. *Nature,* **360**, 336-339.

Arima, H. & Sugawa, H. (2004). Correlation between the pitch of calls and external measurements of streaked shearwaters *Calonectris leucomelas* breeding on Kanmuri Island. *Japanese Journal of Ornithology*, **53**, 40-44 (in Japanese).

Ashmole, N. P. (1971). Sea bird ecology and the marine environment. in *Avian Biology* vol. 1, Farner, D S & King, J R (eds), pp. 223-286, Academic Press.

Baayen, R. H. (2009). languageR: Data sets and functions with "Analyzing Linguistic Data: A practical introduction to statistics".. R package version 0.955. http://CRAN.R-project.org/package=languageR.

Bailleul, F., Lesage, V. & Hammill, M. O. (2010). Spherical First Passage Time: a tool to investigate area-restricted search in three-dimensional movements. *Ecological Modelling,* **221**, 1665-1673.

Barry, J. P. & Dayton, P. K. (1988). Current patterns in McMurdo Sound, Antarctica and their relationship to local biotic communities. *Polar Biology,* **8**, 367–376

Bates, D. & Maechler, M. (2009). lme4: Linear mixed-effects models using S4 classes. R package version 0.999375-32. http://CRAN.R-project.org/package=lme4.

Bijlsma, R. G. & van den Brink, B. (2005). A barn swallow *Hirundo rustica* roost under attack: timing and risks in the presence of african hobbies *Falco cuvieri*. *Ardea*, **93**, 37-48.

Biro, D., Meade, J. & Guilford, T. (2004). Familiar route loyalty implies visual pilotage in the homing pigeon. *Proceedings of the National Academy of Sciences of the United States of America*, **101**, 17440-17443.

Block, B. A., Jonsen, I. D., Jorgensen, S. J., Winship, A. J., Shaffer, S. A., Bograd, S. J., Hazen, E. L., Foley, D. G., Breed, G. A., Harrison, A. L., Ganong, J. E., Swithenbank, A., Castleton, M., Dewar, H., Mate, B. R., Shillinger, G. L., Schaefer, K. M., Benson, S. R., Weise, M. J., Henry, R. W. & Costa, D. P. (2011). Tracking apex marine predator movements in a dynamic ocean. *Nature,* **475**, 86-90.

Bonadonna, F., Bajzak, C., Benhamou, S., Igloi, K., Jouventin, P., Lipp, H. P. & Dell'Omo, G. (2005). Orientation in the wandering albatross: Interfering with magnetic perception does not affect orientation performance. *Proceedings of the Royal Society B-Biological Sciences,* **272**, 489-495.

Bradshaw, C. J. A., McMahon, C. R. & Hays, G. C. (2007). Behavioral inference of diving metabolic rate in free-ranging leatherback turtles. *Physiological and Biochemical Zoology,* **80**, 209-219.

Bundle, M. W., Hansen, K. S. & Dial, K. P. (2007). Does the metabolic rate-flight speed relationship vary among geometrically similar birds of different mass? *Journal of Experimental Biology*, **210**, 1075-1083.

Burger, A. E. & Shaffer, S. A. (2008). Application of tracking and data-logging technology in research and conservation of seabirds. *Auk* **125**, 253-264.

Butler, P. J. & Jones, D. R. (1997). Physiology of diving of birds and mammals. *Physiological Reviews,* **77**, 837-899.

Cade, B. S. & Noon, B. R. (2003). A gentle introduction to quantile regression for ecologists. *Frontiers in Ecology and the Environment,* **1**, 412-420.

Cade, B. S., Terrell, J. W. & Schroeder, R. L. (1999). Estimating effects of limiting factors with regression quantiles. *Ecology,* **80**, 311-323.

Cherel, Y. & Kooyman, G. L. (1998). Food of emperor penguins (*Aptenodytes forsteri*) in the western Ross Sea, Antarctica. *Marine Biology*, **130**, 335-344.

Clark, B. D. & Bemis, W. (1979). Kinematics of swimming penguins at the Detroit Zoo. *Journal of Zoology*, **188**, 411–428

Crystal, J. D. (2009). Theoretical and conceptual issues in time-place discrimination. *European Journal of Neuroscience*, **30**, 1756-1766.

Daan, S. & Koene, P. (1981). On the timing of foraging flights by oystercatchers, *Haematopus ostralegus*, on tidal mudflats. *Netherlands Journal of Sea Research*, **15**, 1-22.

Davis, R. B., Herreid, C. F. & Short, H. L. (1962). Mexican free-tailed bats in Texas. *Ecological Monographs*, **32**, 311-346.

Davis, R. W., Fuiman, L. A., Williams, T. M., Collier, S. O., Hagey, W. P., Kanatous, S. B., Kohin, S., & Horning, M. (1999). Hunting behavior of a marine mammal beneath the Antarctic fast ice. *Science*, **283**, 993–996

Davis, R. W., Fuiman, L. A., Williams, T. M., & Le Boeuf, B. J. (2001). Three-dimensional movements and swimming activity of a northern elephant seal. *Comparative Biochemistry and Physiology A,* **129**, 759–770

DeVries, A. L. & Wohlschlag, D. E. (1964). Diving depths of Weddell seal. *Science,* **145**, 292.

Ellis, H. I. & Gabrielsen, G. W. (2002). Energetics of free-ranging seabirds. In *Biology of Marine Birds* (ed. E. A. Schreiber and J. Burger), pp. 359-408. Boca Raton: CRC Press.

Gabriel, W. & Thomas, B. (1988). Vertical migration of zooplankton an evolutionarily stable strategy. *American Naturalist*, **132**, 199– 216.

Gaston, A. J. (2004). *Seabirds: a natural history*. New Haven and London, the United Kingdom: Yale University Press.

Girard, C., Sudre, J., Benhamou, S., Roos, D. & Luschi, P. (2006). Homing in green turtles *Chelonia mydas*: oceanic currents act as a constraint rather than as an information source.

Marine Ecology Progress Series, **322**, 281-289.

Guilford, T. C., Meade, J., Freeman, R., Biro, D., Evans, T., Bonadonna, F., Boyle, D., Roberts, S. & Perrins, C. M. (2008). GPS tracking of the foraging movements of Manx shearwaters *Puffinus puffinus* breeding on Skomer Island, Wales. *Ibis*, **150**, 462-473.

Gwinner, E. (1996a). Circadian and circannual programmes in avian migration. *Journal of Experimental Biology*, **199**, 39-48.

Gwinner, E. (1996b). Circannual clocks in avian reproduction and migration. *Ibis*, **138**, 47-63.

Hansen, E. S. & Ricklefs, R. E. (2004). Foraging by deep-diving birds is not constrained by an aerobic diving limit: A model of avian depth-dependent diving metabolic rate. *Amrican Naturalist,* **163**, 358-374.

Harcourt, R. G., Hindell, M. A., Bell, D. G., & Waas, J. R. (2000). Three dimensional dive profiles of free-ranging Weddell seals. *Polar Biology*, **23**, 479–487

Hartnoll, R. G. & Wright, J. R. (1977). Foraging movements and homing in limpet *Patella vulgata* L. *Animal Behaviour*, **25**, 806-810.

Hays, G. C., Hochscheid, S., Broderick, A. C., Godley, B. J. & Metcalfe, J. D. (2000). Diving behaviour of green turtles: dive depth, dive duration and activity levels. *Marine Ecology Progress Series,* **208**, 297-298.

Henderson, J., Hurly, T. A., Bateson, M. & Healy, S. D. (2006). Timing in free-living rufous hummingbirds, *Selasphorus rufus*. *Current Biology*, **16**, 512-515.

Hind, A. T. & Gurney, W. S. C. (1997). The metabolic cost of swimming in marine homeotherms. *Journal of Experimental Biology*, **200**, 531–542.

Hindell, M. A., Harcourt, R., Waas, J. R., & Thompson, D. (2002). Finescale three-dimensional spatial use by diving, lactating female Weddell seals *Leptonychotes weddellii.*

Marine Ecology Progress Series, **242**, 275–284

Hobson, E. S. (1972). Activity of hawaiian reef fishes during the evening and morning transitions between daylight and darkness. *Fishery Bulletin*, **70**, 715-740.

Houston, A. I. & Carbone, C. (1992). The optimal allocation of time during the diving cycle. *Behavioral Ecology,* **3**, 255-265.

Houston, A. I. & McNamara, J. M. (1985). A general theory of central place foraging for single prey loaders. *Theoretical Population Biology,* **28**, 233-262.

Jander, R. (1975). Ecological aspects of spatial iruentation. *Annual Review of Ecology and Systematics,* **6**, 171-188.

Johnson, M. P. & Tyack, P. L. (2003). A digital acoustic recording tag for measuring the response of wild marine mammals to sound. *IEEE Journal of Oceanic Engineering*, **28**, 3–12

Jouventin, P., Barbraud, C. & Rubin, M. (1995). Adoption in the emperor penguin, *Aptenodytes forsteri*. *Animal Behaviour,* **50**, 1023-1029.

Kato, A., Watanuki, Y. & Naito, Y. (2003). Foraging behaviour of chick-rearing Rhinoceros auklets *Cerorhinca monocerata* at Teuri Island, Japan, determined by acceleration-depth recording micro data loggers. *Journal of Avian Biology*, **34**, 282-287.

Koenker, R. (2009). quantreg: Quantile Regression. R package version 4.44. http://CRAN.R-project.org/package=quantreg.

Koenker, R. & Bassett, G. (1978). Regression quantiles. *Econometrica,* **46**, 33-50.

Koenker, R. & Park, B. J. (1996). An interior point algorithm for nonlinear quantile regression. *Journal of Econometrics,* **71**, 265-283.

Kooyman, G. L. (1966). Maximum diving capacities of Weddell seal *Leptonychotes weddelli*.

Science, **151**, 1553-1554.

Kooyman, G. L. (1968). An analysis of some behavioral and physiological characteristics related to diving in the Weddell seal. *Antarctic Research Series*, **11**, 227–261

Kooyman, G. L. & Kooyman, T. G. (1995). Diving behavior of emperor penguins nurturing chicks at Coulman Island, Antarctica. *Condor,* **97**, 536-549.

Kooyman, G. L. & Ponganis, P. J. (1998). The physiological basis of diving to depth: Birds and mammals. *Annual Review of Physiology,* **60**, 19-32.

Kooyman, G. L., Wahrenbrock, E. A., Castellini, M. A., Davis, R. W. & Sinnett, E. E. (1980). Aerobic and anaerobic metabolism during voluntary diving in Weddell seals - evidence of preferred pathways from blood chemistry and behavior. *Journal of Comparative Physiology,* **138**, 335-346.

Kooyman, G. L., Ponganis, P. J., Castellini, M. A., Ponganis, E. P., Ponganis, K. V., Thorson, P. H., Eckert, S. A. & Le Maho, Y. (1992). Heart rates and swim speeds of emperor penguins diving under sea ice. *Journal of Experimental Biology,* **165**, 161-180.

Kronfeld-Schor, N. & Dayan, T. (2003). Partitioning of time as an ecological resource. *Annual Review of Ecology Evolution and Systematics*, **34**, 153-181.

Lagardère, J. P., Ducamp, J. J., Favre, L., Dupin, J. M., & Spèrandio, M. (1990). A method for the quantitative evaluation of fish movements in salt ponds by acoustic telemetry. *Journal of Experimental Marine Biology and Ecology*, **141**, 221–236

Lehikoinen, E., Sparks, T. H., & Zalakevicius, M. (2004). Arrival and departure dates. *Advances in Ecological Research, Birds and Climate Change*, **35**, 1-31.

Lewis, S., Schreiber, E. A., Daunt, F., Schenk, G. A., Wanless, S. & Hamer, K. C. (2004). Flexible foraging patterns under different time constraints in tropical boobies. *Animal Behaviour*, **68**, 1331-1337.

Matsumoto, K. (2008). The relationship between long- and short-distanced foraging strategy and marine environment in chick-rearing streaked shearwaters. PhD thesis, Hokkaido University (in Japanese).

Matsumura, M., Watanabe, Y. Y., Robinson, P. W., Miller, P. J. O., Costa, D. P. & Miyazaki, N. (2011). Underwater and surface behavior of homing juvenile northern elephant seals. *Journal of Experimental Biology,* **214**, 629-636.

Matthews, G. V. T. (1953). Navigation in the Manx shearwater. *Journal of Experimental Biology*, **30**, 370-396.

Maus, S., Macmillan, S., Chernova, T., Choi, S., Dater, D., Golovkov, V., Lesur, V., Lowes, F., Luhr, H., Mai, W., McLean, S., Olsen, N., Rother, M., Sabaka, T., Thomson, A. & Zvereva, T. (2005). The 10th-generation international geomagnetic reference field. *Geophysical Journal International*, **161**, 561–565

McFarland, D. J. (1977). Decision-making in animals. *Nature,* **269**, 15-21.

McKechnie, A. E., Freckleton, R. P. & Jetz, W. (2006). Phenotypic plasticity in the scaling of avian basal metabolic rate. *Proceedings of the Royal Society B-Biological Sciences*, **273**, 931–937.

Meir, J. U., Stockard, T. K., Williams, C. L., Ponganis, K. V. & Ponganis, P. J. (2008). Heart rate regulation and extreme bradycardia in diving emperor penguins. *Journal of Experimental Biology,* **211**, 1169-1179.

Mitani, Y. (2002). The analysis of three-dimensional diving behavior of Weddell seals using geomagnetic intensity and acceleration data. PhD dissertation, The Graduate University for Advanced Studies, Sokendai, Tokyo (in Japanese)

Mitani, Y., Sato, K., Ito, S., Cameron, M. F., Siniff, D. B., & Naito, Y. (2003). A method for reconstructing three-dimensional dive profiles of marine mammals using geomagnetic intensity data: results from two lactating Weddell seals. *Polar Biology*, **26**, 311–317

Mitani, Y., Watanabe, Y., Sato, K., Cameron, M. F., & Naito, Y. (2004). 3D diving behavior of Weddell seals with respect to prey accessibility and abundance. *Marine Ecology Progress Series*, **281**, 275–281

Miyazaki, M. (1996). Vegetation cover, kleptoparasitism by diurnal gulls, and timing of arrival of nocturnal Rhinoceros auklets. *Auk*, **113**, 698-702.

Mori, Y., Takahashi, A., Mehlum, F. & Watanuki, Y. (2002). An application of optimal diving models to diving behaviour of Brünnich's guillemots. *Animal Behaviour,* **64**, 739-745.

Nagy, M., Akos, Z., Biro, D. & Vicsek, T. (2010). Hierarchical group dynamics in pigeon flocks. *Nature*, **464**, 890-899.

Naito, Y. (2004). New steps in bio-logging science. *Memoirs of National Institute of Polar Research, Special issue,* **58**, 50-57.

Narazaki, T., Sato, K., Abernathy, K. J., Marshall, G. J., & Miyazaki, N. (2009). Sea turtles compensate deflection of heading at sea surface during directional travel. *Journal of Experimental Biology,* **212**, 4019–4026

Narazaki, T. & Shiomi, K. (2010). Reconstruction of 3-D path (ThreeD_path). http://bre.soc.i.kyoto-u.ac.jp/bls/index.php?3D_path.

Narendra, A., Reid, S. F. & Hemmi, J. M. (2010). The twilight zone: ambient light levels trigger activity in primitive ants. *Proceedings of the Royal Society B-Biological Sciences*, **277**, 1531-1538.

Nathan, R., Getz, W. M., Revilla, E., Holyoak, M., Kadmon, R., Saltz, D. & Smouse, P. E. (2008). A movement ecology paradigm for unifying organismal movement research. *Proceedings of the National Academy of Sciences of the United States of America,* **105**, 19052-19059.

Norberg, U. M. (1990). *Vertebrate Flight: Mechanics, Physiology, Morphology, Ecology and*

Evolution. Berlin: Springer-Verlag.

Oka, N. (2004). The distribution of streaked shearwater colonies, with special attention to population size, area of sea where located and surface water temperature. *Journal of the Yamashina Institute for Ornithology,* **35**, 164-188 (in Japanese).

Orians, G. H., & Pearson, N. E. (1979). On the theory of central place foraging, In *Analysis of Ecological Systems* (D.J. Horn, R.D. Mitchell, and G.R. Stairs, eds.), pp.155-177, Ohio State Univ. Press, Columbus, Ohio.

Passos, C., Navarro, J., Giudici, A. & Gonzalez-Solis, J. (2010). Effects of extra mass on the pelagic behavior of a seabird. *Auk,* **127**, 100-107.

Pennycuick, C. J., Klaassen, M., Kvist, A., & Lindstrom, A. (1996). Wingbeat frequency and the body drag anomaly: Wind-tunnel observations on a thrush nightingale (*Luscinia luscinia*) and a teal (*Anas crecca*). *Journal of Experimental Biology*, **199**, 2757-2765.

Pennycuick, C. J. (2008). *Modelling the Flying Bird.* London: Academic Press.

Piatkowski, U. & Putz, K. (1994). Squid diet of emperor penguins (*Aptenodytes forsteri*) in the Eastern Weddell Sea, Antarctica during late summer. *Antarctic Science,* **6**, 241-247.

Ponganis, P. J., Van Dam, R. P., Marshall, G., Knower, T. & Levenson, D. H. (2000). Sub-ice foraging behavior of emperor penguins. *Journal of Experimental Biology,* **203**, 3275-3278.

Ponganis, P. J., Van Dam, R. P., Levenson, D. H., Knower, T., Ponganis, K. V. & Marshall, G. (2003). Regional heterothermy and conservation of core temperature in emperor penguins diving under sea ice. *Comparative Biochemistry and Physiology A,* **135**, 477-487.

Prop, J., Black, J. M. & Shimmings, P. (2003). Travel schedules to the high arctic: barnacle geese trade-off the timing of migration with accumulation of fat deposits. *Oikos*, **103**, 403-414.

Rayner, J. M. V. (1979). A vortex theory of animal flight. II. The forward flight of birds. *Journal of Fluid Mechanics*, **91**, 731-763.

R Development Core Team (2009). R: A language and environment for statistical computing. R Foundation for Statistical Computing, Vienna, Austria. ISBN 3-900051-07-0, http://www.R-project.org.

Riou, S. & Hamer, K. C. (2008). Predation risk and reproductive effort: impacts of moonlight on food provisioning and chick growth in Manx shearwaters. *Animal Behaviour*, **76**, 1743-1748.

Robertson, G., Williams, R., Green, K., & Robertson, L. (1994). Diet composition of emperor penguin chicks *Aptenodytes forsteri* at 2 Mawson coast colonies, Antarctica. *Ibis*, **136**, 19-31.

Rodway, M. S. & Cooke, F. (2001). Effect of food availability on arrival and departure decisions of harlequin ducks at diurnal feeding grounds. *Condor*, **103**, 870-874.

Rutz, C. & Hays, G. C. (2009). New frontiers in biologging science. *Biology Letters,* **5**, 289-292.

Sato, K., Mitani, Y., Cameron, M. F., Siniff, D. B., & Naito, Y. (2003). Factors affecting stroking patterns and body angle in diving Weddell seals under natural conditions. *Journal of Experimental Biology,* **206**, 1461–1470

Sato, K., Charrassin, J. B., Bost, C. A. & Naito, Y. (2004). Why do macaroni penguins choose shallow body angles that result in longer descent and ascent durations? *Journal of Experimental Biology,* **207**, 4057-4065.

Sato, K., Ponganis, P. J., Habara, Y., & Naito, Y. (2005). Emperor penguins adjust swim speed according to the above-water height of ice holes through which they exit. *Journal of Experimental Biology*, **208**, 2549–2554

Sato, K., Sakamoto, K. Q., Watanuki, Y., Takahashi, A., Katsumata, N., Bost, C.-A. & Weimerskirch, H. (2009). Scaling of soaring seabirds and implications for flight abilities of giant Pterosaurs. *Plos One,* **4**, e5400.

Sato, K., Shiomi, K., Watanabe, Y., Watanuki, Y., Takahashi, A. & Ponganis, P. J. (2010). Scaling of swim speed and stroke frequency in geometrically similar penguins: they swim optimally to minimize cost of transport. *Proceedings of the Royal Society B-Biological Sciences,* **277**, 707-714.

Sato, K., Shiomi, K., Marshall, G., Kooyman, G. L. & Ponganis, P. J. (2011). Stroke rates and diving air volumes of emperor penguins: implications for dive performance. *Journal of Experimental Biology,* **214**, 2854-2863.

Sato, K., Watanuki, Y., Takahashi, A., Miller, P. J. O. Tanaka, H., Kawabe, R., Ponganis, P. J., Handrich, Y., Akamatsu, T., Watanabe, Y., Mitani, Y., Costa, D. P., Bost, C-A., Aoki, K., Amano, M., Trathan, P., Shapiro, A., & Naito, Y. (2007). Stroke frequency, but not swimming speed, is related to body size in free-ranging seabirds, pinnipeds and cetaceans. *Proceedings of the Royal Society B-Biological Sciences,* **274**, 471–477

Schofield, G., Bishop, C. M., MacLean, G., Brown, P., Baker, M., Katselidis, K. A., Dimopoulos, P., Pantis, J. D. & Hays, G. C. (2007). Novel GPS tracking of sea turtles as a tool for conservation management. *Journal of Experimental Marine Biology and Ecology,* **347**, 58-68.

Shepard, E. L. C., Wilson, R. P., Halsey, L. G., Quintana, F., Laich, A. G., Gleiss, A. C., Liebsch, N., Myers, A. E., & Norman, B. (2008). Derivation of body motion via appropriate smoothing of acceleration data. *Aquatic Biology*, **4**, 235–241

Shiomi, K., Narazaki, T., Sato, K., Shimatani, K., Arai, N., Ponganis, P. J. & Miyazaki, N. (2010). Data-processing artefacts in three-dimensional dive path reconstruction from geomagnetic and acceleration data. *Aquatic Biology,* **8**, 299-304.

Shiomi, K., Sato, K., Arai, N., Naito, Y., & Ponganis, P. J. (2009). Distribution of emperor

penguins' dive directions under the fast sea ice. In: *Proceedings of 4th International Symposium on SEASTAR 2000 and Asian Bio-logging Science*, 89-91, Graduate School of Informatics, Kyoto University

Shiomi, K., Sato, K., Mitamura, H., Arai, N., Naito, Y., & Ponganis, P. J. (2008). Effect of ocean current on the dead-reckoning estimation of 3-D dive paths of emperor penguins. *Aquatic Biology*, **3**, 265–270

Shiomi, K., Sato, K., & Ponganis, P.J. (2012a). Point of no return in diving emperor penguins: is the timing of the decision to return limited by the number of strokes? *Journal of Experimental Biology,* **215**, 135-140

Shiomi, K., Yoda, K., Katsumata, N., & Sato, K. (2012b). Temporal tuning of homeward flights in seabirds. *Animal Behaviour,* **83**, 355-359

Sisak, M. M. (1998). Animal-borne GPS and the deployment of a GPS based archiving datalogger on Hawaiian monk seal (*Monachus schauinslandi*). *Marine Technology Society Journal,* **32**, 30-36.

Steiner, I., Burgi, C., Werffeli, S., Dell'Omo, G., Valenti, P., Troster, G., Wolfer, D. P. & Lipp, H. P. (2000). A GPS logger and software for analysis of homing in pigeons and small mammals. *Physiology & Behavior*, **71**, 589-596.

Studds, C. E. & Marra, P. P. (2011). Rainfall-induced changes in food availability modify the spring departure programme of a migratory bird. *Proceedings of the Royal Society B-Biological Sciences*, **278**, 3437-3443.

Tanaka, H., Takagi, Y., & Naito, Y. (2001). Swimming speeds and buoyancy compensation of migrating adult chum salmon *Oncorhynchus keta* revealed by speed/depth/acceleration data logger. *Journal of Experimental Biology,* **204**, 3895–3904

Thalmann, S. J., Baker, G. B., Hindell, M. & Tuck, G. N. (2009). Longline fisheries and foraging distribution of flesh-footed shearwaters in eastern Australia. *Journal of Wildlife*

Management, **73**, 399-406.

Thompson, D. & Fedak, M. A. (2001). How long should a dive last? A simple model of foraging decisions by breath-hold divers in a patchy environment. *Animal Behaviour,* **61**, 287-296.

Thompson, D., Hiby, A. R., & Fedak, M. A. (1993). How fast should I swim? Behavioural implications of diving physiology. *Symposium of the Zoological Society of London,* **66**, 349-368.

Tobalske, B. W. (2007). Biomechanics of bird flight. *Journal of Experimental Biology*, **210**, 3135-3146.

Tobalske, B. W., Hedrick, T. L., Dial, K. P. & Biewener, A. A. (2003). Comparative power curves in bird flight. *Nature*, **421**, 363-366.

van Dam, R. P., Ponganis, P. J., Ponganis, K. V., Levenson, D. H. & Marshall, G. (2002). Stroke frequencies of emperor penguins diving under sea ice. *Journal of Experimental Biology,* **205**, 3769-3774.

Videler, J. J. (2005). *Avian Flight.* Oxford, Oxford University Press

von Hünerbein, K., Hamann, H. J., Ruter, E. & Wiltschko, W. (2000). A GPS-based system for recording the flight paths of birds. *Naturwissenschaften*, **87**, 278-279.

Wakefield, E. D., Phillips, R. A. and Matthiopoulos, J. (2009). Quantifying habitat use and preferences of pelagic seabirds using individual movement data: a review. *Marine Ecology Progress Series*, **391**, 165-182.

Warham, J. 1958. The nesting of the shearwater *Puffinus carneipes*. *Auk*, **75**, 1-14.

Watanabe, Y., Baranov, E. A., Sato, K., Naito, Y. & Miyazaki, N. (2006). Body density affects stroke patterns in Baikal seals. *Journal of Experimental Biology,* **209**, 3269-3280.

Watanabe, Y. Y., Takahashi, A., Sato, K., Viviant, M. & Bost, C.-A. (2011). Poor flight performance in deep-diving cormorants. *Journal of Experimental Biology,* **214**, 412-421.

Watanuki, Y., Kato, A., Naito, Y., Robertson, G. & Robinson, S. (1997). Diving and foraging behaviour of Adélie penguins in areas with and without fast sea ice. *Polar Biology,* **17**, 296-304.

Weihs, D. (1974). Energetic advantages of burst swimming of fish. *Journal of Theoretical Biology,* **48**, 215-229.

Weimerskirch, H., Bonadonna, F., Bailleul, F., Mabille, G., Dell'Omo, G. & Lipp, H. P. (2002). GPS tracking of foraging albatrosses. *Science*, **295**, 1259-1259.

Weimerskirch, H., Pinaud, D., Pawlowski, F. & Bost, C. A. (2007). Does prey capture induce area-restricted search? A fine-scale study using GPS in a marine predator, the wandering albatross. *American Naturalist*, **170**, 734-743.

Wienecke, B., Robertson, G., Kirkwood, R. & Lawton, K. (2007). Extreme dives by free-ranging emperor penguins. *Polar Biology,* **30**, 133-142.

Wikelski, M., Kays, R. W., Kasdin, N. J., Thorup, K., Smith, J. A. & Swenson, G. W. (2007). Going wild: what a global small-animal tracking system could do for experimental biologists. *Journal of Experimental Biology,* **210**, 181-186.

Williams, C. L., Meir, J. U. & Ponganis, P. J. (2011). What triggers the aerobic dive limit? Patterns of muscle oxygen depletion during dives of emperor penguins. *Journal of Experimental Biology,* **214**, 1802-1812.

Williams, T. M. (2001). Intermittent swimming by mammals: a strategy for increasing energetic efficiency during diving. *American Zoology,* **41**, 166-176.

Williams, T. M., Fuiman, L. A., Horning, M. & Davis, R. W. (2004). The cost of foraging by a marine predator, the Weddell seal *Leptonychotes weddellii*: pricing by the stroke. *Journal of*

Experimental Biology, **207**, 973-982.

Wilson, R. P. & Wilson, M. P. (1988). Dead reckoning—a new technique for determining penguin movements at sea. *Kieler Meeresforsch*, **32**, 155–158

Wilson, R. P., Wilson, M. P., Link, R., Mempel, H., & Adams, N. J. (1991). Determination of movement of African penguins *Spheniscus demersus* using a compass system: dead reckoning may be an alternative to telemetry. *Journal of Experimental Biology,* **157**, 557–564

Wilson, R. P., Hustler, K., Ryan, P. G., Burger, A. E. & Noldeke, E. C. (1992). Diving birds in cold water: do Archimedes and Boyle determine energetic costs? *American Naturalist*, **140**, 179–200.

Wilson, R. P., Putz, K., Peters, G., Culik, B., Scolaro, J. A., Charrassin, J. B., & Ropert-Coudert Y. (1997). Long-term attachment of transmitting and recording devices to penguins and other seabirds. *Wildlife Society Bulletin*, **25**, 101–106

Wilson, R. P., White, C. R., Quintana, F., Halsey, L. G., Liebsch, N., Martin, G. R., & Butler PJ (2006). Moving towards acceleration for estimates of activity-specific metabolic rate in free-living animals: the case of the cormorant. *Journal of Animal Ecology*, **75**, 1081–1090

Wilson, R. P., Liebsch, N., Davies, I. M., Quintana, F. Weimerskirch, H., Storch, S., Lucke, K., Siebert, U., Zankl, S., Muller, G., Zimmer, I., Scolaro, A., Campagna, C., Plotz, J., Bornemann, H., Teilmann, J., & McMahon, C. R. (2007). All at sea with animal tracks; methodological and analytical solutions for the resolution of movement. *Deep-Sea Research Part II*, **54**, 193–210

Wiltschko, R. & Wiltschko, W. (2003). Avian navigation: from historical to modern concepts. *Animal Behaviour*, **65**, 257-272.

Yoshida, N. (1962). Biology of streaked shearwaters at Kanmuri Island. *Tori*, **17**, 83-108 (in Japanese).

Yoshida, N. (1981). *'Kini noboru umidori' (Tree-climbing seabirds)* Tokyo: Cho-bunsya (in Japanese).

Zar, J. H. (1999). *Biostatistical analysis, 4th edn.* Prentice-Hall, Englewood Cliffs, NJ

Zavalaga, C. B., Halls, J. N., Mori, G. P., Taylor, S. A. & Dell'Omo, G. (2010). At-sea movement patterns and diving behavior of Peruvian boobies *Sula variegata* in northern Peru. *Marine Ecology Progress Series*, **404**, 259-274.